

Crustal uplift and subsidence due to the interaction
between tectonic and surface processes – an integrated
3D numerical approach for spatial quantification

Zur Erlangung des akademischen Grades eines
DOKTORS DER NATURWISSENSCHAFTEN

von der Fakultät für Physik der
Universität Karlsruhe (TH)

genehmigte

DISSERTATION

von

Diplom-Physiker Daniel Kurfeß
aus Karlsruhe

Tag der mündlichen Prüfung:

5. Dezember 2008

Referent:

Prof. Dr. Friedemann Wenzel

Korreferent:

Prof. Dr. Karl Fuchs

Crustal uplift and subsidence due to the interaction between tectonic and surface processes – an integrated 3D numerical approach for spatial quantification

by Daniel Kurfesß
(E-mail: physik@kurfess.net)

Geophysikalisches Institut, Universität Karlsruhe (TH)

Contents

Abstract	9
1 Introduction	11
1.1 Motivation	11
1.2 Objectives of this thesis	13
2 Theoretical foundations	17
2.1 Uplift and subsidence	17
2.1.1 Feedback between tectonic and surface processes	18
2.1.2 Orders of crustal displacement rates	19
2.1.3 Definition of “uplift” and “subsidence”	20
2.2 Isostasy and erosion	21
2.2.1 Simple erosion models	21
2.2.2 Local isostasy	22
2.2.3 Regional isostasy	23
2.3 Numerical landscape evolution modeling	25
2.3.1 FE modeling with ABAQUS/Standard TM	27
2.3.2 Surface processes modeling	30

3	Coupled simulation integrating surface processes modeling and geomechanical FE modeling	35
3.1	Technique	35
3.2	Benchmark models	39
3.2.1	Model A (flexure)	39
3.2.2	Model B (feedback)	42
3.3	Discussion	46
3.3.1	Limitations	47
3.3.2	Capabilities	47
4	Feedback process study	49
4.1	Impact of isostatic tectonic response	49
4.2	Model setup	50
4.3	Results and discussion	53
4.3.1	Impact of isostasy on erosion and sedimentation rates . .	53
4.3.2	Impact of isostasy on vertical crustal displacement rates	57
5	Contribution of surface processes to vertical displacement rates in the SE Carpathian region	61
5.1	Background	62
5.1.1	Seismicity in Romania	62
5.1.2	Tectonic situation in the SE Carpathian region	65
5.1.3	Observed vertical displacement rates	67
5.2	Model setup	72
5.2.1	Subsurface model	72
5.2.2	Surface model	75
5.2.3	Model adjustment	75

CONTENTS **7**

5.3 Results	79
5.4 Discussion	85
5.5 Conclusions for slab attachment or detachment	92
6 Conclusions of the thesis	93
Acknowledgments	95
References	97

Abstract

Vertical crustal displacements control the topographic evolution of our continents. Due to its social impact, temporal changes of continental topography in the form of uplift and subsidence are studied with growing interest by the geoscience community. Constantly improved remote sensing techniques such as GPS and InSAR allow us to determine uplift and subsidence rates in the sub-mm/a range. Even such small vertical displacement rates lead to centimeters of vertical displacement within human-life time spans, enough to change the habitability of complete regions, such as coastal areas, e.g.

Besides purely tectonic causes for vertical crustal displacements, also the redistribution of masses by surface processes (i.e. erosion and sedimentation) contributes to crustal uplift and subsidence. It is still an open issue to what extent the interaction between surface processes and tectonic activity of the subsurface is able to contribute to vertical crustal displacement rates.

Analytically the feedback mechanism between tectonic and surface processes can be calculated only for homogeneous models of the subsurface and with simple erosion laws. Both for heterogeneous subsurface models and for the consideration of fluvial mass redistribution numerical models are needed. In this thesis, a newly developed numerical tool is presented that simulates the interaction between tectonic processes of a 3D heterogeneous subsurface and fluvial surface processes. The new tool is used to analyze the feedback process by means of conceptual models and to quantify vertical displacement rates induced by surface processes for a 3D model of a natural region.

The results from the conceptual numerical models reveal that for time spans of less than approximately a few thousand years, erosion/sedimentation rates are not significantly affected by the feedback between tectonic and surface processes, whereas on longer time scales, this feedback does significantly affect erosion and sedimentation rates and thus also uplift and subsidence rates.

Furthermore, the numerical experiments show that fluvial erosion and sedimentation is able to contribute to vertical crustal displacement rates by up to

a few mm/a. These results imply the following for particular regions of the Earth where erosion and sedimentation lead to significant mass redistribution: Active tectonic processes, except those that are purely isostatic compensation processes, are not necessarily needed to explain the vertical crustal displacement rates observed there, because these rates might completely be explained by surface processes and their interaction with the subsurface.

In the SE Carpathian region, observed vertical displacement rates are commonly interpreted as an indicator for whether the subducted lithospheric slab beneath this region is either still attached to the crust, or whether it has already broken off and is now decoupled from the crust. Considering the strong earthquakes that frequently occur in the region, this is an important question to answer as an attached slab could transfer significant stresses into the crust and vice versa. The results from a numerical model of the SE Carpathians show that the significant vertical signal observed by GPS and by geomorphological investigations can be explained to a large extent by fluvial surface processes and their interaction with the subsurface. These results support the hypothesis that the slab is not longer attached to the crust.

Chapter 1

Introduction

1.1 Motivation

Continental topography exerts a major control on climate, and it controls the distribution of natural habitats for plants, animals, and humans. The changes of continental topography with time are affected by tectonic activity as well as by surface processes which shape the landscape by erosion and sedimentation. Whereas tectonically induced natural catastrophes such as earthquakes or volcanic eruptions are singular and local events, erosion and sedimentation take place continuously and on large regional scales. Tectonic and surface processes interact with each other, and it is this feedback that plays the key role in changing continental topography. Topographic evolution in the form of continental uplift or subsidence also influences human society as it affects life within the habitats. Low-lying areas subsiding relative to sea-level or surface water level are exposed to an increased flood risk. Areas that are uplifted are exposed to an increased risk of erosion or even desertification [Cloetingh et al., 2003, 2005]. For some areas, vertical displacements of few centimeters are sufficient to change the natural flow of river systems, or to shift coast-lines or shore-lines of rivers and lakes significantly. Even uplift or subsidence rates below 1 mm/a lead to centimeters of vertical displacement within a few decades, changing the face of cities or the habitability of complete areas within the same period of time.

Due to the social impact of topography and its changes with time, scientific research in this field becomes more important today. This trend is supported by the growing amount of data from modern technologies like GPS (Global Positioning System) and InSAR (Interferometric Synthetic Aperture Radar) that are able to measure recent vertical displacement rates within the sub-mm/a

range [Kaniuth and Vetter, 2005; Burgmann et al., 2006]. Future remote sensing techniques, a number of planned satellite missions for SAR interferometry, and new global navigation satellite systems such as the European Galileo positioning system will even increase data density and accuracy for recent vertical displacement rates. Likewise, the benefit from this observed data for geosciences will rise. Accordingly, new research projects are established in this field, for example the multinational Topo-Europe program of the European Science Foundation, covering the “4-D Topography Evolution in Europe: Uplift, Subsidence and Sea Level Change” [Cloetingh et al., 2007].

Besides anthropogenic changes to the landscape that are getting more and more important today, topographic evolution is controlled by two types of geological processes: (1) tectonic processes and (2) surface processes, i.e., geomechanical processes within the lithosphere and erosion and sedimentation processes that redistribute masses at the Earth’s surface [Press and Siever, 2001]. Today it is well known that tectonic and surface processes interact with each other [Allen, 1997; Stüwe, 2000; Burbank and Anderson, 2001]. Their interaction provides a critical feedback mechanism for vertical displacements of the Earth’s crust. This feedback controls the evolution of landscapes featuring mountains, river valleys, sediment basins, and other landforms. And it does not only affect the surface: Recent studies show that even processes below the crust – in the deep lithosphere and in the mantle – are probably affected by surface processes, proposing a possibly more important impact of the feedback for plate tectonics as a whole than accepted so far [Pysklywec, 2006; Burov and Toussaint, 2007].

In order to quantify the evolution of continental topography, it is vital to quantify the relationship between surface processes and internal solid Earth processes. Tectonic and surface processes vary on a wide range of time scales: For example, recurrence intervals of earthquakes are typically of the order of (10...1000) a, e.g. at the North Anatolian Fault system; ice ages are considered to occur approximately each (10...100) ka, accompanied by glaciation and deglaciation of large parts of the Earth’s surface and drastic changes in climate; and continental collisions happen on time scales of several (1...10) Ma. The present-day topographic changes result from the overlap of all processes active on different time scales. Thus it is reasonable to reconstruct geological history on longer time scales in order to understand today’s evolution and to be able to forecast the evolution of Earth’s surface in the near future (on human-life time scales) [Cloetingh et al., 2005]. But the geodetic and remote sensing techniques mentioned previously provide us with information only for a short time window of a few decades before present. So, in order to be able to quantitatively reconstruct long-term landscape evolution, additional data is required that allows us to estimate historic rates of topographic changes [Friedrich et al., 2003]. Geological data can help here, geomorphological data such as river

incision rates for time scales of several (10 . . . 100) ka [Burbank and Anderson, 2001], or data gained by new thermochronological analysis techniques that were developed through the 1990s, giving information about topographic changes on time scales of (1 . . . 10) Ma [Gallagher et al., 1998; Ehlers and Farley, 2003].

Due to the increasing amount of both geological and geodetic/remote sensing data, since about 1990 scientific interest in the field of long-term landscape evolution grows [Molnar and England, 1990; Allen, 1997; Burbank and Pinter, 1999; Burbank and Anderson, 2001; Press and Siever, 2001; Codilean et al., 2006; Bishop, 2007]. Accordingly, earth scientists have been studying the feedback between tectonic and surface processes and their quantitative relationship more intensely than before [Masek et al., 1994; Koons, 1995; Avouac and Burov, 1996; Kooi and Beaumont, 1996; Willett, 1999; Snyder et al., 2000; Molnar, 2001; Basile and Allemand, 2002; Garcia-Castellanos, 2002; Garcia-Castellanos et al., 2003; Simpson and Schlunegger, 2003; Persson et al., 2004; Cloetingh et al., 2004; Pysklywec, 2006; Burov and Toussaint, 2007]. A lot of questions in this field are still unsolved [Molnar, 2003; Bishop, 2007]. For instance, there is an ongoing discussion whether the present uplift of the European Alps is dominated by tectonically induced processes due to ongoing convergence between Eurasia and Africa [Coward et al., 1989; Haas et al., 2000], or whether it is solely caused by mass redistribution due to erosion [Champagnac et al., 2007; and references therein].

The trend in geosciences towards a greater interest in landscape evolution is also supported by the development of numerical models to analyze the links between tectonics and surface processes. During the last years, computers have reached such a performance level that it is now possible to perform detailed numerical analyses of high-resolution models for long-term landscape evolution, which are inevitably computationally expensive [Burbank and Pinter, 1999; Burbank and Anderson, 2001; Bishop, 2007]. With growing computer power, numerical models will contribute to the scientific progress in this field to a great extent.

1.2 Objectives of this thesis

The overall objective of the accomplished work is to contribute to a better quantitative understanding of the feedback mechanism between mass redistribution by rivers (by fluvial erosion and sedimentation) and tectonic uplift and subsidence. The following two general questions will be addressed in this thesis:

1. On which time scales does the feedback between tectonic and surface processes significantly contribute to observed erosion/sedimentation rates and vertical displacement rates? (Chapter 3)
2. To what extent can fluvial erosion and sedimentation contribute to vertical crustal displacement rates? (Chapter 4)

In the general case, neither erosion and sedimentation by rivers nor the geomechanical behavior of a heterogeneous subsurface can be calculated analytically. Thus, models addressing the coupling between tectonic and surface processes that incorporate either fluvial surface processes or subsurface heterogeneities require numerical modeling techniques. Several of such numerical models have been developed during the last two decades. But none of the existing coupled models had been able to simulate heterogeneous subsurface structures of arbitrary geometrical shape in 3D. So, in the framework of this thesis, a new numerical modeling technique has been developed. The resulting software is able to analyze the impact of the interaction between tectonic activity and surface processes on vertical crustal displacement rates. In contrast to previously developed software, the newly developed tool allows for the numerical representation of heterogeneous subsurface structures including tectonic faults.

The thesis is part of the work of project A6 “Stress Field and Geodynamics”¹ within the Collaborative Research Center 461 “Strong Earthquakes: A Challenge for Geosciences and Civil Engineering”² funded by the German research foundation DFG. This research center focusses on the Vrancea region, located in the south-eastern bend of the Carpathian arc, which has been struck by several strong earthquakes during the last century. Their hypocenters are concentrated within a small seismogenic volume at intermediate depth delineating the seismically active part of a subducting lithospheric slab.

One of the key questions to be assessed by this project is whether the slab has already broken off, or still is in the process of decoupling. In order to answer this question and thus to discuss possible tectonic causes for the strong Vrancea earthquakes, vertical displacement rates observed at the surface are used as constraints. However, before they are used it has to be analyzed whether these displacement rates have their origin in the decoupling process of the subducting lithosphere, or whether they can be explained by erosion and sedimentation processes and are thus not related to the break-off. From this consideration, a third question is derived particularly for the Vrancea region and discussed in the thesis:

¹<http://www-sfb461.ipf.uni-karlsruhe.de/pub/A6/index.html>

²<http://www-sfb461.ipf.uni-karlsruhe.de>

3. To what extent can fluvial mass redistribution explain vertical crustal displacement rates in the region around the south-eastern Carpathians, both in terms of absolute rates and in terms of spatial distribution of uplift and subsidence? (Chapter 5)

After the software had been developed during the first technical part of this thesis, it turned out that Dr. Andrea Hampel, head of an Emmy-Noether Research Group at the Ruhr-Universität Bochum, intended to develop a very similar software tool. This led to a close collaboration with the Bochum group, where I focused on the benchmarking of my software code that was further improved and provided to our colleagues, whereas the Bochum group dismissed the idea of developing another code and used mine. The first result of this collaboration is a conjoint paper on the impact of fluvial erosion and sedimentation on fault slip rates.³ Besides, the newly developed software is also tested in the research and development department of Chevron, in order to check whether the code can be adapted to include submarine sedimentation which is important for numerical simulations of reservoir development.

³Maniatis, G., Kurfeß, D., Hampel, A. and Heidbach, O., Slip acceleration on normal faults due to erosion and sedimentation – results from a new three-dimensional numerical model coupling tectonics and landscape evolution, Submitted to *Earth and Planetary Science Letters*.

Chapter 2

Theoretical foundations

2.1 Uplift and subsidence

Vertical displacements of the Earth's crust are generated by tectonic processes or by the interaction between tectonic and surface processes. The term *tectonic processes* as used in this thesis is a quite general expression encompassing all types of deformation within the lithosphere, including the motion of tectonic plates, slip on individual faults, ductile deformation, and isostatic processes [Burbank and Anderson, 2001].

The term *surface processes* here refers to the three consecutive geological processes of *erosion*, *transportation*, and *sedimentation* (or *deposition*) on Earth's surface. These are “the processes that loosen soil and rock and move them downhill or downstream, where they are laid down as layers of sediment” [Press and Siever, 2001]. Surface processes are responsible for a significant spatial redistribution of masses, associated with changes of the gravitational loads acting onto the lithosphere. The subsurface reacts to these changes by vertical displacements, generally by uplift in regions where erosion exceeds sedimentation, and by subsidence where more material is deposited than eroded.

For a large part of Earth's land area, erosion by channeled water flow (*fluvial*, *stream* or *river erosion*) is the most powerful of the erosive processes, moving more material than gravitational mass movements (*mass wasting*), glaciers (*glacial erosion*), or wind (*aeolian erosion*) [Allen, 1997]. But river systems do not only erode a large amount of material. Also, they often have the power to transport this material as sediment load over distances up to hundreds, sometimes thousands of kilometers, leading to a long-range redistribution of masses on the Earth's surface [Allen, 1997; Press and Siever, 2001].

Besides tectonic and surface processes, there is another process generating significant vertical crustal displacements: Earth's body tide. The gravity of the Sun and the Moon generates a periodic vertical displacement on the sub-meter scale with periods of about 12 hours [Kertz, 1969]. But due to its periodicity, Earth's tide does not result in permanent uplift or subsidence over longer time scales. It does not change the shape of the Earth's surface and can therefore be neglected as far as the evolution of topography is concerned. Strictly speaking, the gravity of the Sun and the Moon can be neglected only as long as we concentrate on the evolution of *continental* topography, because ocean tides do have the power to shape the shallow sea floor and shorelines due to erosion effects by the induced sea currents.

2.1.1 Feedback between tectonic and surface processes

Tectonic processes or the interaction between tectonic and surface processes lead to a considerable amount of uplift or subsidence of rocks over geological time scales. Both tectonic and surface processes shape our planet, building the topography that can be observed at the surface. Though these two types of processes have different driving mechanisms, they are coupled; they affect each other mutually [Ahnert, 1970].

This can be made clear if we consider the evolution of a mountain. This mountain is created by the convergence of tectonic plates, accompanied by an uplift of rock masses as well as by the development of a lithospheric root that balances the gravitational load of these rock masses by isostatic compensation. The rock uplift goes on as long as the convergence continues. This tectonic uplift also increases the rate of erosion as topography gets steeper, because slope gradient is another primary controlling parameter for surface processes besides climate. While the mountain is eroded, below more rock material rises from depth due to isostasy and due to the mountain-building tectonic processes. This process would not continue permanently if erosion did not take material off from the mountain top. Once the mountain would have attained a critical elevation, its gravitational load would have reached a static equilibrium with the force pushing the mountain upward. So in tectonically active mountain ranges a positive feedback may arise, where tectonic uplift accelerates erosion and erosion accelerates uplift [Molnar and England, 1990; Burbank, 1992; Masek et al., 1994; Avouac and Burov, 1996]. In tectonically *inactive* mountain ranges erosion is the only process that generates uplift, and a positive feedback increases both erosion and uplift rates there as well. This clearly shows that the interaction between tectonic and surface processes provides a critical feedback mechanism for vertical displacements of the Earth's crust.

2.1.2 Orders of crustal displacement rates

Characteristic relative velocities of horizontal tectonic plate motions are in the order of cm/a, sometimes even dm/a [DeMets et al., 1990]. Near plate boundaries, horizontal plate motions can be transformed into vertical crustal displacements, which reach orders of mm/a. This can be observed very clearly at converging plate boundaries, like the India–Eurasia collision zone. The ongoing orogeny of the Himalaya has even led to tectonic uplift rates of about 1 cm/a, considered to be equal to the stream erosion rates found there due to the balance between uplift and erosion [Press and Siever, 2001].

As tectonic plates are not rigid blocks, relative velocities between two points within one tectonic plate are compensated by various processes, including aseismic creep, brittle failure, and frictional sliding along existing faults. Where strain between two distant points is released by brittle failure, often not a single fault, but a system of faults that compensates the deformation occurs. Thus horizontal fault slip rates are typically smaller than relative velocities between tectonic plates, of the order of ($10^{-1} \dots 1$) mm/a [e.g.: Friedrich et al., 2003]. In the case of a normal or a thrust fault, horizontal displacement directly results in vertical displacement, with displacement rates of the same order of magnitude, assuming a typical fault dip between 30° and 60° .

With respect to vertical crustal displacements controlled by climate, glaciation and deglaciation during and after ice ages play the major role. Glacial loads depress the crust, and deglaciation results in an upward rebound.¹ The present-day uplift of Scandinavia of about 1 cm/a is attributed to isostatic recovery due to deglaciation after the last ice age [Johansson et al., 2002; Kuo et al., 2004]. Hetzel and Hampel [2005] propose that the development and the melting of glaciers located above normal faults also have the potential to affect the slip rate of this fault significantly, for their example by some 10^{-1} mm/a, which may even lead to a possible locking of the fault during glacial loading [also: Hampel and Hetzel, 2006].

Also controlled by climate, vertical crustal displacement rates induced by erosion and sedimentation are generally significantly smaller than those due to glaciation and deglaciation. This is because of the different mass redistribution rates. Glaciers emerge and vanish much faster than it is possible for erosion or sedimentation processes to ablate or deposit masses of rock or sediment, respectively, that are comparable with the ice mass of a glacier. Thus characteristic vertical displacement rates due to erosion and sedimentation are at most of the order of 1 mm/a, but often they only reach the sub-mm/a range

¹Comparing the density of ice and rock, the gravitational load of a 3 km thick glacier corresponds to a mountain higher than 1 km.

[Avouac and Burov, 1996; Cloetingh et al., 2003; Garcia-Castellanos et al., 2003].

2.1.3 Definition of “uplift” and “subsidence”

In this thesis the terms *uplift* or *subsidence* will often be used in conjunction with *vertical movement*, *motion* or *displacement*. Though it is clear that the word *uplift* denotes a vertical upward displacement and *subsidence* a vertical downward displacement, respectively, the words themselves do not make clear what is uplifting or subsiding, and relative to what frame of reference. So using these terms without proper definition may lead to misunderstandings. England and Molnar [1990] recognized the problem and specified the terms for geoscientific context. They differentiate between three cases: (1) *Surface uplift/subsidence* is defined as the displacement of Earth’s surface with respect to the geoid; (2) *uplift/subsidence of rock(s)* is the displacement of rocks with respect to the geoid; and (3) *exhumation/burial* is the displacement of rocks with respect to the Earth’s surface. Considering the two different reference frames, the three types of displacement are related by (cf. figure 2.1):

$$\underbrace{\text{surface uplift}}_{\Delta h} = \underbrace{\text{uplift of rock}}_{u_{ro}} - \underbrace{\text{exhumation}}_{u_{ex}} \quad . \quad (2.1)$$

Likewise, the displacement rates are related by:

$$\frac{\partial h}{\partial t} = \dot{u}_{ro} - \dot{u}_{ex} \quad , \quad (2.2)$$

where h is local elevation and t is time. The text in hand will follow this convention. Whenever the term *crustal uplift*, *rock uplift* or *tectonic uplift* is used, or *uplift* on its own, then uplift according to definition 2 is meant. Equivalently, the same holds true for the term *subsidence*.

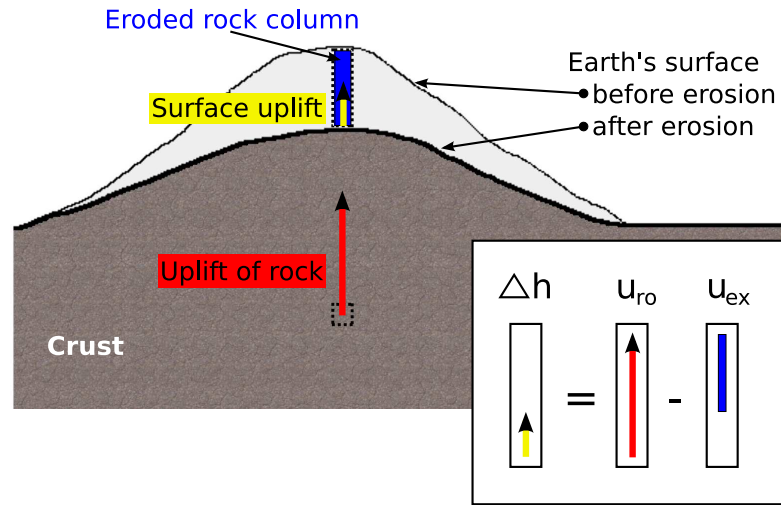


Figure 2.1 – Surface uplift (Δh), uplift of rock (u_{ro}), and exhumation/erosion (u_{ex}) are three types of vertical displacement that are related as shown in the figure.

2.2 Isostasy and erosion

In order to restrain when numerical techniques are needed to quantify vertical displacement rates, analytical solutions for rock uplift and subsidence due to the interaction between tectonic and surface processes will be presented in this section. These solutions are based on simple erosion laws and on homogeneous properties of the lithosphere.

2.2.1 Simple erosion models

Four very simple models for erosion exist that can be applied as one-dimensional erosion laws to a topographic profile [Stüwe, 2000]: Erosion rate is (1) constant, (2) proportional to elevation, (3) proportional to local slope, or (4) proportional to local curvature of topography. Models 2 and especially 4 are the most commonly used models [Ahnert, 1970; Pinet and Souriau, 1988; Stüwe, 2000; Watts, 2001], where

$$\dot{u}_{ex} = K_d \cdot h \quad , \quad \text{or} \quad (2.3)$$

$$\dot{u}_{ex} = -K_s \cdot \frac{\partial^2 h}{\partial x^2} \quad , \quad (2.4)$$

respectively; here \dot{u}_{ex} is erosion/exhumation rate, h is elevation, x is horizontal position, and K_d as denudational coefficient and K_s as subduing coefficient are the constants of proportionality. Equation 2.4 is based on the observation that mass fluxes q found at hillslopes are often proportional to local slope,

$q = -K_s \cdot \partial h / \partial x$, and on mass conservation, $\dot{u}_{ex} = \partial q / \partial x$. If the rock uplift rate $\dot{u}_{ro} = 0$, it follows from equation 2.2 that $\dot{u}_{ex} = -\partial h / \partial t$. Then equation 2.4 takes the form of a diffusion law, $\partial h / \partial t = K_s \cdot \partial^2 h / \partial x^2$, and K_s is called erosional diffusivity.

2.2.2 Local isostasy

The concept of isostasy describes an equilibrium between the gravitational force and the buoyancy force that acts on lithospheric material dipping into denser mantle material. Isostatic compensation can be achieved as the lithosphere essentially floats on a relatively inviscid² substrate, the asthenosphere [Berckhemer, 1997].

Definition of “local isostasy”

The hypothesis of *local* isostatic compensation assumes that this equilibrium is achieved for every small-sized rock column of the lithosphere. Unlike the Pratt-Hayford model for local isostasy proposing that different topographic heights are accommodated by lateral changes in density of lithospheric rocks, the Airy-Heiskanen model proposes that different topographic heights are accommodated by changes in lithospheric thickness [Watts, 2001]. In a reference depth of constant pressure within the mantle, the height of topography h is isostatically compensated by a lithospheric root of thickness T , so that

$$T(\rho_m - \rho_c) = h\rho_c \quad , \quad (2.5)$$

where ρ_c is the average density of the lithosphere, mainly consisting of crustal rocks, and ρ_m is the density of the upper mantle material forming the asthenosphere.

Denudational isostasy (local)

If material is eroded from top of the rock column, the lithospheric root is uplifted together with the rock column, where $\dot{u}_{ro} = -\dot{T}$. From equations 2.5 and 2.2 it follows for the crustal uplift rate that

$$\dot{u}_{ro} = \frac{\rho_c}{\rho_m} \dot{u}_{ex} \quad . \quad (2.6)$$

²A fluid with zero viscosity is *inviscid*.

Assuming erosion model 2 with an exhumation rate proportional to elevation (equation 2.3), the crustal uplift rate can be calculated as

$$\dot{u}_{ro}(x, t) = \frac{K_d \rho_c}{\rho_m} \cdot h(x, t) \quad . \quad (2.7)$$

Using equation 2.2 and solving the resulting relation where $\partial h / \partial t \propto h$, the Airy response to erosional unloading follows as

$$h(x, t) = h_0(x) \cdot \exp \left[- \left(1 - \frac{\rho_c}{\rho_m} \right) K_d \cdot t \right] \quad , \quad (2.8)$$

where $h_0(x) = h(x, t)|_{t=0}$, i.e., elevation decays exponentially with time at every point of the landscape [Watts, 2001].

Assuming erosion model 4 with an exhumation rate proportional to local curvature of topography (equation 2.4), the crustal uplift rate can be calculated as

$$\dot{u}_{ro}(x, t) = - \frac{K_s \rho_c}{\rho_m} \cdot \frac{\partial^2 h(x, t)}{\partial x^2} \quad . \quad (2.9)$$

Using equation 2.2, the Airy response to erosional unloading is here determined by

$$\frac{\partial h(x, t)}{\partial t} = K_s \left(1 - \frac{\rho_c}{\rho_m} \right) \cdot \frac{\partial^2 h(x, t)}{\partial x^2} \quad . \quad (2.10)$$

This relation has the form of a linear diffusion equation for which general solutions for specific boundary conditions exist [Bronstein et al., 1999; Ehlotzky, 2007]. Assuming the specific case where the initial profile of topography is periodic with the wavenumber k ,³

$$\tilde{h}_0(x) = h(x, t)|_{t=0} = \hat{h}_0 \cos(kx) \quad , \quad (2.11)$$

the Airy response to erosional unloading follows as

$$h(x, t) = \tilde{h}_0(x) \cdot \exp \left[- \left(1 - \frac{\rho_c}{\rho_m} \right) K_s k^2 \cdot t \right] \quad . \quad (2.12)$$

2.2.3 Regional isostasy

Definition of “regional isostasy”

In contrast to local isostasy, *regional* isostasy additionally takes the flexural elastic behavior of the lithosphere into account. In the most general form, the

³ $k = 2\pi/\lambda$ where λ is wavelength

downward (in $-z$ direction) deflection w of a thin elastic plate is given by the fourth-order linear differential equation

$$\frac{d^2}{dx^2} \left(D(x) \frac{d^2 w(x)}{dx^2} \right) = l(x) - P \frac{d^2 w(x)}{dx^2} \quad , \quad (2.13)$$

where D is the flexural rigidity of the plate,

$$D = \frac{Eh^3}{12(1 - \nu^2)} \quad , \quad (2.14)$$

with E being the Young's modulus, ν the Poisson's ratio, and h the thickness of the plate; $l(x)$ is a downward force, per unit length in y direction, exerted on the plate by an arbitrarily distributed load, and P is a horizontal compressional force, per unit length in y direction [Bodine and Watts, 1979; Watts, 2001; Turcotte and Schubert, 2002].

Considering the elastic flexure of the lithosphere, horizontal forces generally have a small influence on its bending behavior, thus the $Pd^2w(x)/dx^2$ term will be neglected in the following [Turcotte and Schubert, 2002]. The $l(x)$ term must address the effects of local Airy isostasy, i.e. the influence of the topographic load, $\rho_c gh(x)$, as well as the buoyancy forces generated by the lithospheric root, $(\rho_m - \rho_c)gw(x)$,⁴ where g is gravitational acceleration. Replacing $l(x)$ accordingly, considering only homogeneous elastic plates where $D(x) = D = \text{const}$, and adding time dependence in equation 2.13, the flexure equation for lithospheric problems is

$$D \frac{\partial^4 w(x, t)}{\partial x^4} + (\rho_m - \rho_c)gw(x, t) = \rho_c gh(x, t) \quad . \quad (2.15)$$

A periodic topographic profile $h(x, t)|_{t=\text{const}} = \hat{h} \cos(kx)$ results in an in-phase periodic deflection $w(x, t)|_{t=\text{const}} = \hat{w} \cos(kx)$ [Turcotte and Schubert, 2002]. As any topographic profile that can be described by a piecewise differentiable function can be expanded by a Fourier series, theoretically for every topographic profile the deflection profile can be calculated as superposition due to the linear character of the flexure equation (2.15).

⁴A foundation that acts with a force that is proportional to the plate deflection at every point is called *Winkler foundation* [Watts, 2001].

Denudational isostasy (regional)

For the periodic topographic profile given in equation 2.11, which is periodic with wavenumber k , the flexural response to erosional unloading according to erosion model 2 or 4 is

$$h(x, t) = \tilde{h}_0(x) \cdot \exp \left[- \left(1 - \frac{\rho_c}{\rho_m} \right) K_d \phi(k) \cdot t \right] , \quad \text{or} \quad (2.16)$$

$$h(x, t) = \tilde{h}_0(x) \cdot \exp \left[- \left(1 - \frac{\rho_c}{\rho_m} \right) K_s k^2 \phi(k) \cdot t \right] , \quad \text{with} \quad (2.17)$$

$$\phi(k) = \left(\frac{Dk^4}{\rho_m g} + 1 \right)^{-1} , \quad (2.18)$$

respectively [Watts, 2001]. From these equations and equations 2.2, 2.3, and 2.4, the rock uplift rates $\dot{u}_{ro}(x, t)$ can be calculated.

The flexure equation has also been used to model the isostatic response to differential denudation based on measured exhumation rate profiles [e.g., Gilchrist and Summerfield, 1990], or to calculate the isostatic response to topographic load redistribution by river systems where fluvial erosion and sedimentation are modeled numerically [e.g., Tucker and Slingerland, 1994].

2.3 Numerical landscape evolution modeling

In the general case, analytical and semi-analytical techniques to calculate rock uplift and subsidence rates cannot be applied if the geomechanical behavior of a heterogeneous subsurface is to be modeled. Furthermore, the realistic simulation of river systems and the associated redistribution of topographic loads cannot be treated analytically. So, in order to quantify vertical displacement rates of a heterogeneous crust due to fluvial erosion and sedimentation processes, numerical models that simulate the coupling between surface processes and tectonics are needed. With increasing computer power over the last decades several such computer models have been developed [Beaumont et al., 1992; Masek et al., 1994; Fullsack, 1995; Batt and Braun, 1997; Braun and Sambridge, 1997; Garcia-Castellanos et al., 1997; Willett, 1999; Garcia-Castellanos et al., 2002; Koons et al., 2003; Fischer et al., 2004; Persson et al., 2004; Simpson, 2004; Toussaint et al., 2004; Pysklywec, 2006; Burov and Toussaint, 2007; Robl et al., 2008].

In the following I will also make use of numerical techniques to quantify vertical displacement rates by means of a coupled model that simulates the feedback between tectonic and surface processes. However, none of the already existing

coupled models is used, but a new simulation tool has been developed that is different from the existing ones: First it is based on commercial Finite Element (FE) software, and secondly it is running fully automatically. Except for the model of Fischer et al. [2004] none of the existing coupled models is based on a commercial FE package for the simulation of the subsurface [Coulthard, 2001; Braun, 2006]. Commercial software packages implementing the FE method allow for the simulation of arbitrary three-dimensional structural heterogeneities including faults in combination with a wide range of different rheologies [Buchmann and Connolly, 2007; Maniatis et al., Subm.]. The availability of corresponding preprocessing software makes a proper definition of such intricate subsurface models possible, in terms of both the geometric setup and the spatial assignment of material properties. For their coupled model Fischer et al. [2004] use the commercial FE package ABAQUSTM for subsurface modeling and additional academic software for surface processes computation. They combine both parts by means of auxiliary programs which iteratively exchange data between the two parts to make a coupled simulation possible [see Fischer, 2001; for technical details]. But their approach has several disadvantages, in particular because their modeling procedure is not fully automated but requires extensive manual user interaction during the computation [Kasper D. Fischer, personal communication].

For my new simulation tool CASQUS I also couple surface processes modeling with truly three-dimensional FE modeling of the subsurface by using ABAQUSTM. The innovation of my approach and its difference to the work of Fischer et al. is that I integrate a surface processes model directly within commercial FE software. I.e., CASQUS is a geoscientific software extension to ABAQUSTM. With this technique a fully automated coupled simulation is obtained; no manual user interaction is needed once the numerical model setup is defined and the computation is started.

The FE solver ABAQUS/StandardTM [ABAQUS, Inc., 2004] that is used here handles the modeling of subsurface structures with arbitrary three-dimensional geometric shapes like tectonic faults or geological layers with topography. A wide range of rheologies is available in ABAQUS/StandardTM, such as a Coulomb failure criterion for ruptures. Temperature dependent or anisotropic material properties can also be defined. Other available features include the possibility of coupled pore fluid-stress analyses, the possibility to define hydrostatic pressure simulating the gravitational effect of water masses, and more. I.e., with the new approach it is possible to simulate a heterogeneous model of the subsurface in 3D, integrating the feedback effects of surface processes in an automated way.

CASQUS integrates the erosion and sediment transport routines of the surface processes model CASCADE written by Braun and Sambridge [1997] into

ABAQUS/StandardTM. The original CASCADE versions have been implemented into CASQUS, incorporating long-range fluvial transport processes by channeled water flow and short-range hillslope processes due to gravitational mass movements. As CASQUS is freely provided to the scientific community, advanced surface processes models based on (or similar to) CASCADE may be implemented by other users to replace the original CASCADE routines. The characteristic feature of CASQUS is its *integration* into ABAQUS/StandardTM that is used in geosciences with growing popularity for geomechanical analyses of spatially complex models of the subsurface.

2.3.1 FE modeling with ABAQUS/StandardTM

ABAQUS/StandardTM is an implicit Finite Element (FE) solver package for the numerical solution of various types of mechanical and thermo-mechanical problems [ABAQUS, Inc., 2004]. With the FE method structures of airplanes are analyzed, for example, as well as the deformation behavior of human bones or the stability of boreholes. ABAQUS/StandardTM handles such static or quasi-static mechanical problems by solving the equation that describes the equilibrium of forces in a continuous medium,

$$\frac{\partial \sigma_{ij}}{\partial x_j} + f_i = 0 \quad , \quad i, j = 1, 2, 3 \quad , \quad (2.19)$$

for a given set of displacement and/or traction boundary conditions. Here $\boldsymbol{\sigma}$ is the stress tensor, \mathbf{f} is the body force per unit volume, ρ is mass density, and $\mathbf{x} = (x_1, x_2, x_3)^T$ is the position vector in a Cartesian reference frame [Davis and Selvadurai, 1996].

This equilibrium equation results from Cauchy's equation of motion,

$$\frac{\partial \sigma_{ij}}{\partial x_j} + f_i = \rho \frac{\partial^2 u_i}{\partial t^2} \quad , \quad (2.20)$$

if the second temporal derivative of the displacement vector \mathbf{u} is negligibly small compared to the terms on the left-hand side of the equation. In order to approximate the magnitude of $\partial^2 u / \partial t^2$ for tectonic problems, consider a part of a tectonic plate, moving at an average velocity of $\partial u / \partial t = 1$ dm/a. If this part was forced to completely stop within a distance of only $\Delta u = 1$ mm, an average acceleration $\partial^2 u / \partial t^2$ of the order of 10^{-14} m/s² = $10^{-15}g$ would be sufficient.⁵ The mass density for lithospheric rock is about $\rho = 3 \times 10^3$ kg/m³,

⁵

$$\Delta u = \left(2 \frac{\partial^2 u}{\partial t^2} \right)^{-1} \left(\frac{\partial u}{\partial t} \right)^2$$

so the resulting inertial force per unit volume $\rho \partial^2 u / \partial t^2$ is only of the order of 10^{-11} Pa/m, which is negligibly small compared to the gravitational body forces $f = \rho g = 3 \times 10^4$ Pa/m and compared to typical stress gradients $\partial \sigma_{ij} / \partial x_j$ in the lithosphere that are of the same or similar order as f .

For a proper definition of a mechanical problem in continuum mechanics, additionally relations must be defined that relate the stress and the displacement field. In place of the displacement field, a quantity derived from it is typically used, the strain field, where $\epsilon = \frac{1}{2}(\nabla \mathbf{u}^T + (\nabla \mathbf{u}^T)^T)$ is the (infinitesimal) strain tensor. These constitutive relations define the rheology of the model, i.e. its deformation behavior. Linear elasticity is one example of rheological behavior; here generalized Hooke's law relates stress and strain by means of the 4th-order elasticity tensor \mathbf{C} [Ranalli, 1987]:

$$\sigma_{ij} = C_{ijkl} \epsilon_{kl} \quad , \quad i, j, k, l = 1, 2, 3 \quad . \quad (2.21)$$

\mathbf{C} contains $3^4 = 81$ components, but can be expressed by only 21 independent parameters in the most general case.⁶ In the particular case of isotropic homogeneous linear elastic media the number of independent elastic parameters reduces to two. For this case the following five interrelated elastic constants exist in literature: Young's modulus E , Poisson's ratio ν , shear modulus G , bulk modulus K , and the Lamé constant λ [Davis and Selvadurai, 1996].⁷

Continuum mechanical problems are typically boundary value problems with displacement and/or traction boundary conditions. A static (or quasi-static) continuum mechanical problem that has been properly formulated is solved by finding stress, strain, and displacement fields for the complete model such that (1) the equilibrium equations as well as (2) the constitutive equations are satisfied everywhere in the model, and (3) the boundary conditions are satisfied at all points of the boundary [Davis and Selvadurai, 1996]. Combining the equilibrium equations and the constitutive equations, a final set of partial differential equations is obtained defining the problem, in case of elastic material behavior (eqs. 2.21 in eqs. 2.19):

$$\frac{\partial}{\partial x_j} \left[\frac{C_{ijkl}}{2} \left(\frac{\partial u_k}{\partial x_i} + \frac{\partial u_l}{\partial x_k} \right) \right] + f_i = 0 \quad . \quad (2.22)$$

Those partial differential equations often cannot be solved analytically if the boundary conditions or the shape of the model body are complicated, and

⁶The balance of moment of momentum requires a symmetric stress tensor $\boldsymbol{\sigma}$, and the strain tensor $\boldsymbol{\epsilon}$ is symmetric due to its definition. I.e., each of them has six independent components. The resulting 6×6 matrix form for \mathbf{C} is also symmetric due to energy reasons, and this results in 21 independent components.

⁷Using G and λ , the generalized Hooke's law for isotropic homogeneous linear elastic material behavior can be simplified to: $\sigma_{ij} = \lambda \delta_{ij} \epsilon_{kk} + 2G \epsilon_{ij}$.

numerical methods are needed. The FE method solves such type of problems numerically by partitioning the model volume into smaller subvolumes, the so-called finite elements. Each finite element is defined by a discrete number of points at its boundary, called nodes. The nodes also interconnect each two neighboring elements, i.e. they form the vertices of the so-called FE mesh.

By default, static mechanical FE problems are formulated in a Lagrangian reference frame, where the nodes are attached to the underlying material (as opposed to an Eulerian reference frame, where material is allowed to flow through the mesh). I.e., the relative displacement between two nodes of a finite element is equivalent to strain within the material represented by this element. Provided that the discretization of the model volume, the FE mesh, is sufficiently fine for the posed problem, the variation of the displacement field variable between two neighboring nodes can be well approximated by a linear or quadratic interpolation. By combining all these local (element-wise) solutions of a given set of partial differential equations to a global solution, the FE method reduces a boundary value problem as stated above to one set of linear equations,

$$\mathbf{K}\tilde{\mathbf{u}} = \mathbf{b} \quad , \quad (2.23)$$

where $\tilde{\mathbf{u}}$ is the solution vector containing the displacement components of all nodes in the model, \mathbf{b} is the load vector containing the contributions of body forces and tractions acting at all finite elements, and \mathbf{K} is the stiffness matrix containing all information about the mesh geometry and material properties. This linear system of equations is solved efficiently by FE solvers that are optimized for this class of problems. A detailed mathematical description of the FE method which is too long to be reproduced in this thesis is given by Zienkiewicz [1977].

A Finite Element discretization can be arbitrary and irregular, i.e., it is not bound to a rectangular or equidistant grid, for example. So three-dimensional models including structures of arbitrary geometrical shape can be analyzed. In commercial FE software packages such as ABAQUS/StandardTM a wide range of rheologies is implemented, and they can handle inhomogeneous and anisotropic material properties and contact definitions [ABAQUS, Inc., 2004]. A contact definition is used where model bodies interact on contact with each other; for example, a contact definition between tectonic blocks can simulate a tectonic fault with friction according to the Amonton-Coulomb law:

$$\tau = C + \mu\sigma_n \quad , \quad (2.24)$$

where τ is the critical shear stress and σ_n is the normal stress on the fault plane, C is cohesion, and μ is the coefficient of friction [Ranalli, 1987].

A growing number of geoscientists uses ABAQUSTM for geomechanical modeling on tectonic scales [e.g., Heidbach and Drewes, 2003; Wu, 2004; Dyksterhuis

et al., 2005; Hetzel and Hampel, 2005; Ellis et al., 2006; Hergert and Heidbach, 2006; Steffen et al., 2006; Buchmann and Connolly, 2007; Masterlark, 2007; Westerhaus et al., 2008]. As accelerations of the Earth's subsurface are negligibly small, tectonic problems are generally static or quasi-static, and thus ABAQUS/StandardTM can be used for their solution.

2.3.2 Surface processes modeling

For the mathematical formulation of the surface processes model CASCADE used in this work, its creators Braun and Sambridge [1997] follow an approach that Kooi and Beaumont [1994] used before: They assume that on tectonic time scales and large spatial scales landscape evolution results from the interplay between two processes, long-range sediment transport by rivers and short-range gravitational mass movements (hillslope processes), see figure 2.2.

Both processes are simulated based on numerical solutions of differential equations. These are basically mass balance equations, shortly introduced in the subsections below and described in detail by Beaumont et al. [1992] and Kooi and Beaumont [1994]. In CASCADE the governing differential equations behind the two types of surface processes are numerically implemented on irregular grids, computing elevation changes as the result of the difference between influx and outflux of sediment at a grid point. Internal redistribution of sediment material within the model is possible, i.e. erosion *and* local deposition. Though, CASCADE needs some grid points where the water that rained onto the model surface is allowed to leave the grid, and where sediment load possibly transported by rivers reaching these grid points is removed from the model. So in CASCADE, the sum of rock plus sediment mass is generally not conserved. Braun and Sambridge [1997] explain the technical design of their code in detail, especially the relevance of the irregular grids that they use for discretizing the surface. As the CASCADE routines themselves only compute surface processes and do not consider crustal uplift and subsidence, $\partial h / \partial t = -\dot{u}_{ex}$ in the following (according to equation 2.2).

Fluvial transport

Rivers incise the landscape and transport sediments from higher to lower ground where they are deposited. One can define a local equilibrium sediment carrying capacity $q_f^{eqb}(x, y, t)$ as a measure of how much sediment a river is able to transport maximally given a point on the landscape. In CASCADE its value depends proportionally on the river discharge per unit width q_r and on the slope in the direction of river drainage $|\nabla h(x, y, t)|$,

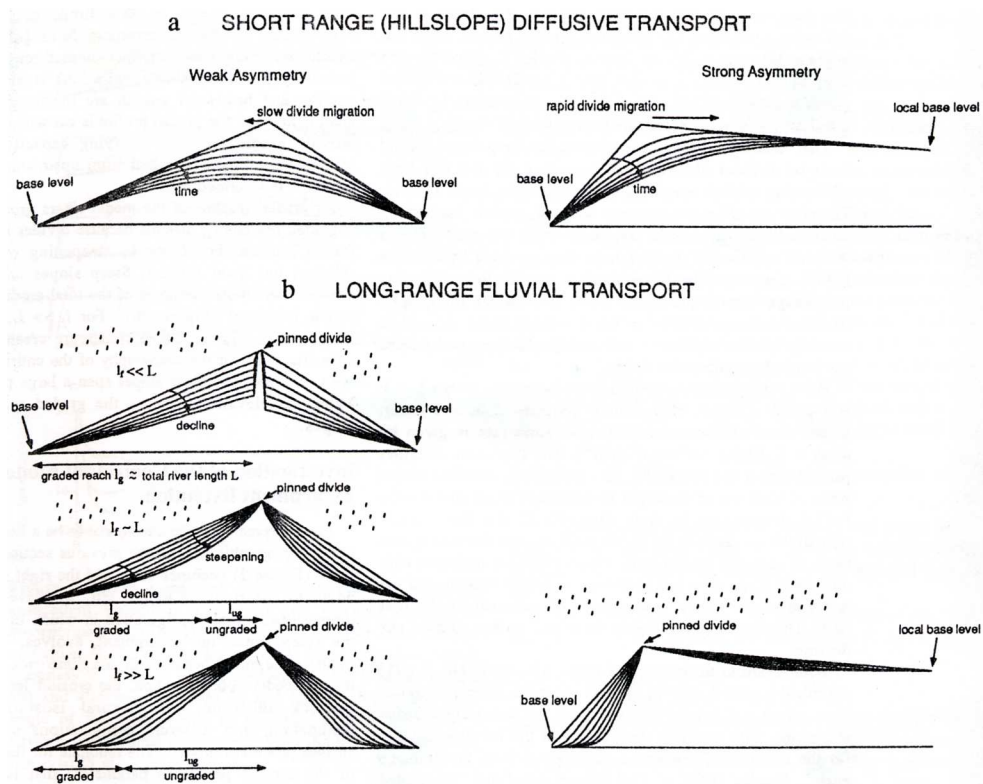


Figure 2.2 – Basic surface processes model behavior, profile of topography. **(a)** Short-range diffusive transport is the cumulative effect of surface processes such as weathering, slope wash, rain splash, and mass wasting (creep, slide, slump, flow, and fall of soil or rocks). It does not require channeled water flow by river systems. These hillslope processes smooth the relief due to their diffusive character. Drainage divides are eroded and move laterally if the topographic profile is asymmetric at the divides, because erosion at the steeper side of the divide exceeds that at the other side. **(b)** Long-range fluvial transport due to channeled water flow by river systems locally steepens relief. The divides are laterally fixed and are not eroded, because no water drains off exactly at the divides. From Kooi and Beaumont [1994].

$$q_f^{eqb}(x, y, t) = K_f q_r(x, y, t) |\nabla h(x, y, t)| \quad . \quad (2.25)$$

Here K_f is a nondimensional empirical transport coefficient, giving consistent dimensions (volume per unit width per unit time) for the fluxes q . The fluvial discharge $q_r(x, y, t)$ depends on climate, it results from conservation of water over the upstream catchment area A_c , $q_r(x, y, t) \propto \int_{A_c} \nu_R(x, y, t) dA$, where $\nu_R(x, y, t)$ is the mean precipitation rate. The approach of Kooi and Beaumont [1994] includes a formulation for fluvial mass removal that is not a priori transport-limited like in some previous surface processes models [e.g., Willgoose et al., 1991a,b], which means rivers are not forced to always carry at capacity. Instead, the disequilibrium between the actual sediment flux $q_f(x, y, t)$ of a river and its sediment transport capacity $q_f^{eqb}(x, y, t)$ controls the rate of erosion (where $q_f < q_f^{eqb}$) or sedimentation (where $q_f > q_f^{eqb}$). Then the temporal height change of a point of the landscape is given by

$$\frac{\partial}{\partial t} h(x, y, t) = -\frac{1}{l_f(x, y)} \left(q_f^{eqb}(x, y, t) - q_f(x, y, t) \right) \quad , \quad (2.26)$$

where $1/l_f(x, y)$ is an empirical constant. It depends on lithology and is a measure of how easily the river substrate can be eroded or how fast sediments are deposited, thus affecting how fast the river locally tends towards equilibrium [Mackin, 1948; Kooi and Beaumont, 1994]. In CASCADE streams never carry more load than their carrying capacity, i.e., the model of Braun and Sambridge [1997] is transport-limited in the sense that $q_f^{eqb}(x, y, t)$ is the upper bound for $q_f(x, y, t)$.

Hillslope processes

Observable fluvial transport only occurs where a significant amount of water drains off. Additionally, hillslope processes that are mainly driven only by gravity can feed the rivers from their flanking slopes. In the CASCADE model the cumulative effect of the different types of these processes (such as weathering, slope wash, rain splash, and mass wasting) is implemented as a linear diffusion equation:

$$\frac{\partial}{\partial t} h(x, y, t) = K_s(x, y, t) \nabla^2 h(x, y, t) \quad , \quad (2.27)$$

where $K_s(x, y, t)$ as the diffusion constant depends on both climate and lithology, controlling the rate of the short-range processes.

As K_f is considered to be uniform within a numerical model, in CASCADE K_f and $\nu_R(x, y, t)$ are combined to one input parameter $K_f \cdot \nu_R(x, y, t)$ (cf. equation 2.25). The resulting three empirical constants entering CASCADE as input parameters $K_f \cdot \nu_R(x, y, t)$, $l_f(x, y)$, and $K_s(x, y, t)$, can spatially vary in a model setup. Typical estimates for these parameters are $K_f \cdot \nu_R = 0.01$ m/a, $l_f = 100$ km, and $K_s = 0.1$ m²/a [van der Beek and Braun, 1998]. However, as precipitation rates in different regions vary by some order of magnitude, $K_f \cdot \nu_R$ varies accordingly, and l_f and K_s may also vary by a few orders of magnitude depending on the local lithology.

Chapter 3

Coupled simulation integrating surface processes modeling and geomechanical FE modeling

3.1 Technique

In order to study the feedback mechanism between surface and tectonic processes we have developed the simulation tool CASQUS, which integrates the surface processes model CASCADE into the FE software ABAQUS/StandardTM [Kurfeß and Heidbach, In Press]. These two programs communicate with each other via the topography of the Earth's surface. In the three-dimensional geomechanical FE model this topography is discretized by the surface nodes. They define the top side of the FE mesh of the subsurface (see figure 3.1). The same surface nodes also make up the vertices of the irregular grid that CASCADE uses [Braun and Sambridge, 1997]. That means, though the Finite Element solver runs separately from the (non-FE) surface processes computation, the discretization that is used for both computation parts is identical.

The morphology defined by the spatial coordinates of the surface nodes controls erosion and sedimentation rates, as these rates strongly depend on quantities like slope and drainage area (equations 2.25–2.27). CASCADE changes the topography as it shifts the vertical position of the surface nodes due to erosion and sedimentation. These node movements lead to volume changes in the FE mesh and thus to changes in the gravitationally induced body forces

This chapter is based on Kurfeß, D. and Heidbach, O., CASQUS: a new simulation tool for coupled 3D Finite Element modeling of tectonic and surface processes based on ABAQUSTM and CASCADE, *Computers & Geosciences*, In Press.

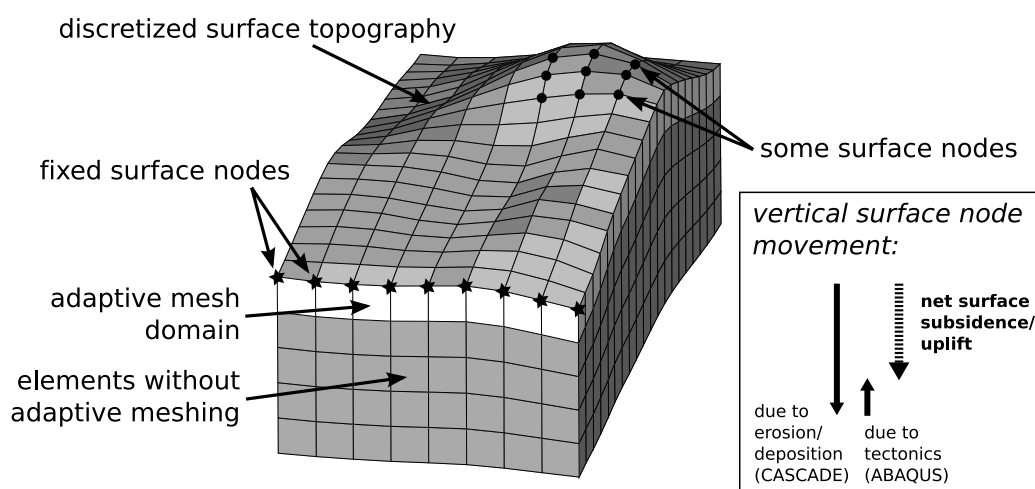


Figure 3.1 – Sketch illustrating the basic layout of a CASQUS FE model. The surface nodes (some are shown as black dots) form the upper face of the uppermost layer of elements that act as an adaptive mesh domain (white). These nodes are defined by the ABAQUSTM input file; they are also used by the CASCADE routines as the discretization of the Earth’s surface to calculate vertical changes in topography due to surface processes. Some of the surface nodes need to be defined as ‘fixed’ (black stars): Their height coordinate is not changed by CASCADE due to erosion or sedimentation; but it can still be changed by ABAQUS/StandardTM due to tectonic processes. All the sediment load of the simulated rivers that reach these fixed surface nodes is transported out of the model. **Inset:** In a CASQUS model the geomechanical stress/displacement analysis by ABAQUS/StandardTM simulates uplift (or subsidence) of rock, and the CASCADE routines mimic exhumation (or burial), according to the relation “surface uplift = uplift of rock - exhumation” [England and Molnar, 1990].

(figure 3.1). In return, ABAQUSTM calculates a new equilibrium of forces (equation 2.19), simulating the tectonic response to the changed gravitational load distribution.¹ This response in general leads to vertical movement of rock, which again modifies the surface topography. The new topography is reported to CASCADE in order to simulate surface processes on the basis of the present, tectonically changed morphology. These computation steps are continuously and automatically repeated by CASQUS.

The technical difficulty with this integrated approach is that the surface nodes must not be fixed to the subsurface material while they undergo vertical movements due to erosion and sedimentation. But by default static stress/displacement analyses in ABAQUS/StandardTM use a Lagrangian formulation: The FE mesh as the discretization of the subsurface is attached to the material and, thus, deforms with the material. I.e., by default node movements are equivalent to deformations, and they may change the stress state of the subsurface due to straining. Hence, for the particular problem of transferring vertical nodal displacements from CASCADE to ABAQUS/StandardTM, the default Lagrangian formulation is not applicable, and an Eulerian reference frame must be used in which material is allowed to flow through the mesh.

For hybrid problems of this type ABAQUS/StandardTM offers the possibility of a so-called Arbitrary Lagrangian-Eulerian (ALE) analysis. This ALE technique is enabled with Adaptive Meshing in ABAQUS/StandardTM. Our approach makes use of Adaptive Mesh Constraints: This allows us to define mesh motion which is detached from the underlying material, i.e. Eulerian-type node movements for the surface nodes [see ABAQUS, Inc., 2004]. Via the ABAQUS/StandardTM user subroutine UMESHMOTION Adaptive Mesh Constraints can be defined that are automatically computed dependent on other quantities like nodal coordinates and time increment. This user subroutine is the essential part of CASQUS: The CASCADE code is called from within this subroutine, and it forms the interface between ABAQUSTM and CASCADE through which the actual position of the surface nodes and other variables are exchanged. A schematic overview of the program flow of CASQUS is given in figure 3.2.

¹ABAQUSTM moves all nodes in the 3D FE model vertically as well as horizontally, whereas the CASCADE routines only compute vertical shifts of the surface nodes.

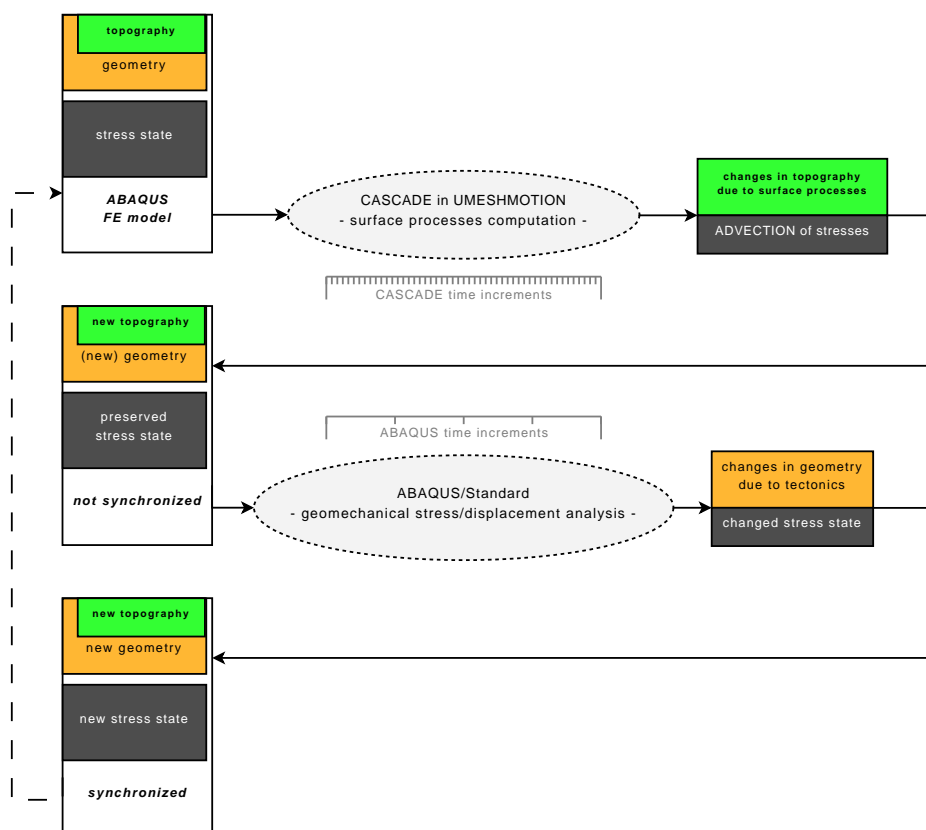


Figure 3.2 – Flow of information in CASQUS. During a first step the surface processes routines compute vertical changes of the surface topography simulating mass redistribution. A technique called Advection maps the mechanical stresses to the new FE mesh that is generated by the surface processes computation. So the stress state of the model is preserved by ABAQUSTM despite the Eulerian-type mesh geometry changes from CASCADE. Afterwards, ABAQUS/StandardTM performs a geomechanical stress/displacement FE analysis, simulating tectonic processes. During this second step the FE model mechanically responds to the changed gravitational loads. These two model steps are repeatedly computed to achieve a realistic feedback. The simulated time span is identical for both steps. As the model is in a synchronized state only after the second step, this synchronization time controls the coupling between surface and tectonic processes.

3.2 Benchmark models

Though CASQUS is designed to simulate the feedback between surface processes and geometrically and rheologically complicated subsurface models this section will introduce two geomechanically simple conceptual models that serve as benchmark examples. The setup of both models is similar, but the aim of the two analyses is different. The first model (A) is similar to the models Braun and Sambridge [1997] used for testing CASCADE. It calculates the mechanical response of a homogenous elastic plate to mass redistribution, and the modeled change in plate deflection will be compared to the analytical solution to this problem. With the second model (B) we will concentrate on the feedback process itself and the appropriate synchronization time needed.

3.2.1 Model A (flexure)

Homogeneous elastic plate models of the lithosphere based on the flexure equation (2.15) are well studied. The analytical solution of this equation in 1D for a concentrated topographic load results in a proportional relationship between the maximum deflection and the magnitude of this load [Turcotte and Schubert, 2002]. In order to show that the FE solver ABAQUS/StandardTM responds to mass redistribution by surface processes in the correct manner we have chosen a model setup that approximates a 1D homogeneous elastic plate model, though the setup is in fact 3D in order to simulate fluvial surface processes and to test CASQUS which is designed for 3D problems.

Model A consists of a homogenous elastic plate of 34 km thickness and 1600 km length representing the lithosphere. In the middle of this plate an island is placed with a length of 80 km at the bottom, that means its dimension is small relative to the underlying elastic plate (for the shape of the island see figure 3.3). The cross section shown in figure 3.3 is linearly extruded by 100 km perpendicular to the viewing plane. This gives a three-dimensional model with dimensions of $1600 \times 100 \times 34 \text{ km}^3$ for the plate and $80 \times 100 \times 2 \text{ km}^3$ for the island. The model is discretized by 8-node linear hexahedral elements², $1600 \times 100 \times 11$ elements for the plate and $80 \times 100 \times 1$ for the island. This gives a total number of 1.8×10^6 finite elements and 5.8×10^6 degrees of freedom in the model. The resulting small characteristic element length of 1.7 km in combination with the sufficient number of 22 integration points in the vertical direction assures the correct convergence of the model. As a perfectly smooth topography prevents the evolution of river networks [Braun and Sambridge, 1997] random noise in elevation is added to the island surface. The magnitude

²ABAQUSTM element type: C3D8

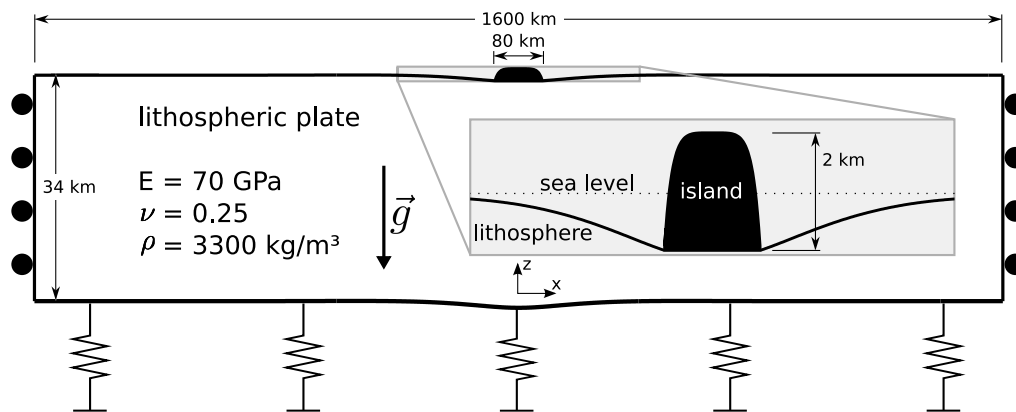


Figure 3.3 – Section of model A, vertically exaggerated. The purely elastic model is composed of a 1600 km long and 34 km thick lithospheric plate that is covered by the water of an ocean and an island in the middle that is 80 km long at its bottom (painted in black, see inset). The model is linearly extruded to a depth of 100 km in the viewing direction (along the y-axis, not shown here). The rheological parameters of the plate are given in the figure, where E is elastic (Young's) modulus, ν is Poisson's ratio and ρ is mass density. For the island $E = 10$ GPa, $\nu = 0.25$, and $\rho = 2800$ kg/m³. The plate is hydrostatically supported at the bottom to take isostasy into account (simulated by spring forces), and all side faces are fixed in normal direction indicated by the rollers. Note the deflection of the lithosphere bottom due to the gravitational load of the island.

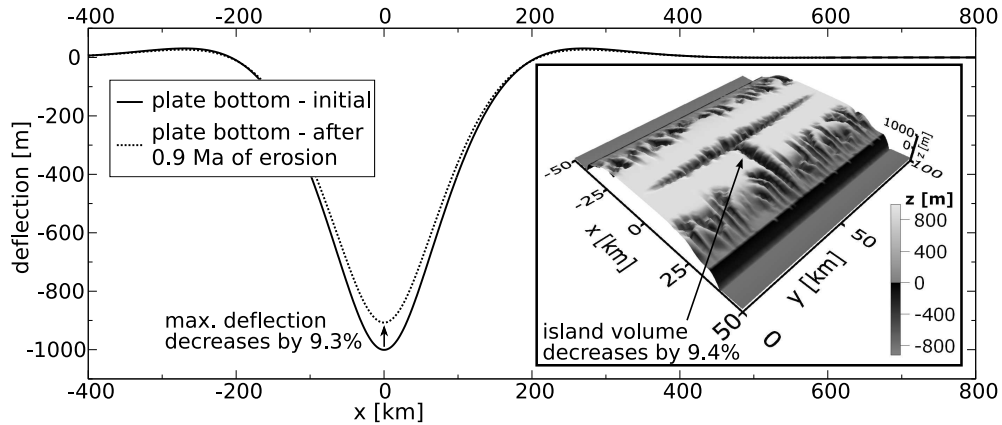


Figure 3.4 – Lithospheric plate deflection computed by model A. In the numerical model, during 0.9 Ma the island loses 9.4% of its volume due to river erosion (see inset) while the maximum deflection of the lithosphere decreases by 9.3%. This model result comes very close to what is expected from the analytical treatment of a similar problem: The maximum deflection of a thin elastic plate under a concentrated load is proportional to the magnitude of this load [Turcotte and Schubert, 2002].

of the noise is uniformly distributed in the range $(-1 \text{ mm}; +1 \text{ mm})$. The four plane side faces of the model are fixed in normal direction. The bottom of the plate is supported by spring forces (elastic foundations in ABAQUSTM). They represent that part of the lithostatic pressure that is generated by the mantle material and the water of the ocean [Turcotte and Schubert, 2002]. Their stiffness per unit area is $(\rho_m - \rho_w) \cdot g = 23 \text{ kPa/m}$ with $\rho_m = 3300 \text{ kg/m}^3$ and $\rho_w = 1000 \text{ kg/m}^3$.

In the first step of the model analysis the isostatic equilibrium is computed for the initial model state. Figure 3.3 shows the model in equilibrium at the end of this first analysis step. In the second step, additionally the computation of surface processes is switched on. During the CASQUS analysis, rivers incise the island and transport eroded material to the ocean for a period of 0.9 Ma. Surface processes only act on that part of the island that is not covered by sea water, which also means that there is no sedimentation in the trenches adjacent to the island. River water that drains into the ocean (i.e. that reaches sealevel, see inset of figure 3.3) is removed from the model, likewise the sediment load that is transported to the sea by these rivers. So there is a net loss of material out of the model system.

Time steps of 10 ka are used for the FE analysis, which means that every 10 ka the mechanical model adjusts to the changed weight of the island. That means that the surface processes modeling and the geomechanical computation are synchronized 90 times during the complete analysis. The parameters for the

computation of surface processes within the CASCADE routines are constant and uniform for the complete model region: The surface processes model is iterated with time increments of 100 a, the constant for stream erosion K_f times the net precipitation rate ν_R is $K_f \cdot \nu_R = 0.03 \text{ m/a}$, the diffusion constant $K_s = 0.3 \text{ m}^2/\text{a}$, the alluvial erosion length scale $l_{f,a} = 10 \text{ km}$ and the erosion length scale for bedrock $l_{f,b} = 100 \text{ km}$. These values are taken from Braun and Sambridge [1997].

The topography of the island at the end of the analysis is shown in the inset of figure 3.4. Due to the steep slope of the two coastal regions rivers go straight to the sea. The plateau in the middle shows a local minimum in elevation due to the bending process at the beginning of the analysis and due to the unnatural initial shape of the island. Despite this artificial feature the evolution of the drainage pattern is plausible: Water that flows inland accumulates in the internal drain until it finds a way out. At this place, where one river carries all the water from the inland area, the surface is deeply incised.

During the complete model time of 0.9 Ma, 9.4% of the initial rock volume of the island is transported to the sea, i.e. out of the model. Likewise, the magnitude of the maximum deflection in the middle of the plate decreases by 9.3%, cf. figure 3.4. This corresponds very well to the analytical solution, where the maximum deflection is proportional to the magnitude of a concentrated load [Turcotte and Schubert, 2002]. It also shows that the mechanical response to surface mass redistribution gives a significant uplift signal, here of the order of 0.1 mm/a due to the used surface transport parameters which are chosen based on literature values (see above).

3.2.2 Model B (feedback)

Model B analyzes the influence of flexural rebound to the rate of erosion and the relevance of the numerical parameter *synchronization time*, which is the time increment after which the FE solver and the CASCADE routines sequentially exchange information. We use a model setup that is similar to model A. Here the lithospheric elastic plate has a square layout of 120 km side length³ and a thickness of 11 km. For the discretization $120 \times 120 \times 6 = 86 \times 10^3$ 8-node linear hexahedral elements⁴ are used, which results in a characteristic element length of 1.3 km and 3.1×10^5 degrees of freedom. In the middle of the plate we place a circular symmetric mountain (inset of figure 3.5). All nodes of the model that are located at the upper edges of the plate (black

³As it is not the aim of this model to simulate quantitatively exact flexural behavior we can accept a laterally small-sized elastic plate in order to minimize computation time.

⁴ABAQUSTM element type: C3D8

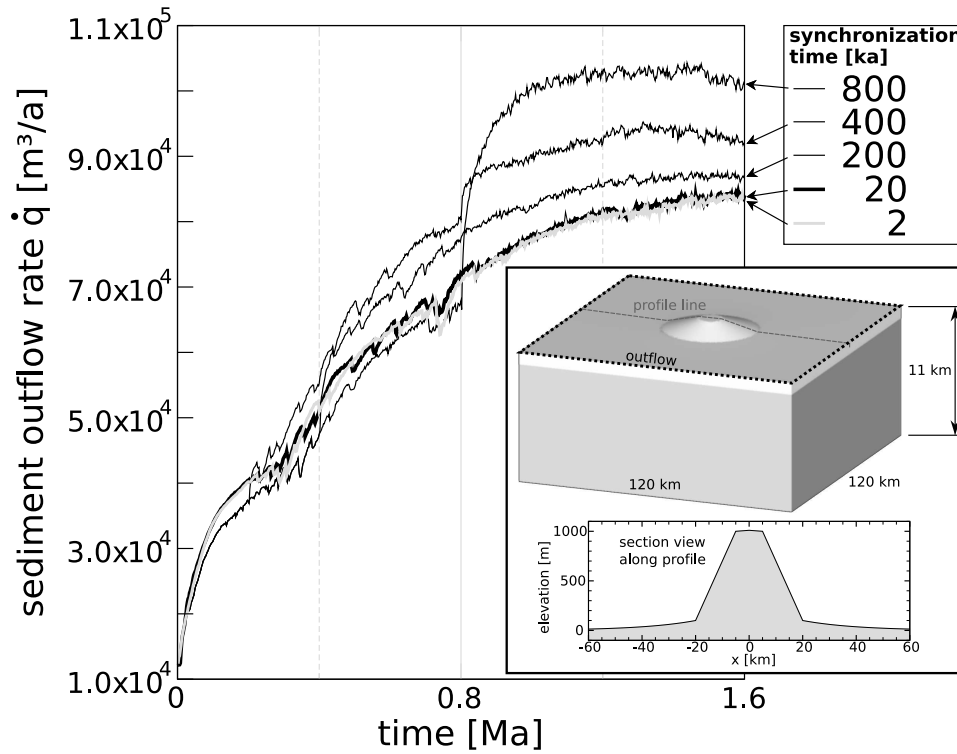


Figure 3.5 – Sediment outflow rate \dot{q} over time for different synchronization times. A synchronization time of 200 ka, e.g., means the computation of surface processes and the geomechanical simulation are synchronized every 200 ka. The topography is steepened while the plate elastically responds to the decreased loading. After synchronization, the surface processes react to the increased mean slope. So in general, after synchronization the outflow rate \dot{q} is increased. Note that this effect is mostly significant for model runs with the greatest synchronization time: Here after 800 ka the deflected elastic plate (that has not moved before) instantaneously springs back upwards due to the large amount of material that has been eroded at the mountain. The smaller the synchronization times are chosen, the smaller these singular effects become. For this model setup, a synchronization time of 20 ka is sufficiently small to suppress these singular effects to the best possible level: Model runs with smaller synchronization times do not show significant changes, cf. the collapse of the 20 ka and the 2 ka curves. **Inset:** Setup of model B, vertically exaggerated. The boundary conditions are the same as in model A (figure 3.3). The rheological parameters are: $E = 20$ GPa and $\rho = 2800$ kg/m^3 for the adaptive mesh domain (white), $E = 70$ GPa and $\rho = 3300$ kg/m^3 for the rest of the plate (gray). $\nu = 0.25$ throughout the model. The initial shape of the circular symmetric mountain topography is shown at the bottom.

dotted lines) are defined as ‘fixed surface nodes’ (cf. figure 3.1). These nodes are not vertically shifted due to surface processes simulated by CASCADE, because they act as outflow zone where water and sediment load leave the model. Yet they can move vertically in the geomechanical analysis performed by ABAQUS/StandardTM; ‘fixed’ only refers to the surface processes computation here. The parameter values for the surface transport processes are equal to the settings used for model A, and the elastic parameters for the FE model are listed in the caption of figure 3.5. The boundary conditions are the same as in model A, with the difference that no ocean is simulated on top of the plate, so the stiffness per unit area for the elastic foundations is just $\rho_m \cdot g = 33 \text{ kPa/m}$.

Just as in model A, the first step of the analysis brings model B to isostatic equilibrium. In the second analysis step, when the CASCADE routines are switched on, 1.6 Ma of coupling between surface mass denudation and isostatic rebound are simulated. The mountain is worn down and sediment is transported out of the model, while the deflected elastic plate springs back.

The synchronization time plays a crucial role in the development of the model during the simulation. After surface processes are simulated for a model time period Δt_s , tectonic processes including the mechanical response to these surface processes are computed for the same model time period Δt_s (figure 3.2). Subsequently, these two steps are repeatedly processed. I.e., after each of these passes a new synchronized model state is reached as a combination of both surface processes modeling and mechanical FE modeling, and the simulation is *not* synchronized in-between these two steps. Accordingly, the interval Δt_s is denoted as synchronization time here. It has to be chosen very carefully. The smaller the model time steps are, i.e., the smaller the synchronization time is, the more accurately the coupling between surface and tectonic processes is simulated. But for a given total model time, the number of analysis steps increases with decreasing synchronization time, and the computation time of an FE analysis generally increases with the number of analysis steps used. This has to be considered for models with a large number of finite elements where computation is time-consuming.

In order to find a reasonable compromise for the synchronization time Δt_s , the outflow rate of sediment material \dot{q} is a characteristic parameter. \dot{q} is the sediment volume transported to the edges of the model per unit time (cf. inset of figure 3.5). It is a measure of the mean erosion rate in the model. Figure 3.5 shows this outflow rate \dot{q} over time for different synchronization times: ‘800 ka’, for example, labels the curve for the model that starts in an a priori synchronized initial state and is only synchronized a second time at $t = 0.8 \text{ Ma}$ (within the complete model time of 1.6 Ma). Directly after synchronization at $t = 0.8 \text{ Ma}$ the outflow rate \dot{q} rapidly increases in this model.

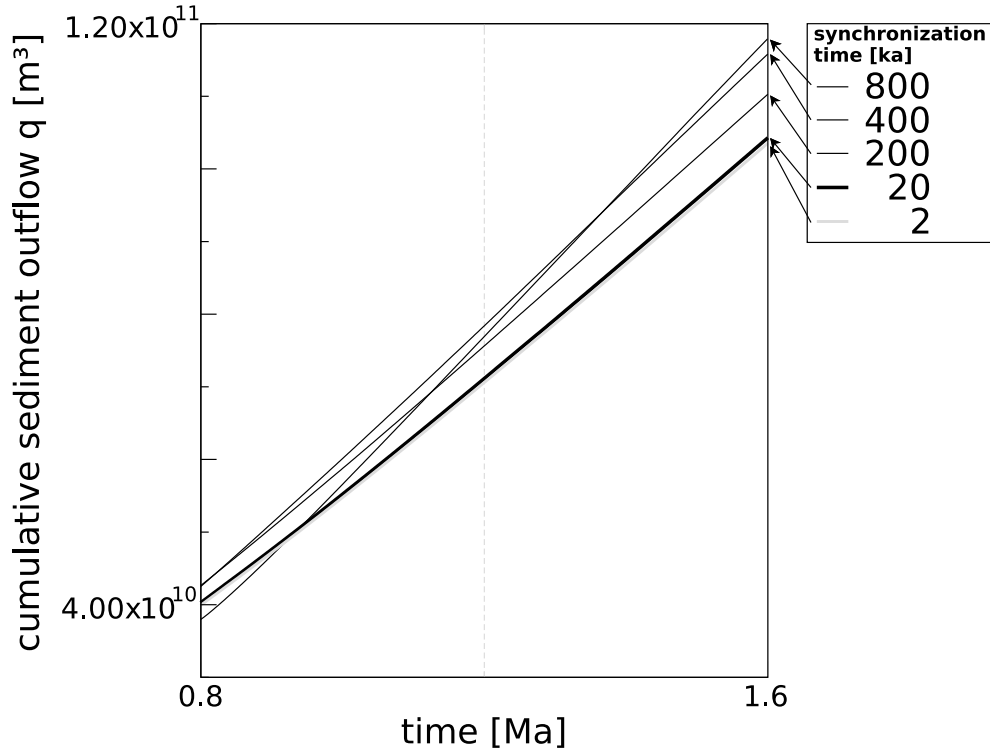


Figure 3.6 – Cumulative sediment outflow $q = \int \dot{q} dt$ over time, for different synchronization times. Only the last 0.8 Ma of the simulation are shown. Note that the difference between the 20 ka and the 2 ka curves is not (significantly) growing, i.e., the absolute, long-time model behavior for these two synchronization times is the same.

The loads acting onto the lithospheric plate significantly decrease before this point in time as a lot of sediment material is removed from the model during 0.8 Ma, without the plate responding to this change. When the plate finally reacts to the changed loading at $t = 0.8$ Ma the maximum deflection of the plate decreases abruptly, associated with a large abrupt increase of the mean slope of the model surface. As slope and the sediment carrying capacity are directly related (cf. equation 2.25), this explains the rapid increase of \dot{q} . After this abrupt change in mean slope, the rivers are far from equilibrium as far as their transport behavior is concerned [Mackin, 1948; Kooi and Beaumont, 1994], and the sediment outflow rate \dot{q} exceeds the curves of the simulation runs with stronger coupling, i.e. with smaller synchronization times. A similar behavior is shown by the curves for the cumulative sediment outflow q in figure 3.6 ($q = \int \dot{q} dt$), which allows a better analysis of the model behavior on longer time scales.

If we iteratively decrease the synchronization time, the curves for both \dot{q} and q show an asymptotic behavior. There is no significant difference between the two models with synchronization times of 20 ka and 2 ka, indicating that a synchronization time of $\Delta t_s = 20$ ka is sufficient for this model example, also on long time scales.

3.3 Discussion

CASQUS enables us to simulate the interaction and feedback mechanism between mechanical deformation within the lithosphere and erosion and sedimentation at the Earth's surface. It allows us to numerically study the long-range redistribution of sediment masses and how the subsurface responds to the changed loading, and – vice versa – how erosion and sedimentation changes due to processes from the interior of the Earth. CASQUS' surface processes routines are taken (with minor modifications) from the academic modeling software CASCADE developed by Braun and Sambridge [1997]. Yet these routines can be replaced by code from similar surface processes models to address particular problems. The *essential* part of CASQUS is the interface to the FE program ABAQUS/StandardTM that makes a simulation of surface processes within ABAQUSTM possible and introduces the feedback mechanism.

The two benchmark models presented in this paper demonstrated that CASQUS is able to appropriately simulate the coupling process. For this feedback the synchronization time between the surface processes modeling and the tectonic simulation is an important numerical parameter. We have shown a way to assess the minimum number of synchronization steps (i.e. the maximum synchronization time) needed for a particular model. This number depends on many properties of the model, including the 3D geometric setup, the geomechanical material behavior and the surface transport parameters. Generally speaking, the minimum number of synchronization steps needed will decrease for models with a stiffer behavior of the subsurface, for example due to a higher effective elastic thickness. It will also decrease if less sediment is transported, for example due to a lower precipitation rate. The opposite holds true as well.

The manner in which the mean erosion rate in a model is determined by the synchronization time also shows how sensitive the feedback between erosion/sedimentation and tectonic processes is. Both types of processes cannot be studied independently on geological time scales in a proper way; understanding their coupling is essential for understanding both surface evolution and tectonic deformations.

Due to its design and architecture our new coupled simulation tool CASQUS has some limitations, but also some advantages compared to other coupled landscape evolution models:

3.3.1 Limitations

It must be well considered whether using CASQUS is reasonable for the type of problem to be solved. Due to its design based on the FE method in 3D computation times are significantly longer than those of other landscape evolution models. For example, computation times for the benchmark model B are 1.3h for a synchronization time of 800 ka and 15 h for 20 ka, on an IntelTM PentiumTM 4 CPU with 3.20GHz. CASQUS is intrinsically designed for problems where the focus is on a proper model representation of a geometrically complex three-dimensional subsurface.

ABAQUS/StandardTM by default uses a Lagrangian formulation for the mechanical FE computation (section 2.3.1). Therefore, by default CASQUS cannot perform simulations over very long model time scales because this will generally lead to severe distortions of the finite elements if deformation rates are not negligible. Consequently, in order to simulate an orogenesis for several million years, for example, the simulation needs to be split in several separate FE model runs to be run consecutively. The model is then re-meshed in-between the model runs to maintain a suitable FE mesh, and results are mapped from the end of one run to the initial state of the next model run. I.e., the necessary remeshing interrupts the non-interactive analysis and requires user input. Another possibility to circumvent excessive FE mesh distortions is the use of the Arbitrary Lagrangian-Eulerian adaptive meshing technique for the whole subsurface model.

Another limitation is that the original CASCADE routines which are used for the provided CASQUS version model only fluvial and hillslope processes in order to simulate erosion and sedimentation. Regions where other types of surface processes prevail are not appropriately simulated without modifications. But this limitation can be overcome by replacing the CASCADE routines by code that is provided by the user and adjusted to the particular problem, for example to simulate glacial or aeolian surface processes.

3.3.2 Capabilities

CASQUS removes some limitations of previous landscape evolution models concerning the complexity of the subsurface. With CASQUS the ability of

CASCADE to simulate surface processes on geological time scales and regional spatial scales is combined with the ability of ABAQUS/StandardTM to simulate truly three-dimensional geomechanical models with tectonic structures of arbitrary geometrical shape, different rheologies, distributed material properties and features like faults with Coulomb friction. Various authors have published the results of such intricate 3D models analyzed by ABAQUSTM [e.g.: Fischer, 2006; Morra and Regenauer-Lieb, 2006; Steffen et al., 2006; Buchmann and Connolly, 2007; Masterlark, 2007; Westerhaus et al., 2008; Schotman et al., In Press]. CASQUS provides more capabilities with regard to the geomechanical behavior of the subsurface and the shape of subsurface structures than other existing landscape evolution models. With a view to simulating natural regions of the Earth our sequentially coupled 3D modeling technique has the potential to provide new insights into the feedback mechanism between tectonic and surface processes. This includes, for example, the effects of viscosity, temperature-dependent material properties, and heterogeneous tectonic boundary conditions for the quantification of vertical crustal displacement rates.

Chapter 4

Feedback process study

This chapter is devoted to the question to what extent fluvial erosion and sedimentation is able to contribute to vertical crustal displacement rates. For this, maximum bounds on vertical crustal displacement rates that are generated solely by the isostatic response to fluvial mass redistribution will be estimated.

4.1 Impact of isostatic tectonic response

The feedback mechanism between tectonic and surface processes leading to vertical crustal displacements will be studied in the following. The software CASQUS is used to numerically analyze the effects of flexural isostasy on the coupling between surface processes and tectonic response due to erosional mass redistribution. Two different numerical models will be analyzed and compared with each other: (1) Model A considers only surface processes and no mechanical response of the subsurface. (2) Model B is a Finite Element model that also includes the mechanical response of an elastic lithosphere in combination with isostatic compensation, i.e., flexural/regional isostasy is simulated.

Both models start with the same topography, divided by an escarpment into a high plateau and a low plane foreland. The evolution of a river network is simulated on top of this initial topography. While rivers evolve during model time, they erode the plateau, and canyons incise the escarpment. The mass of rock that is thereby ablated is transported by the rivers as sediment load to the lowlands. There it is either deposited or further transported out of the model. The impact of the isostatic tectonic response to this mass redistribution at the

model surface is quantified both for (1) crustal uplift rates and (2) erosion rates. As these models are aimed at estimating upper bounds for crustal uplift rates that can be generated by fluvial erosion, a model setup with an extremely small effective elastic thickness, i.e. with a small flexural rigidity, is chosen. For the same reason, viscous behavior of the subsurface is not considered, as in general this would dampen subsurface movements, i.e., it would decrease crustal uplift rates.

4.2 Model setup

The geometric FE model setup of model B before isostatic compensation is illustrated as a side view in figure 4.1. Note the surface topography where the mountain range on the left will become a high plateau limited by an escarpment *after* isostatic compensation. Little noise in elevation is added to the smooth topography to allow river networks to develop. The crust and the lithospheric mantle are implemented as isotropic homogeneous linear elastic layers; the elastic parameters are given in figure 4.1. Winkler foundations at the bottom of the lithospheric mantle mimic the isostatic buoyancy of the asthenosphere. Their stiffness per unit area is $\rho_m \cdot g \cong 31 \times 10^3 \text{ Pa/m}$ with $\rho_m = 3200 \text{ kg/m}^3$ and $g = 9.8 \text{ m/s}^2$.

Here the concept of a symmetrical model setup is used, where only one half of a symmetrical topographic profile of a mountain range is modeled. The vertical left boundary of the model shown in figure 4.1 can be imagined as the axis of symmetry, and a vertically mirrored image of the shown 200 km long lithospheric plate is considered to exist to the left of the model. Because the very left point of the shown topography is the highest point, this point is considered to be the watershed between the two river networks that evolve on the shown model part and on the mirrored model part that is not shown. Like all side faces, the left vertical model boundary is fixed in normal direction. The reaction forces that act at this side mimic the mechanical effect of the mirrored part of the plate that is not shown. Due to this symmetry in both surface river network evolution and mechanical behavior of the subsurface, it is sufficient to model only the right half of the imaginary symmetrical 400 km long lithospheric plate in order to save computation time.

The 200 km long model cross section as shown in figure 4.1 is extruded by 100 km in Y direction, and so the complete 3D model dimensions are $200 \times 100 \times 18 \text{ km}^3$. It is discretized by 8-node linear hexahedral elements¹ with an

¹ABAQUS™ element type: C3D8

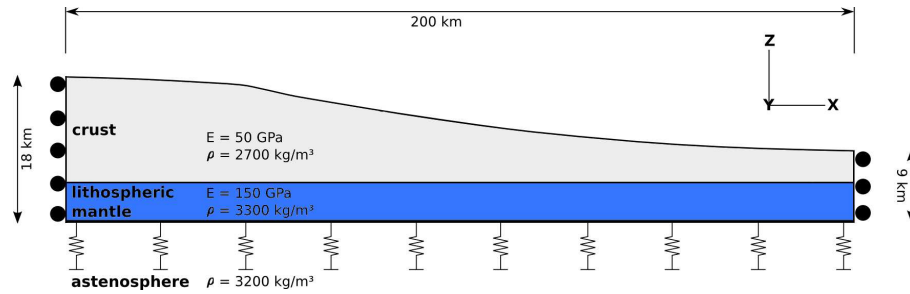


Figure 4.1 – Setup of the FE model (model B) for the feedback process study, shown as a $2\times$ vertically exaggerated side view of the 3D model. Young’s modulus E and density ρ for the elastic crust and the elastic lithospheric mantle are shown in the figure; Poisson’s ratio $\nu = 0.25$ for the complete lithosphere. The elastic model is supported by Winkler foundations that mimic the isostatic buoyancy forces generated by the underlying asthenosphere (indicated by the springs). The vertical side boundary faces are fixed in normal direction (indicated by the rollers). The model as shown here is extruded by 100 km perpendicular to the viewing plane (in Y direction).

average horizontal element edge length of 1.25 km, see figure 4.2. That means that 160×80 nodes discretize the surface topography in the model.

Once gravity is switched on in model B, internal compaction of the lithospheric material occurs. Additionally, the plate bends to compensate the gravitational load of the mountain range by flexural isostasy (figure 4.2 top). Bending stresses and the isostatic buoyancy forces now keep the model in mechanical equilibrium. This model state is the initial state for model B, and this state also defines the initial topography for model A which only simulates surface processes without tectonic response.

Then, based on this initial setup, CASQUS starts the computation of surface processes, both for model A and for model B. Water is precipitated onto the model surface, eroding material in the mountain range and transporting sediment load to lower ground, thereby establishing river networks. When river water and sediment load reach the right edge of the model that marks the line of lowest surface elevation, they are transported out of the model (figure 4.2 bottom). I.e., conservation of mass does not hold here for the complete model. The mean precipitation rate is uniformly distributed over the model. The surface transport parameters according to equations 2.25, 2.26, and 2.27 are identical for model A and model B: Stream erosion times net precipitation rate $K_f \cdot \nu_R = 0.3 \text{ m/a}$, diffusion constant $K_s = 3.0 \text{ m}^2/\text{a}$, alluvial erosion length scale $l_{f,a} = 10 \text{ km}$ and for bedrock $l_{f,b} = 100 \text{ km}$. These input parameters are within realistic bounds considering characteristics of natural river systems [Braun and Sambridge, 1997; van der Beek and Braun, 1998], and the abso-

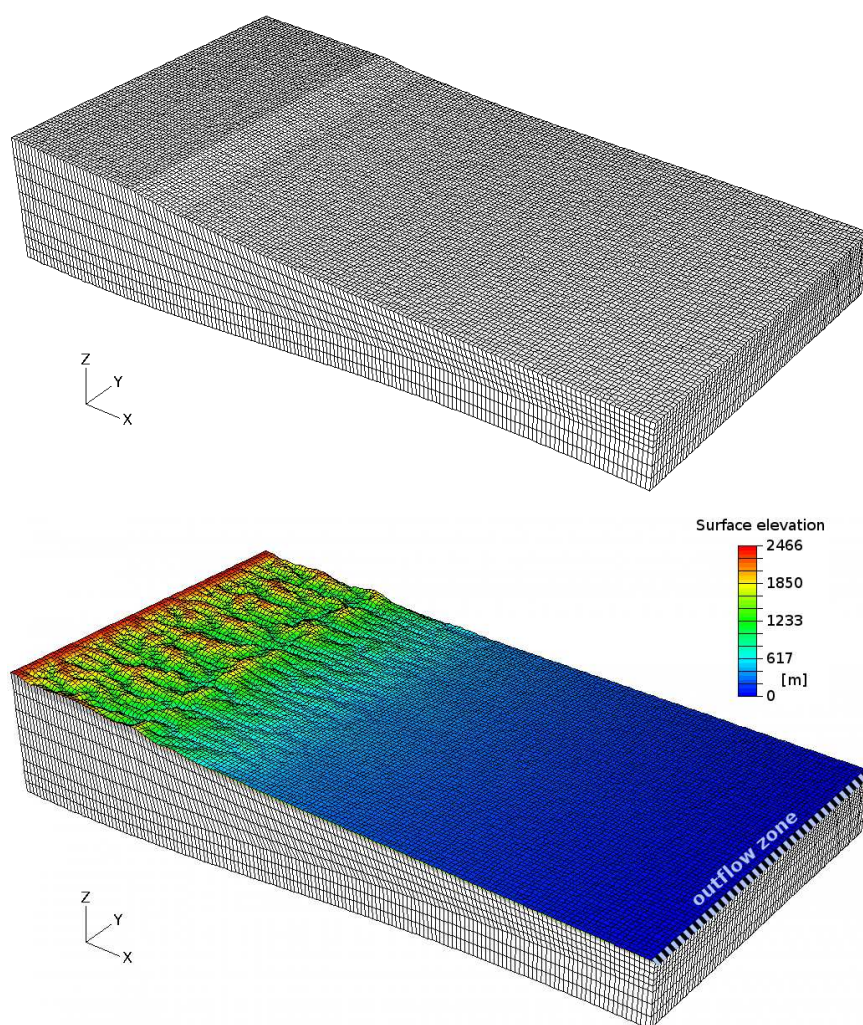


Figure 4.2 – Finite Element model (model B) in isostatic equilibrium ($2\times$ vertically exaggerated). Gravitational loads are compensated by buoyancy and bending stresses. **(top)** FE mesh at the initial model state. **(bottom)** Erosion and sedimentation processes have generated a river network at the surface.

lute values of $K_f \cdot \nu_R$ and K_s are around the same (high) values that will be determined for the SE Carpathian region in the next chapter.

The numerical surface processes computation is iterated with time steps of 5 a for model A and for model B. The complete model time for both models is 320 ka. For model B, the surface processes computation is synchronized with the geomechanical subsurface simulation $80\times$ during the complete model time, i.e., 4 ka is the synchronization time for model B. This is tested to be sufficient, as a smaller synchronization time of 750 a does not result in significant changes for the evolution of model B (figure 4.5).

4.3 Results and discussion

The differences in the results of model A and model B identify the impact of isostatic tectonic response to fluvial mass redistribution. Model A only simulates surface processes, whereas mechanical coupling between the subsurface and the surface is suppressed, i.e., there is no crustal uplift or subsidence. For model B, the feedback between tectonic and surface processes is active.

4.3.1 Impact of isostasy on erosion and sedimentation rates

The landforms and the course of the rivers that have evolved after the complete model time of 320 ka differ only slightly between model A and B, cf. figure 4.3. This is as expected because the initial artificial noise in topography (which is the same for both models) defines the pattern of the evolving river network. However, significant differences of the maximum elevations within the mountains can be observed. Peak elevations in model B are increased by several 100 m compared to those found in model A, because the mountains in model B are significantly uplifted due to the isostatic response to erosion. This will be discussed in the following subsection.

Crustal uplift within the mountain region also increases the erosion rates found there which are around 2 mm/a (figure 4.4). Because crustal uplift compensates the flattening due to erosion to a large extent, the mean slope in topography is increased for model B compared to model A. Consequently, fluvial erosion rates that are controlled by slope (equations 2.25 and 2.26) are higher for model B than for model A, cf. figure 4.4. As a consequence to the increased erosion, sedimentation rates in the foreland are also higher for model B than for model A.

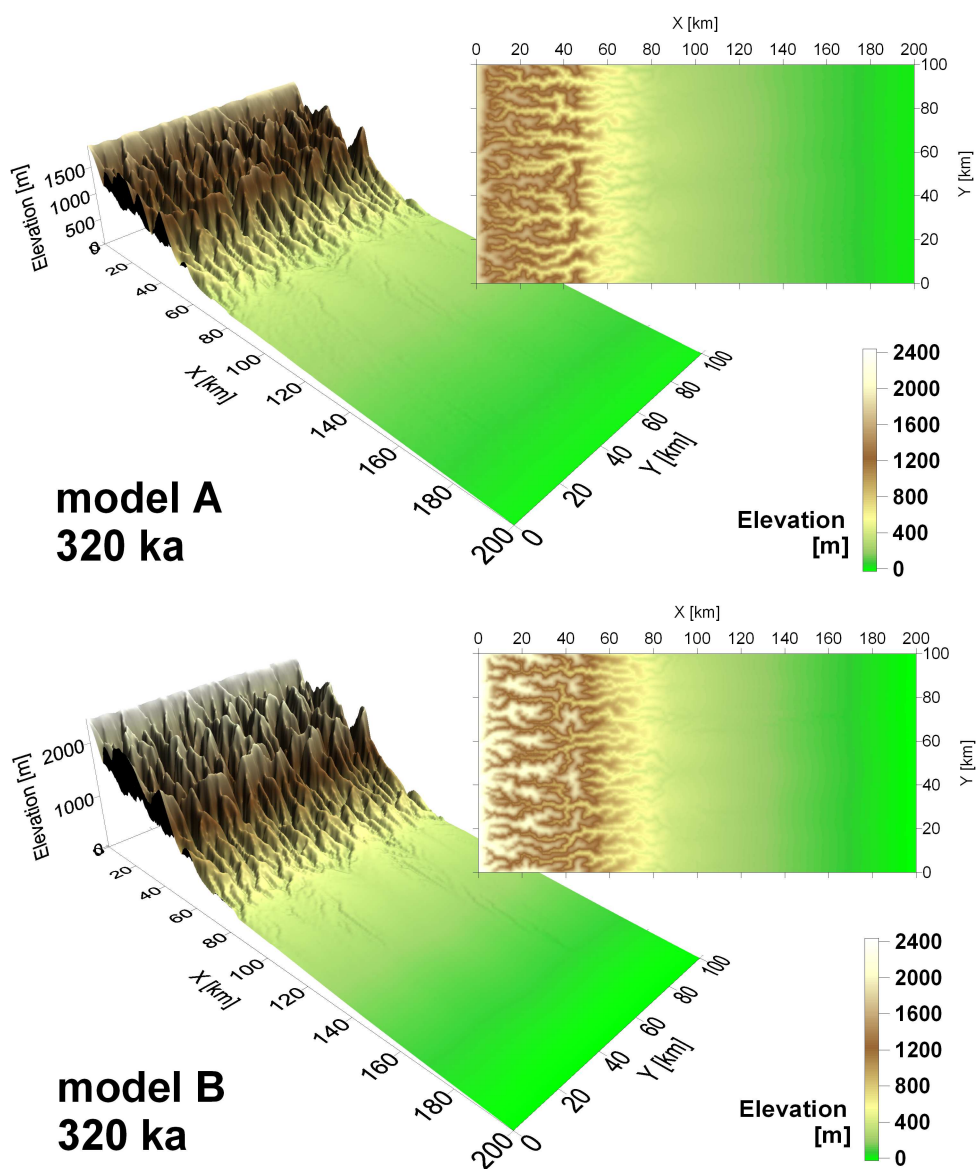


Figure 4.3 – Topography after 320 ka of surface processes computation, **(top)** without tectonic response, **(bottom)** with isostatic response of the subsurface. Note the increased maximum elevation for model B resulting from the isostatic response to erosion in the mountain range.

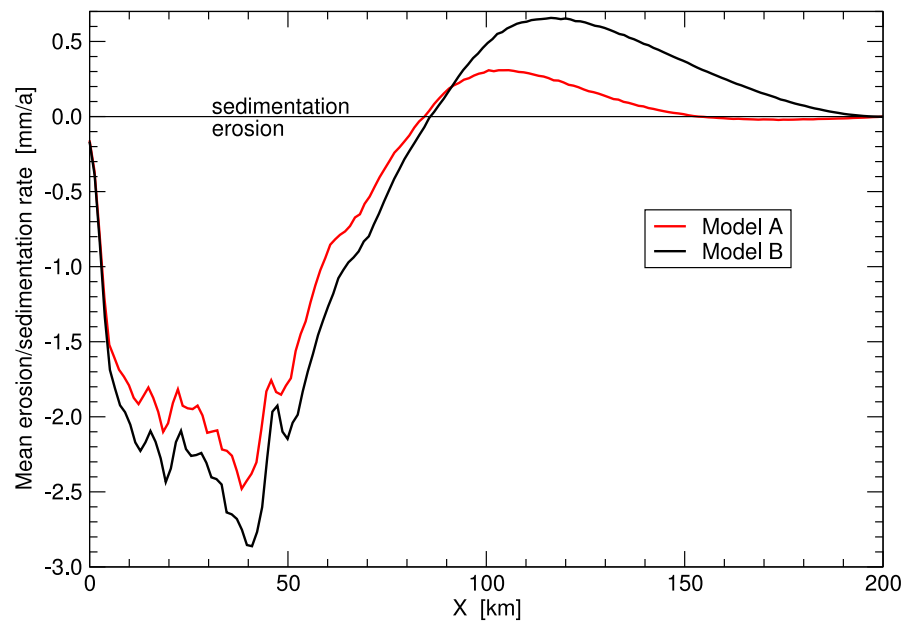


Figure 4.4 – Mean erosion and sedimentation rates for the model without tectonic response (A) and the one with isostatic response of the subsurface (B). Values are averaged over Y and over the complete model time of 320 ka.

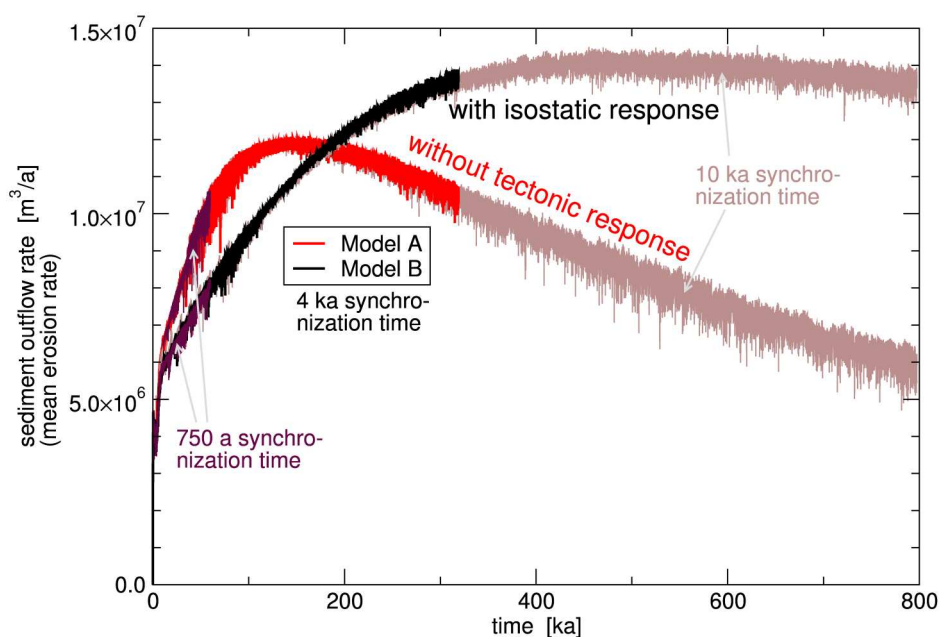


Figure 4.5 – Sediment outflow rate over model time (as a measure of mean erosion rate), for the model without tectonic response (A) and the model with isostatic response of the subsurface (B). Sediment outflow rate is the sediment volume per unit time that is transported out of the model via the outflow zone, cf. figure 4.2. At the beginning, the sediment outflow rate increases while river profiles continuously come closer to a shape that allows maximum sediment transport. The development of this most efficient river profile is disturbed by crustal uplift in model B, and thus the sediment outflow rate in model B is not increasing as fast as in model A. After the maximum sediment outflow rate has reached, the rate only slightly decreases for model B, whereas the rate significantly decreases for model A because the topography is flattened much faster without isostatic response. Both models are also analyzed for synchronization times of 750 a and 10 ka, as shown in the figure, in order to make sure that the used synchronization time of 4 ka (light red and dark black curves) is sufficiently small.

The outflow rate of sediment material that is transported out of the model is shown in figure 4.5 for both models. This rate is a measure of the mean erosion rate in the model. The clear differences between the curves for model A and B also show the influence of isostasy on erosion.

For the first 200 ka, the mean erosion rate for model A exceeds the one for model B. According to the “concept of the graded river” [Mackin, 1948], streams tend towards a stable concave longitudinal profile with a downstream decreasing slope. Graded streams are in equilibrium with uplift, erosion and deposition, and a graded river profile is the most efficient profile for river flow and sediment transport. The first 200 ka are interpreted to be dominated by the effect that river profiles in model A are closer to the state of a graded river than those in model B, because the profiles in model B are continuously disturbed by crustal uplift.

After around 200 ka, sediment outflow rates for model A are decreasing much faster than those for model B. For model A, this period is dominated by the flattening of topography due to erosion, whereas in model B crustal uplift counteracts erosion with regard to topographic elevation. Thus in model A mean slope is decreasing constantly, associated with a constantly decreasing mean erosion rate. In contrast, in model B the mean erosion rate stays nearly constant as crustal uplift compensates the flattening due to erosion almost completely.

These differences clearly show the influence that tectonic processes exert on surface processes.

4.3.2 Impact of isostasy on vertical crustal displacement rates

The evolution of model B which considers the response of the subsurface to the long-range mass redistribution by the evolving rivers is shown in figure 4.6. The elastic deflection of the simulated lithospheric plate is controlled by the gravitational loads that are changed by surface mass redistribution. As expected, the lithosphere is uplifted below the mountain range where erosion takes place and rock material is removed. This material is deposited as sediments in the lower plane foreland, where the plate subsides.

The resulting crustal uplift rates for model B are shown in figure 4.7. They are up to 1.7 mm/a, averaged over 320 ka model time. So crustal uplift rates nearly reach the values for maximum erosion rates of (2...3) mm/a found within the mountain range. Because the foreland is not a basin but a plane area and thus

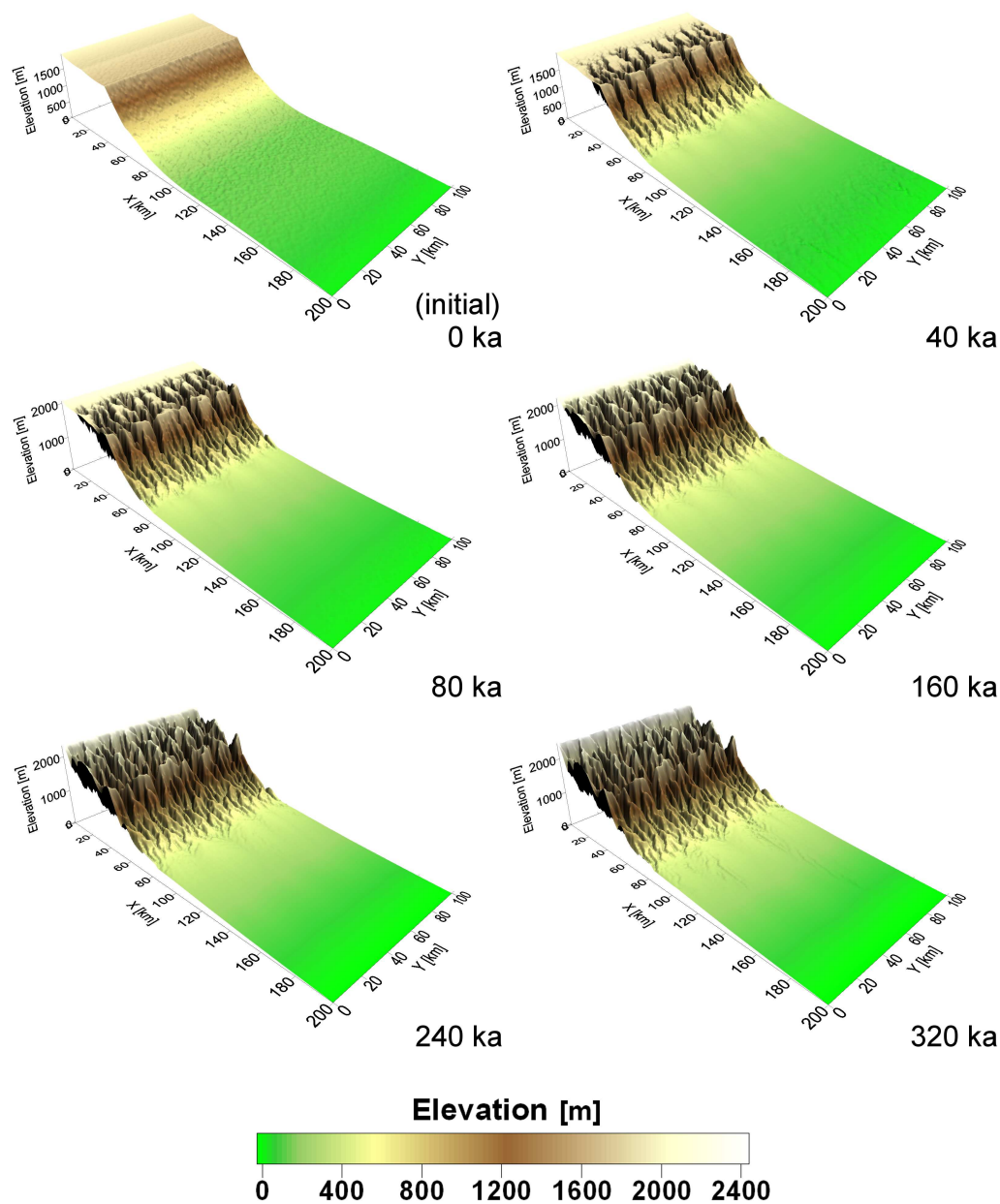


Figure 4.6 – Topographic evolution of the FE model (model B) with time. The escarpment is incised by canyons that evolve where major rivers drain into the foreland. Note that the maximum elevation of mountain peaks rises while the lithosphere is uplifted.

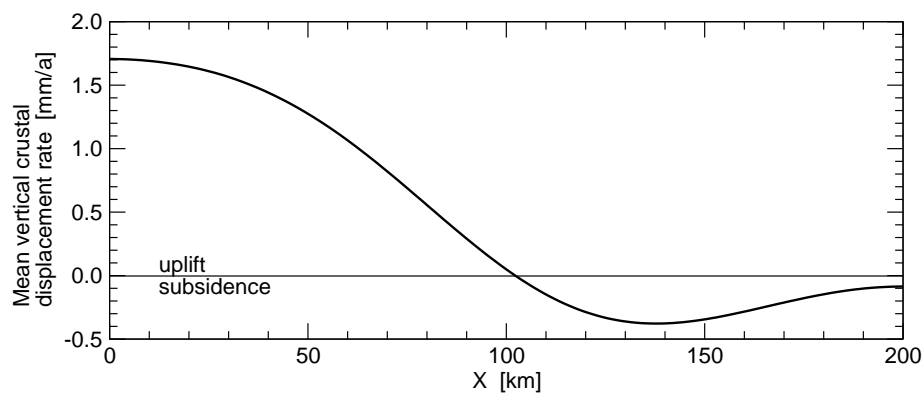


Figure 4.7 – Mean crustal uplift and subsidence rates for model B. Values are averaged over Y and over the complete model time of 320 ka.

the sedimentation rates found there are significantly smaller than the erosion rates in the mountains, subsidence rates in the foreland are also significantly smaller than the uplift rates in the mountains.

For this feedback model, a perfect elastic plate with a very small thickness is chosen as model representation of the lithosphere, and input parameters for the surface processes computation are chosen which correspond to high precipitation rates considering a plateau with an elevation of 2 km. Thus, the maximum crustal uplift rates resulting from the simulation of the feedback between tectonic and surface processes are estimated to be an approximate upper bound for the rates found in nature.

As a conclusion, maximum vertical crustal displacement rates that are induced by fluvial mass redistribution at the Earth's surface can reach orders of few mm/a.

Chapter 5

Contribution of surface processes to vertical displacement rates in the SE Carpathian region

The Vrancea region in the SE Carpathians of Romania is one of the rare places on Earth where the process of slab break-off after subduction can be studied, when continental collision has ended and when the previously subducted lithosphere finally detaches from the overriding plate and begins to sink deeper into the mantle [Fuchs et al., 1979; Linzer, 1996; Gvirtzman, 2002; Houseman and Gemmer, 2007; Lister et al., 2008]. Besides the Bucaramanga region in Colombia and the Hindu Kush region in Afghanistan, the Vrancea region belongs to the only three well-known intermediate-depth earthquake nests where the seismicity is concentrated in a small volume, located in an old subducted slab [Zarifi and Havskov, 2003]. Unlike at plate boundaries with ongoing convergence or at active transform plate boundaries such as the San Andreas Fault or the North Anatolian Fault system, here lateral crustal displacement rates are minor and exceeded by the vertical displacement rates that are an important indicator for processes occurring in depth [Schmitt et al., 2007].

In particular, vertical crustal displacement rates are used to discuss whether the lithospheric slab beneath Vrancea is still coupled to the crust or whether it has already completely detached. High subsidence rates in the Vrancea region that can only be explained by deep tectonic processes would be an indicator that the slab still pulls down the crust. Knowledge about the degree of attachment between the slab and the crust is important because this slab-

crust coupling controls the transfer of tectonic stresses from and into the crust and thus has a major impact on possible earthquakes.

5.1 Background

In the years 1940–1990, Romania was shaken by a sequence of five strong earthquakes with moment magnitudes $M_w \geq 6.8$ ¹ [Oncescu et al., 1999], cf. figures 5.1 and 5.2. They also struck the Romanian capital city Bucharest that is on the list of the ten largest cities in Europe, populated by about two million inhabitants. Due to this impact, the area where those frequent and strong earthquakes occur at intermediate depth, namely the Vrancea region located in the bend zone of the SE Carpathians, is subject of recent geoscientific research [Oncescu and Bonjer, 1997; Wenzel et al., 1999, 2002]. Particularly the possibility of stress transfer from and into the crust from a coupled slab is an open question and is still discussed.

5.1.1 Seismicity in Romania

The hypocenters of sub-crustal earthquakes in Romania are all concentrated at intermediate depths between 70 km and 180 km within a confined seismogenic volume with lateral dimensions of $25 \times 55 \text{ km}^2$ [Zarifi and Havskov, 2003]², see figure 5.1. Its position coincides with the location of subducted lithosphere within the mantle, observed as a high-velocity body by seismic tomography [Wortel and Spakman, 2000; Martin et al., 2006], cf. figures 5.1 and 5.2. This high-velocity body beneath Vrancea extends today to a depth of more than 350 km. Its shape indicates a lateral tear-off of the vertically dipping subduction slab starting from its SW edge in a depth of about 170 km. The two parts above and below this disruption are distorted against each other (figure 5.2). The intermediate-depth earthquakes occur where those two parts of the slab are still connected, in the NE part of the slab [Heidbach et al., 2007a]. As earthquakes occur spatially distributed over the whole seismogenic volume within the cold core of the subducted lithosphere, a Wadati-Benioff zone cannot explain sub-crustal seismicity in the Vrancea region. It is assumed that these seismic events are triggered by slab pull forces as most extension axes from earthquake focal mechanism solutions are vertical [Radulian et al., 2000].

¹up to $M_w = 7.7$ in 1940

² $M_w \geq 5$ earthquakes are concentrated in (60...170) km depth according to Oncescu et al. [1999].

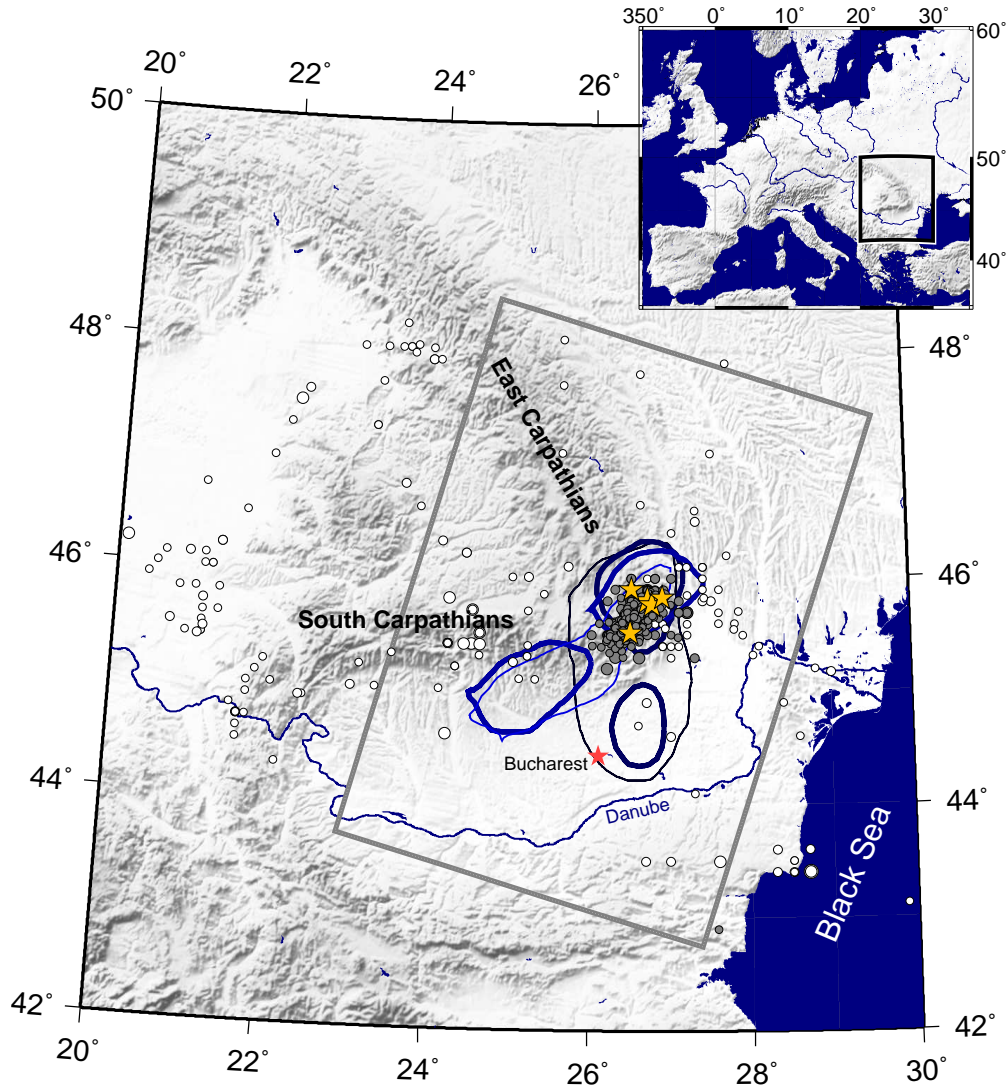


Figure 5.1 – Epicenters of recent and historical earthquakes in the region around the SE Carpathians. Only earthquakes with moment magnitudes $M_w \geq 4.0$ are plotted, crustal earthquakes (with depths ≤ 60 km) as white circles, and deeper earthquakes as gray circles, where the five $M_w \geq 6.8$ earthquakes during 1940–1990 are indicated by yellow stars. Additionally, the +2.2% isoline of the P-wave velocity anomaly is plotted for different depths (100 km: thin blue line, 150 km: thick blue line, 200 km: thick dark blue line, 250 km: thin dark line), cf. figure 5.2. Note the strong concentration of sub-crustal earthquakes within the anomaly. Earthquake data is taken from the continuously updated Romanian Earthquake Catalogue ROMPLUS^a [Onescu et al., 1999], version 2007-02-10 including events of the years 984–2006. P-wave tomography data is taken from Martin et al. [2006]. Map in UTM projection, zone 35.

^a <http://www.infp.ro/catal.php>

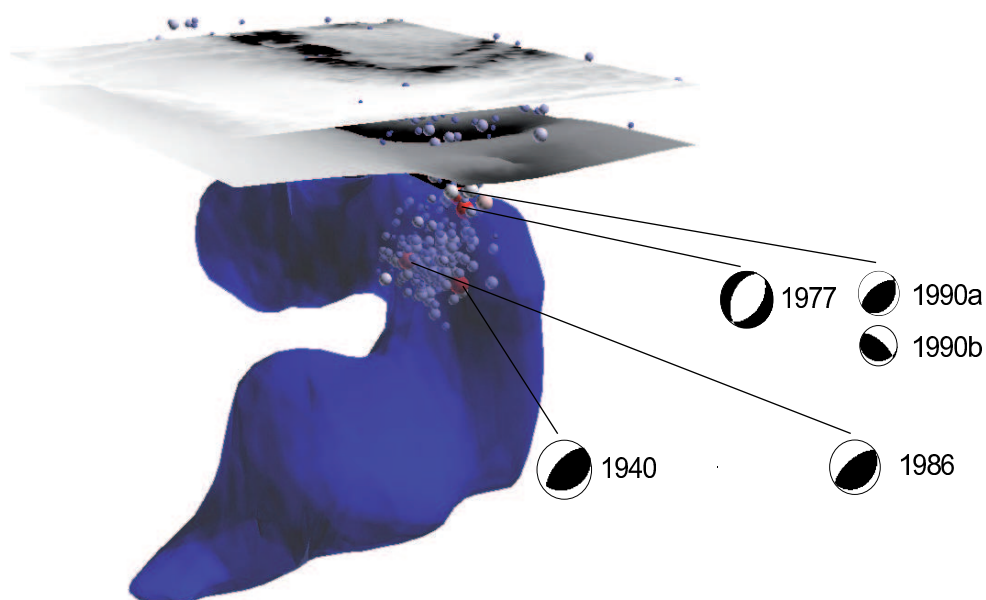


Figure 5.2 – +2.2% isosurface of P-wave velocity anomaly beneath Vrancea, from seismic tomography [Martin et al., 2006]. Perspective view from above in NW direction. Earthquake hypocenter locations are plotted as spheres, strong earthquakes in red. Beachballs of the focal mechanism solutions apply relative to map view, the compressional quadrant is plotted in black. Additionally, surface topography and Moho are plotted. Note the lateral disruption in the middle of the high-velocity body, and the concentration of intermediate-depth earthquakes within the body at the same depth. From Heidbach et al. [2007a].

5.1.2 Tectonic situation in the SE Carpathian region

The Neogene tectonic evolution of the Carpathian region is dominated by a subduction process starting during the late Cretaceous when the intra-Carpathian blocks including the Tisia-Dacia block moved N(W)-ward, cf. figure 5.3. An oceanic embayment in the European foreland provided additional space for the NE- and E-wards movement of the intra-Carpathian blocks [Sperner et al., 2004]. In the Miocene, continental collision in the Carpathians first took place in the western part (18 Ma). Then it shifted to the north, where continental collision of the Tisia-Dacia block with the European foreland started in the Badenian (13 Ma). At the same time, subduction was still continuing in the eastern part of the Carpathian arc, until subduction finally stopped completely in this region when continental collision reached the SE Carpathians (9 Ma) [Sperner et al., 2004]. Before, at around 12 Ma (Sarmatian), the dip direction of the subducting lithospheric slab had changed from W to NW while the retreat of the subduction zone had changed from a NE- to an E-ward direction [Csontos, 1995], see figure 5.3.

Today's tectonic situation in the SE corner of the Carpathian Mountains represents the final and short-lived stage of a ceased subduction, dominated by postcollisional processes like slab detachment and break-off [Fuchs et al., 1979; Linzer, 1996; Gvirtzman, 2002; Houseman and Gemmer, 2007; Lister et al., 2008]. The degree of attachment between the slab and today's crust, as resulting from the tectonic evolution of the area, is under controversial discussion [Girbacea and Frisch, 1998; Girbacea et al., 1998; Girbacea and Frisch, 1999; Sperner et al., 2001; Matenco et al., 2003; Cloetingh et al., 2004; Sperner et al., 2004; Matenco et al., 2007]. A slab that is attached to the crust could be expected due to the subsidence of the Focsani Basin in the Vrancea region [Bertotti et al., 2003; Matenco et al., 2007; Schmitt et al., 2007], cf. figure 5.4. Gvirtzman [2002] proposes that the cold mantle body under the SE Carpathians is already partly detached from the overriding lithosphere, but still viscously coupled to it. On the other hand, both the heterogeneous crustal stress pattern found in Romania and the low seismic velocity zone found between the Moho and the high-velocity body beneath Vrancea indicate that the slab-crust coupling is very weak or not longer existing, which means that the slab has probably detached on its complete width from today's crust [Hauser et al., 2007; Heidbach et al., 2007b; Müller et al., Subm.]. If the latter holds true, an important question is whether present-day vertical crustal displacement rates are controlled by a rebound process induced by the slab detachment, or whether the rebound has already finished in the past. Postseismic relaxation or lateral tectonic activity may also contribute to recent displacement rates.

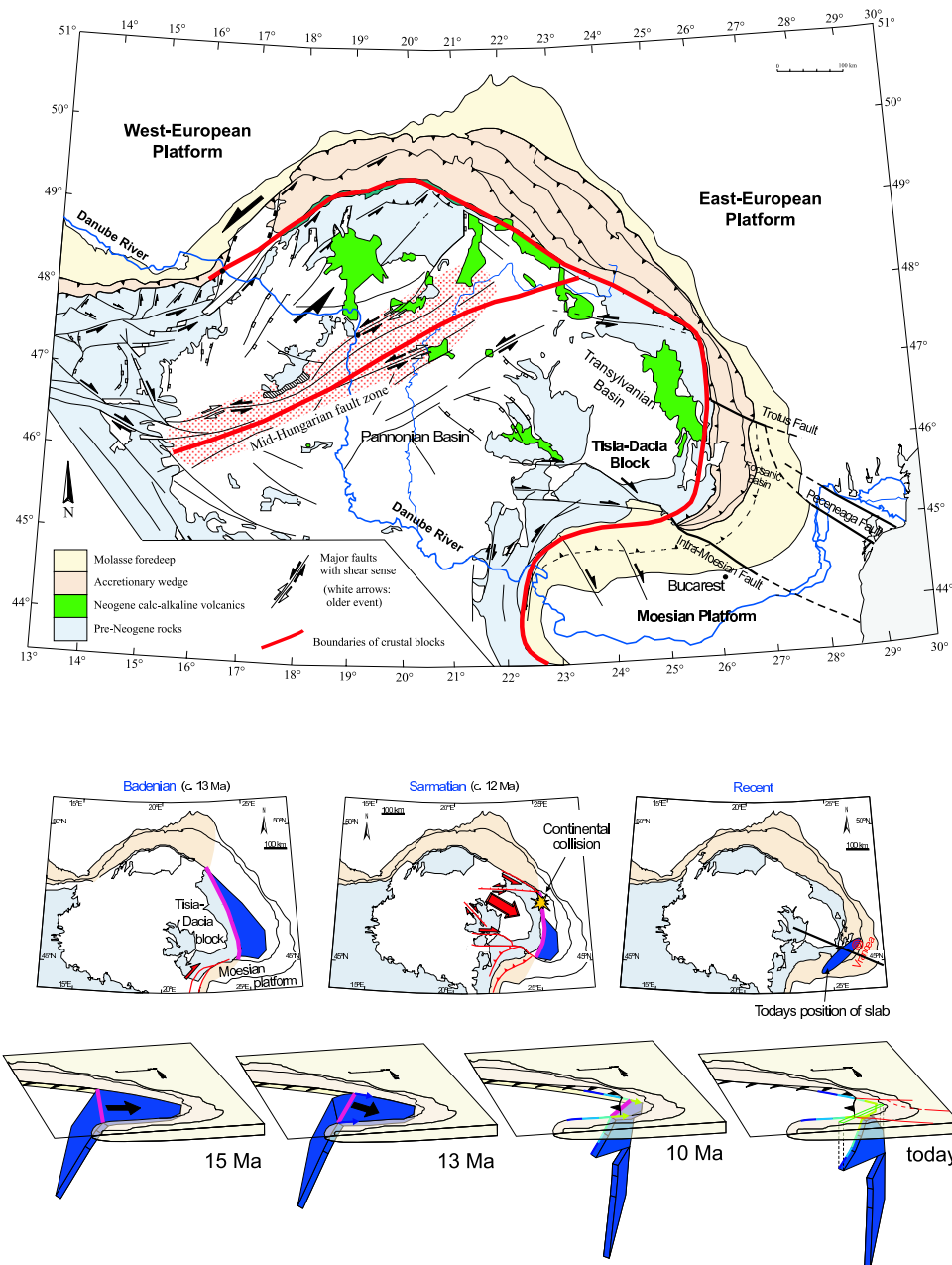


Figure 5.3 – (top) Tectonic map of the Carpathian-Pannonian region showing Tertiary–Quaternary structures, after Sperner et al. [2004] and Sperner and the CRC 461 team [2005], with geology based on Horvath [1993]. **(bottom)** Miocene–Recent tectonic evolution of the SE Carpathians after Sperner and the CRC 461 team [2005] based on Sperner et al. [1999], showing the subduction of the lithosphere (blue). The direction of subduction changes at around 12 Ma before present (Sarmatian) from W to NW, which has probably initiated the lateral tear-off of the subduction slab. Note the retreat of the subduction zone indicated by the black arrow.

In order to investigate the different tectonic scenarios for the present state of subduction and slab break-off beneath Vrancea, vertical crustal displacement rates are important constraints. Concerning strong earthquakes in Romania, a better understanding of the degree of coupling between the crust and the subducting lithospheric slab will lead to an improved estimation of seismic hazard in that region. However, before vertical crustal displacement rates can be used to draw conclusions about the tectonic processes in the interior of the Earth, observed rates have to be corrected for effects due to surface processes. This chapter will quantify to which extent observed vertical displacement rates in the SE Carpathian region are affected by mass redistribution due to fluvial erosion and sedimentation.

5.1.3 Observed vertical displacement rates

In the following two subsections, observed data of vertical displacement rates will be presented that gives information about two different time scales: contemporary data from GPS observations as an average value over the last decade, and geomorphological data as long-term average values over (10...100) ka for different time spans during the last (100...200) ka.

GPS data

Figure 5.4 shows vertical displacement rates from GPS observations using a network of roughly 50 stations in Romania. The GPS network was established in the framework of the CRC 461 in cooperation with the geodetic working group of ISES³ at the Department of Earth Observation and Space Systems of Delft University of Technology [Nuckelt et al., 2005; van der Hoeven et al., 2005]. Station velocities are estimated using observations of 15 GPS field campaigns in the years 1997–2006 [Nuckelt, 2007; Schmitt et al., 2007]. The fact that the results are not derived from permanent GPS stations, but from field campaign measurements, gives an explanation why standard deviations are significantly large, cf. figure 5.4. For several stations, even the sign of the vertical displacement rate measured by GPS is not savely determined.

The pattern of uplift and subsidence from GPS indicates strong short-range fluctuations in the SE Carpathian region. Whereas GPS stations located in the Focsani Basin show subsidence as expected [Bertotti et al., 2003; Matenco et al., 2007], and most stations in the Carpathian Mountains show uplift, stations in other parts of the region show unexpected signs in the vertical GPS

³Netherlands Research Centre for Integrated Solid Earth Science

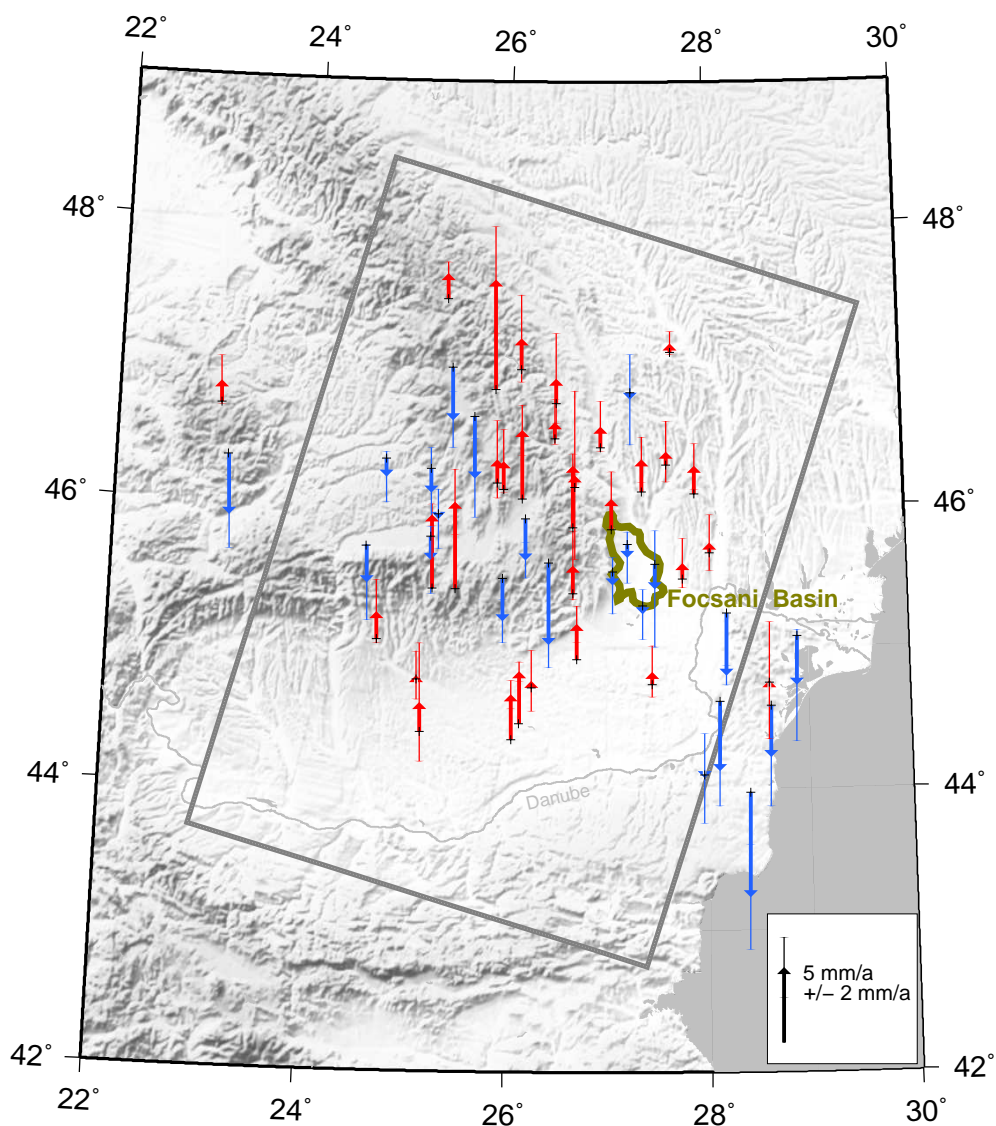


Figure 5.4 – Average vertical displacement rates from observations of 15 GPS field campaigns in the years 1997–2006 [Schmitt et al., 2007]. GPS measurement sites are marked by black crosses. Uplift is plotted as red arrows, subsidence as blue arrows, each with standard deviation. Note the subsidence of the Focsani Basin whose approximate location is indicated by the 500 m thickness isoline of Quaternary sediments. Sediment data is from Matenco et al. [2007].

River region	Time interval [ka]	River incision rate [mm/a]	Reference
Arges – Olt	100 – 10	0.63	Peters
	50 – 10	0.98	
	20 – 10	1.7	
	10 – 0	2.5	
Putna	781 – 200	0.4	Necea et al.
	200 – 0	0.2	
Siret – Trotus	300 – 12	0.47	Peters
	100 – 10	0.45	
	20 – 10	2.3	
	10 – 0	5.	
Birlad	50 – 0	1.2	Peters

Table 5.1 – Fluvial incision rates for various time intervals and different river regions, cf. figure 5.5. The river incision rates can be taken as an estimate of uplift rates in the corresponding regions. The data is derived from fluvial terrace analyses for the rivers Arges, Olt, Siret, Trotus, and Birlad by Gwendolyn Peters [personal communication, and Heidbach et al., 2008] and for the river Putna by Necea et al. [2005].

signal. For example, most stations in the foreland, both to the S and to the E of the SE Carpathians, also show uplift, and three stations located directly within the SE Carpathians show subsidence. This strongly fluctuating pattern is in agreement with stress observations that also reveal a heterogeneous stress pattern for the region [Müller et al., Subm.]. The absence of a homogeneous long-range pattern for both stresses and vertical displacements indicates that there is no strong coupling between the lithospheric slab and the crust beneath Vrancea.

Geomorphological data

Table 5.1 shows river incision rates from two studies for the foreland of the SE Carpathians where river terraces of Quaternary age are exposed: (1) Gwendolyn Peters [personal communication, and Heidbach et al., 2008] correlated the relative height position of these river terraces with their age in order to determine incision rates for the five rivers Arges, Olt, Siret, Trotus, and Birlad incising into their terraces (figure 5.5). The terraces had been mapped by the Structural Geology and Basin Analysis Group of the Department of Geology and Paleontology at the University of Bucharest. As the used terrace ages are mainly relative and based on the height position of the terrace surfaces [Gradstein et al., 2004], they are only estimates, which means that the resulting

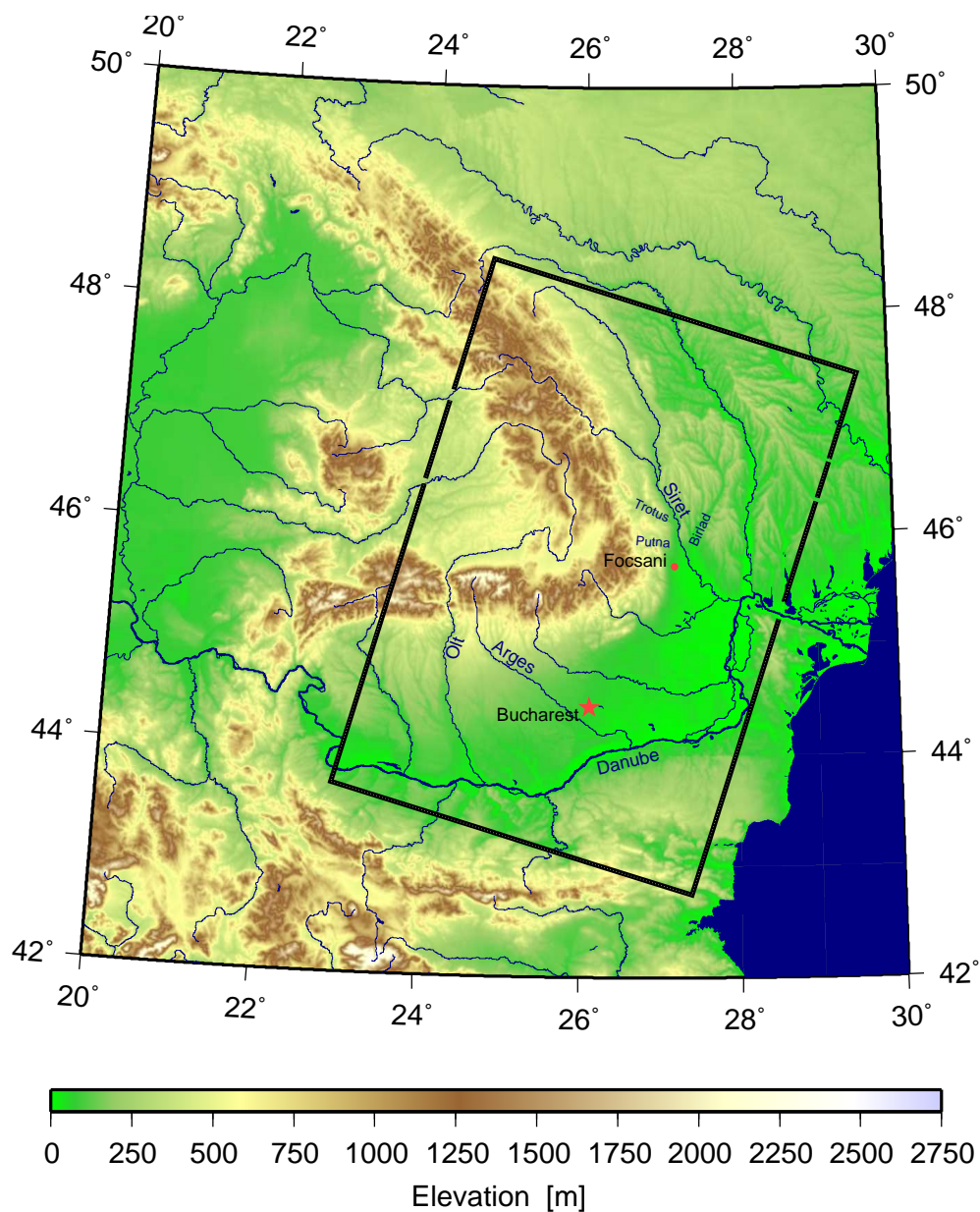


Figure 5.5 – Elevation map of the SE Carpathians, with major rivers, the Romanian capital city Bucharest, and the capital city of the Vrancea region, Focsani, included. The black rectangle marks the boundary of the numerical model. Note the openings in the boundary where the water precipitating onto the model is allowed to leave the model surface. The map is based on the GTOPO30 digital elevation model^a and the GSHHS high-resolution shoreline data set^b [Wessel and Smith, 1996].

^a <http://edc.usgs.gov/products/elevation/gtopo30/gtopo30.html>

^b <http://www.ngdc.noaa.gov/mgg/shorelines/gshhs.html>

fluvial incision rates are also only estimated. (2) Necea et al. [2005] mapped the surfaces of the terraces along the river Putna in detail (figure 5.5) and determined their ages based on the relative height position in order to determine incision rates.

The longitudinal terrace profiles along all six rivers show a parallel distribution of the individual terrace units and a consistent lowering in terrace heights downstream, which suggests a constant incision of the rivers into continuously uplifting terraces [Necea et al., 2005; Heidbach et al., 2008]. This means that the river incision rates can be taken as an estimate of uplift rates in the corresponding regions. The fluvial terrace analyses also reveal that major faults have no effect on the elevations of the terraces. This indicates that no significant vertical motions have occurred on these faults in Quaternary times.

To summarize the incision rates shown in table 5.1, the results from both studies are consistent for older terraces (before about 50 ka), as corresponding incision rates are in the order of 0.5 mm/a for all six rivers. For younger terraces, the studies are inconsistent: Whereas Peters determined rates increasing by up to one order in magnitude compared to the older time intervals, Necea et al. [2005] document a decreasing rate. Though the latest time intervals of both studies differ greatly, this cannot explain the differences: An assumed incision rate of 5 mm/a during the last 10 ka for the river Putna, as determined for the Siret–Trotus region located next to it, would result in 50 m absolute river incision for the last 10 ka. The results of 0.2 mm/a actually determined for the river Putna give $200 \text{ ka} \times 0.2 \text{ mm/a} = 40 \text{ m}$ absolute river incision for the last 200 ka. Even when accepting some tolerances for these two very different results, an incision rate of nearly zero for the time interval (200...10) ka for the river Putna seems to be unrealistic.

The great increase of incision rates in Late Pleistocene and Holocene times according to the study of Peters cannot be explained by tectonic processes, because tectonic activity is relatively low for the Late Pleistocene and the Holocene [Necea et al., 2005; Matenco et al., 2007]. The increase is more likely to be explained by climatic changes [Heidbach et al., 2008]. After the last glacial maximum at around 20 ka, glaciers in the Alps significantly retreated as the climate in Europe gradually got warmer [Major et al., 2006]. As a consequence, rivers feeding the Black Sea (Dneper in Belarus and Dniester in Ukraine) showed increased incision [Kalicki and Sanko, 1998; Huhmann et al., 2004]. Thus, it is possible that also the Danube river and consequently also its tributaries in the SE Carpathian foreland actively incised during this period. This means that the increase of incision rates is likely not to represent increased uplift during the last 20 ka. Based on this argumentation and on the results of both terrace studies, it is more probable that the SE Carpathian foreland is still uplifting at a rate of around 0.5 mm/a or lower. This value is one order of

Tectonic unit	Mass density ρ [kg/m ³]	Young's modulus E [GPa]	Poisson's ratio ν
Carpathians	2700	50	0.250
Foredeep	2500	30	0.275
Focsani Basin	2000	20	0.300
East-Europ. Platform	2700	75	0.250
East Moesia	2700	35	0.250
Moesian Platform	2700	60	0.250
Lower crust	3000	85	0.450

Table 5.2 – Mass density and isotropic elastic material properties assigned to the tectonic units in the numerical crustal model, cf. figure 5.6. Values after Thies Buchmann [personal communication], based on Turcotte and Schubert [2002].

magnitude lower than the rates from GPS observations, and of such an order that the contribution of surface processes can be significant.

5.2 Model setup

In order to quantify vertical crustal displacement rates generated by fluvial erosion and sedimentation, the software CASQUS (as described in chapter 3) is used for a numerical simulation of the SE Carpathian region. The location of the numerical model is indicated by the gray rectangle in figures 5.1 and 5.4. Its dimensions are roughly 380×550 km².

5.2.1 Subsurface model

The subsurface model used for the coupled FE analysis of the Vrancea region is shown in figure 5.6. It is a linear elastic model of the Earth's crust assembled from seven tectonic units that have been discretized by Thies Buchmann [personal communication]. Each unit consists of an isotropic homogeneous linear elastic medium whose material properties are given in table 5.2. The lower boundary of the model is the Moho, i.e., the slab is not simulated as the only aim of this model is to quantify the contribution of surface processes to vertical crustal displacement rates, and not the superposition of all possible contributions to these rates.

The crustal model has already been introduced by Heidbach et al. [2007a, 2008]. The data for the tectonic units and the faults is derived from the work of Matenco et al. [2007; and references therein]. The data for the Moho,

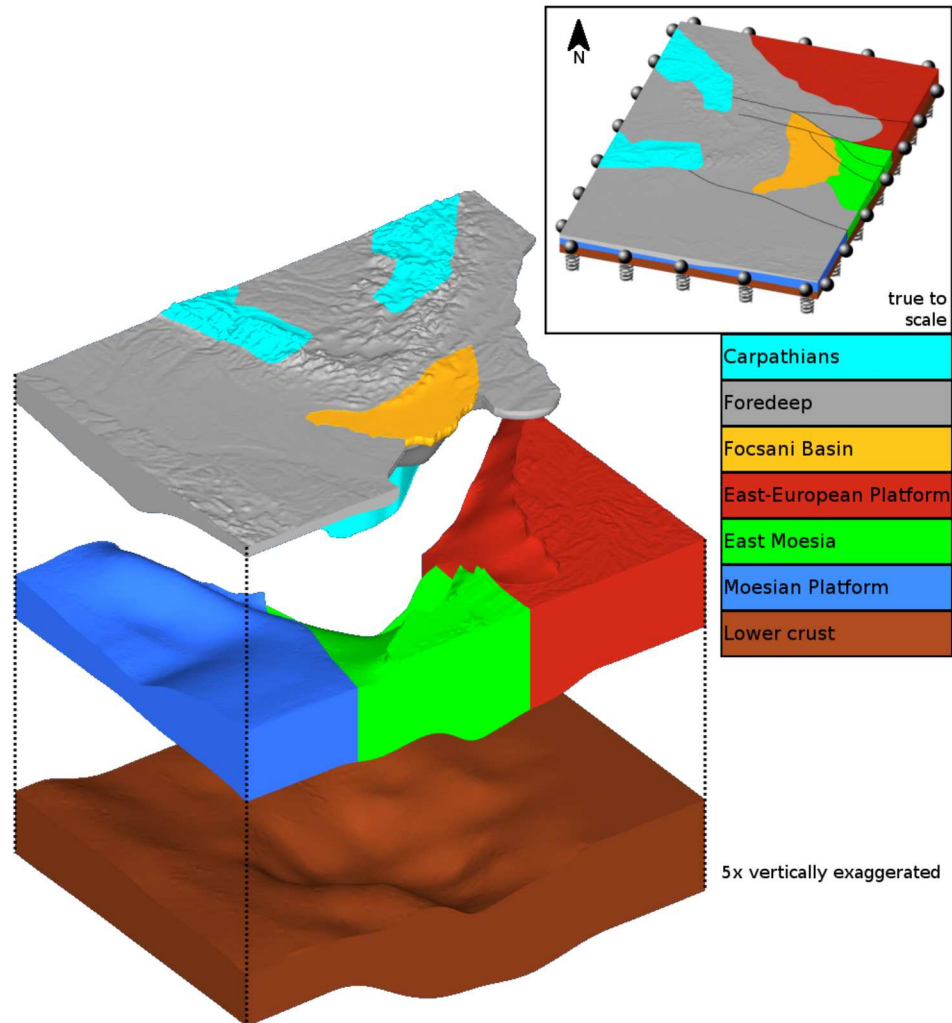


Figure 5.6 – Crustal model of the SE Carpathian region, 3D perspective view from above towards NW with $5\times$ vertical exaggeration. The model consists of seven tectonic units where different material properties are assigned to each unit, cf. table 5.2. In the figure, the units are grouped into three layers that are separated from each other for better identification. The lower model boundary is defined by the Moho in a depth of (30 . . . 45) km. **Inset:** Figure of the assembled crustal model, true to scale and looking from above towards N. The included faults are drawn as black lines. The model is supported by Winkler foundations to account for the buoyancy forces due to the underlying mantle material (indicated by the springs), and all side faces of the model are fixed in normal direction (indicated by the rollers).

the Conrad, and the basement topography is from Martin et al. [2005; and references therein] [Joachim Miksat, personal communication]. The surface topography of the numerical model is based on the GTOPO30 digital elevation model.⁴

The uppermost layer of elements in the FE subsurface model are 8-node linear hexahedral elements⁵, where around 2×10^5 nodes discretize the surface, resulting in average element edge lengths of 1.0 km horizontally and similar vertically. The other element layers consist of 4-node linear tetrahedral elements⁶ whose size increases towards the bottom of the model, where around 3×10^3 nodes discretize the Moho, resulting in element edge lengths of the order of 10 km at the bottom of the model. The faults shown in figure 5.6 have been included as discrete contact surfaces into the FE model. A contact surface cuts the continuum of the FE model, and slip of the two fault walls relative to each other is only allowed in-plane of the contact surface. In the model run in which the included faults are active, slip on the faults is controlled by the Amonton-Coulomb friction law according to equation 2.24 with no cohesion ($C = 0$) and $\mu = 0.05$ as coefficient of friction. For the other runs the faults are removed from the FE model, which corresponds to setting $\mu = \infty$ for all faults.

Zero displacement boundary conditions constrain the four vertical side faces of the model in normal direction, i.e. no horizontal displacements normal to the plane side faces are allowed. The bottom of the model is supported by Winkler foundations. They incorporate the lithostatic pressure generated by the mantle material (not included as a finite element domain), cf. section 2.2.3. Their stiffness per unit area is $\rho_m \cdot g \cong 31 \times 10^3$ Pa/m with $\rho_m = 3200$ kg/m³ and $g = 9.8$ m/s². In order to prevent any instant displacements at the start of the model, the model is initially set to a state of equilibrium by means of two initial conditions for stresses in the model: (1) The Winkler foundations are prestressed by a magnitude that is equal to the lithostatic pressure generated by the gravitational load of the crust at the Moho, so that the complete model is not subsiding when the computation is switched on. (2) The full stress tensor that keeps the model in static equilibrium is prescribed for every finite element in the model, which prevents the model from compacting internally due to its own weight.⁷

⁴<http://edc.usgs.gov/products/elevation/gtopo30/gtopo30.html>

⁵ABAQUSTM element type: C3D8

⁶ABAQUSTM element type: C3D4

⁷This rough estimate of the initial stress state is allowed here as the results of the linear elastic model are only aimed at displacements, not at stresses.

5.2.2 Surface model

According to the design of CASQUS, the same nodes discretizing the surface of the subsurface FE model are used as discretization for the surface processes computation. I.e., erosion and sedimentation start on top of the present-day topography (figure 5.5), and a forward computation of the next several thousand years is performed.

The openings in the black rectangle in figure 5.5 mark the parts of the model boundary where water and sediment load is allowed to leave the model surface. In other words, all surface nodes of the FE model located at the boundary where the black boundary line is not continuous are fixed surface nodes as defined in chapter 3. These outflow zones are chosen based on the location of major rivers leaving the model.

Different from the numerical models presented in the previous chapters, here the precipitation rate is not uniform. As for the complete model region the mean annual precipitation rate is highly correlated with mean elevation, cf. figure 5.7, the relative distribution of rainfall in the model is orographically controlled by surface elevation. Corresponding to the precipitation increase of about 50% between 300 m and 1000 m, the constant for stream erosion K_f times the net precipitation rate ν_R is $K_f \cdot \nu_R = 0.250$ m/a for elevations ≤ 300 m, $K_f \cdot \nu_R = 0.375$ m/a for elevations ≥ 1000 m, and increases linearly with elevation in between. The other surface transport parameters are uniform in the model, where the diffusion constant $K_s = 0.75$ m²/a, the alluvial erosion length scale $l_{f,a} = 10$ km, and the erosion length scale for bedrock $l_{f,b} = 100$ km. The values for the ratio $K_s/(K_f \cdot \nu_R)$ and for $l_{f,a}$ and $l_{f,b}$ are taken as typical values from literature. They are considered to be within valid bounds giving realistic results with respect to the fractal characteristics of natural landscapes [van der Beek and Braun, 1998]. The absolute values for K_s and $K_f \cdot \nu_R$ are chosen based on considerations presented in the following subsection.

The surface processes computation is iterated with time increments of 2 a. Different synchronization times are used for different model runs, 200 a or 1000 a, respectively. In each run, surface processes computation and geomechanical computation are synchronized 20 times. This gives total model times of 4 ka or 20 ka, respectively.

5.2.3 Model adjustment

The proper absolute adjustment of the input parameters K_s and $K_f \cdot \nu_R$ used by the surface processes modeling routines requires particular attention. Their

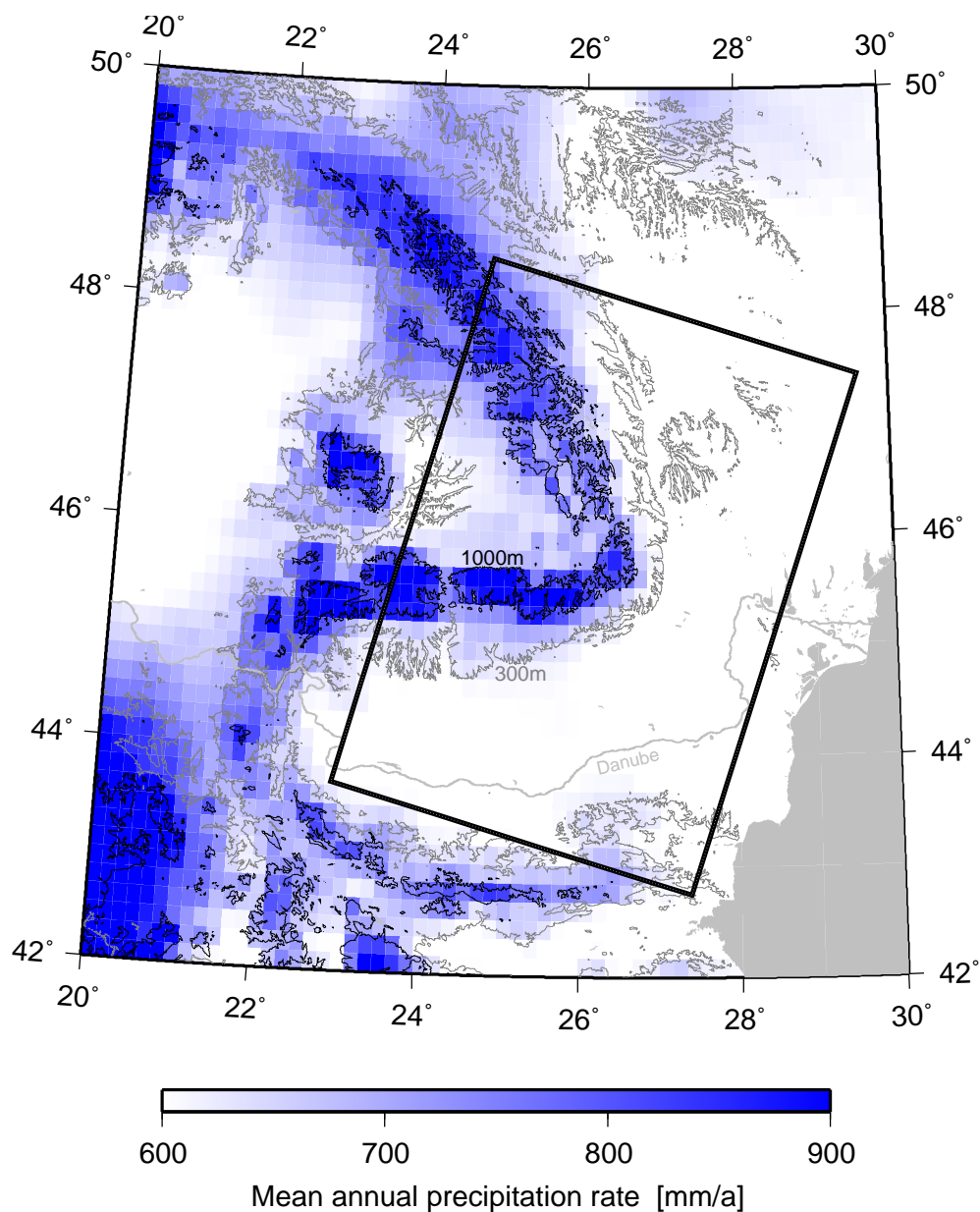


Figure 5.7 – Precipitation map of the SE Carpathians, showing mean annual precipitation rates for the years 1961–1990 at a 10 minute spatial resolution. Additionally, the elevation contour lines for 300 m and 1000 m (from GTOPO30) are plotted. Note the high correlation between mean precipitation and elevation in the model region. Precipitation data is taken from the CRU CL 2.0 data set^a [New et al., 2002].

^a http://www.cru.uea.ac.uk/~timm/grid/CRU_CL_2.0.html

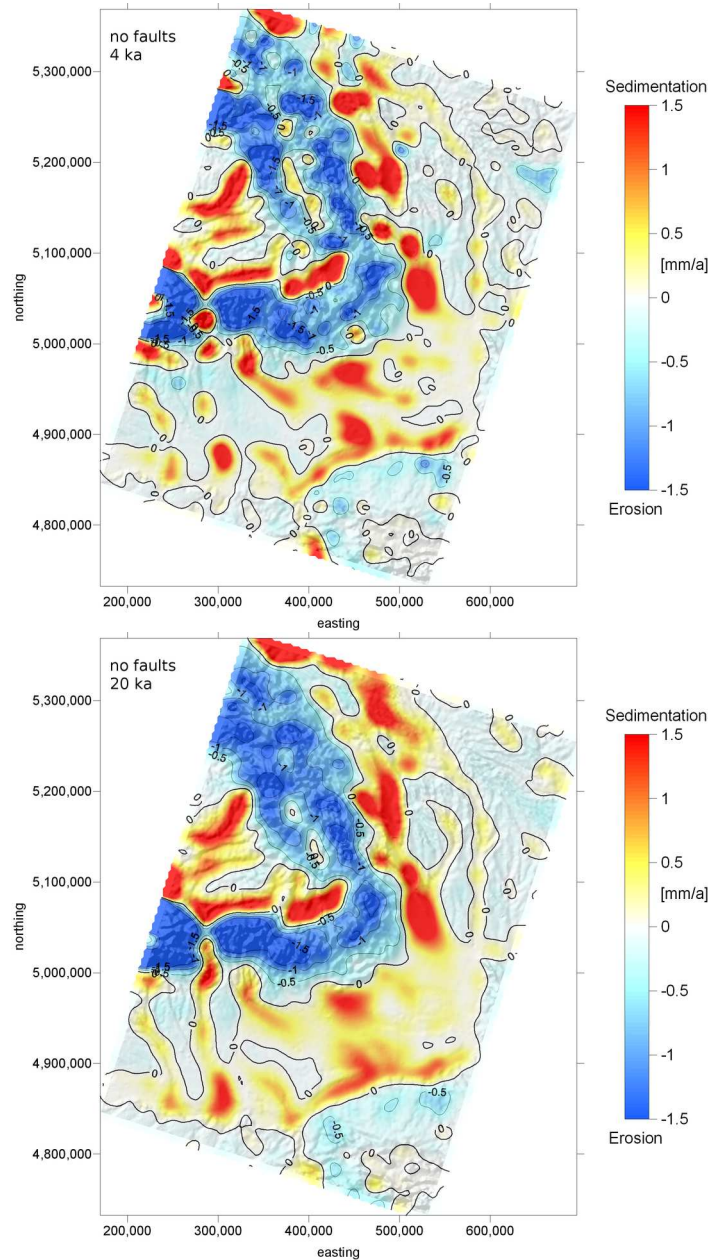


Figure 5.8 – Smoothed maps showing erosion and sedimentation rates color coded, resulting from two runs of the coupled numerical model without faults. Contour lines are drawn for erosion areas only. Northing and easting are UTM coordinates for UTM zone 35 (in meters). **(top)** Total model time is 4 ka. **(bottom)** Total model time is 20 ka. Note that the erosion/sedimentation pattern here shows larger-scale structures than the above 4 ka model run, where the sedimentation areas roughly trace the major rivers in the plane SE Carpathian foreland as expected, cf. figure 5.5.

absolute values control the process rates of erosion and sedimentation, i.e. the mass transport rates. The direct correlation between the input parameters and the process rates cannot be determined before running the numerical model, because the complex topography affects this correlation in an unpredictable way.

However, the linear character of the relationships governing surface processes in CASQUS (cf. equations 2.25–2.27) leads to a linear time-scaling of the surface processes model. Rescaling both K_s and $K_f \cdot \nu_R$ by a common factor Γ and using numerical time increments of $\Gamma^{-1} \Delta t$ will lead to exactly the same landform evolution as using unscaled parameters K_s and $K_f \cdot \nu_R$ and time increments of Δt . Both models will reach the same final topography, the rescaled model only Γ times as fast as the unscaled one [van der Beek and Braun, 1998]. As the subsurface model only makes use of linear elastic rheology, linear time-scaling does also apply to the complete coupled model combining surface and subsurface simulation. This consideration justifies the approach used for the coupled model of the SE Carpathians, which is first computed based on estimated values for K_s and $K_f \cdot \nu_R$, and whose results are then rescaled in time after computation to obtain realistic erosion rates. All times and time-dependent values (rates) given in the text and shown in the figures of this chapter have already been rescaled, including the input parameters defined in the previous subsection.

In order to constrain the absolute values of K_s and $K_f \cdot \nu_R$, geological data on denudation rates is used [as suggested by van der Beek and Braun, 1998]. Time-integrated Pliocene-recent (5 Ma) erosion rates for the bend zone of the SE Carpathians are in the order of 1 mm/a, as deduced from fission track thermochronological analyses [Sanders et al., 1999; Cloetingh et al., 2005]. Sedimentation rates in the foreland of the East Carpathians, calculated until around 2.5 Ma before present, do not vary significantly from the beginning of the Pliocene [Panaiotu et al., 2007]. As they are directly related to erosion rates, and assuming no significant changes during the last 2.5 Ma, the long-term erosion rate of 1 mm/a is considered to be a realistic estimate of the present-day erosion rate in the SE Carpathians. The (rescaled) input parameters for the surface processes computation as stated above have been adjusted to such values that this erosion rate of 1 mm/a is reached within the SE Carpathian bend zone, see figure 5.8.

5.3 Results

The results from three runs of the coupled numerical model will be presented in the following, showing the influence of mass redistribution by surface erosion on vertical crustal displacement rates. Two runs have been performed without faults, one for 4 ka and one for 20 ka total model time, and a third run has been performed with faults for 4 ka total model time.

Surface uplift and subsidence rates for the model runs without faults are shown in figure 5.9. The rates for the run with faults and the difference between the runs with and without faults are shown in figure 5.10. As crustal uplift rates are very small compared to the values shown in the figures, these maps also represent sedimentation and erosion rates similar to the smoothed maps shown in figure 5.8. Therefore the shown pattern of surface uplift and subsidence resembles the fine structures of the river network of the SE Carpathian region, except for basin areas where surface uplift/sedimentation occurs at larger spatial scales. As expected, the mountainous region of the SE Carpathians is dominated by erosion, whereas sedimentation dominates the foreland and the basin areas: the Brasov Basin directly to the W of the Carpathian bend zone, surrounded by the S and the E Carpathians, the Transsylvanian Basin further to the W, and the foreland to the S and to the E of the Carpathians, here especially the Focsani Basin. High sedimentation rates are found along segments of major rivers close to the mountains, cf. figure 5.5, whereas the topography of large parts of the foreland does not change significantly.

The results for surface uplift and subsidence rates do not vary strongly between the three model runs. The high similarity between the 4 ka and the 20 ka model run indicates that the discretization of the model surface appropriately represents the natural topography of the model region, because rivers generally follow their river beds and do not change their course with time. The results from the 4 ka model runs with and without faults are also highly similar for most areas in the model, except for the Brasov Basin, along the river Siret following the eastern flank of the E Carpathians, and along the river Olt (see arrow in figure 5.10). High variations at the river Olt mainly occur near the faults crossing the river. For the Brasov Basin and the river Olt, the changes in erosion and sedimentation rates due to the existence of faults is not obvious, because all faults are at least 50 km away from each of these two places.

Crustal uplift and subsidence rates for the model runs without faults are shown in figure 5.11. The rates for the run with faults and the difference between the runs with and without faults are shown in figure 5.12. As expected, the shown pattern of crustal uplift and subsidence reflects a smoothed image of the pattern of erosion and sedimentation, respectively. All parts of the SE

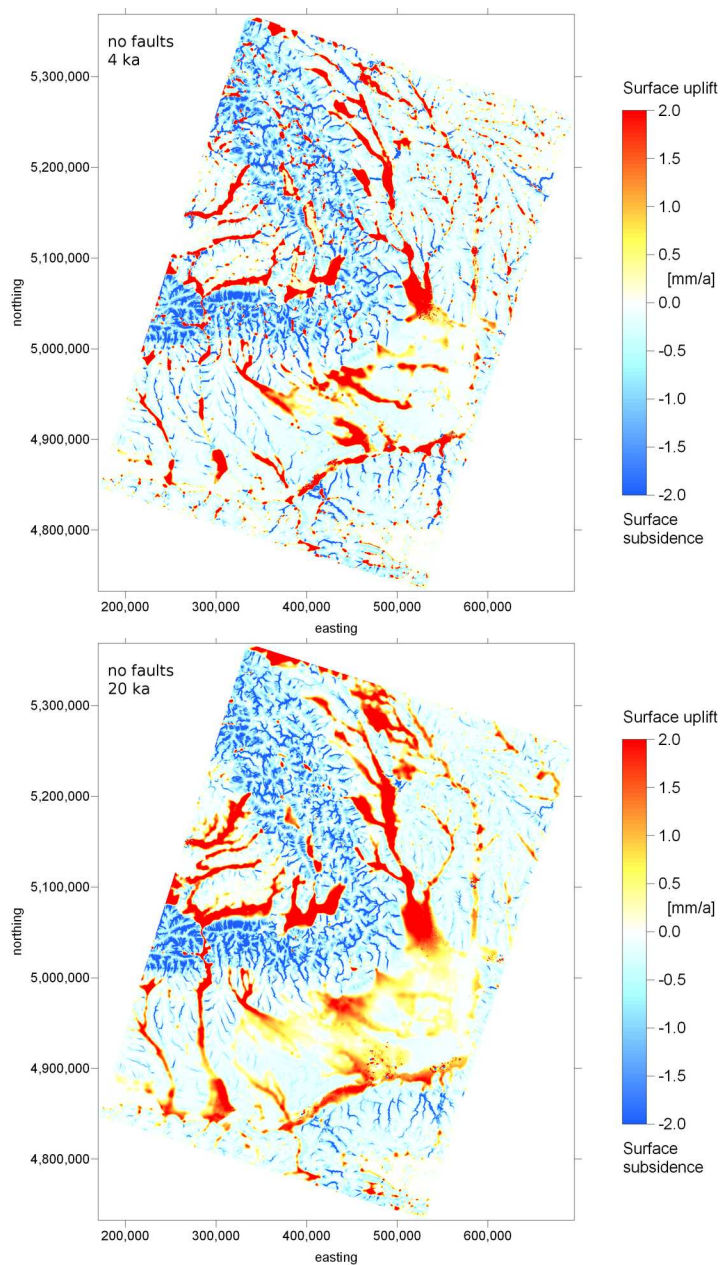


Figure 5.9 – Maps showing surface uplift and subsidence rates color coded. **(top)** 4 ka model run without faults. **(bottom)** 20 ka model run without faults. The pattern here shows larger-scale subsidence structures than the above 4 ka model run, and surface subsidence in the Focsani Basin is a bit more pronounced.

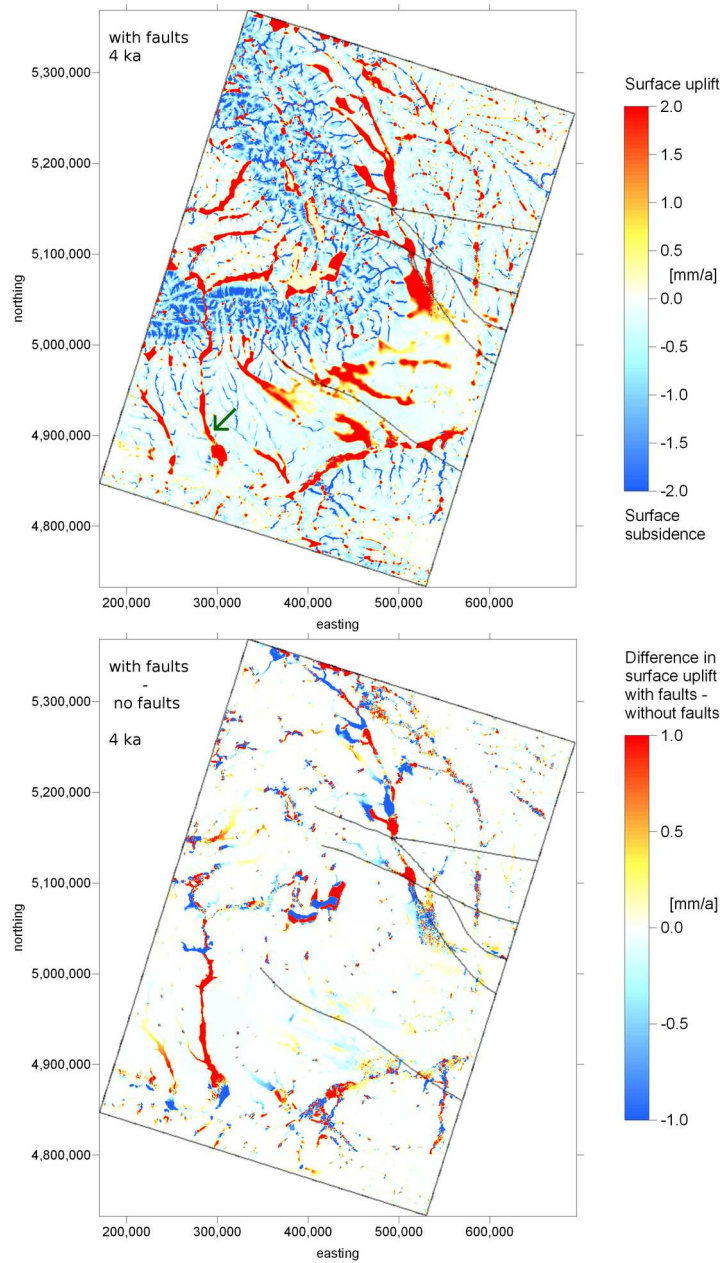


Figure 5.10 – (top) Map showing surface uplift and subsidence rates for the 4 ka model run with active faults. The pattern does not vary significantly between the runs with and without faults, except of small changes (e.g., see arrow). **(bottom)** Map showing the difference between the 4 ka model runs with and without faults, $(\partial h/\partial t)_{faults} - (\partial h/\partial t)_{nofaults}$. Note the increased surface uplift/sedimentation rates along the river Olt.

Carpathians are uplifted, whereas the complete foreland is subsiding. Distinct local features cannot be found, except the Focsani Basin showing locally increased subsidence relative to its surrounding area. This results from the high sedimentation rates for a large area of the Focsani Basin. Maximum uplift rates of more than 0.15 mm/a are found for a long band along the Carpathians. Maximum subsidence rates of the same order are found for a region of about 100 km diameter to the E of Bucharest. A large area in the NE part of the model does not show significant vertical crustal displacement rates.

As was expected due to the similarity of the results for surface displacement rates, the results for crustal uplift and subsidence rates do also not vary strongly between the three model runs. For the runs without faults, maximum uplift rates within the Carpathians slightly increase for a longer model time, whereas maximum subsidence rates in the foreland slightly decrease. This can be explained by the fact that the complete model is slightly uplifted due to the sediment mass that is completely removed from the model via the rivers leaving the model surface. The results from the model runs with and without faults are also highly similar for most areas in the model, except along the river Olt, where the change towards higher sedimentation rates for the model with faults results in a significant change towards higher subsidence rates, though the differences are one order of magnitude smaller than the absolute rates.

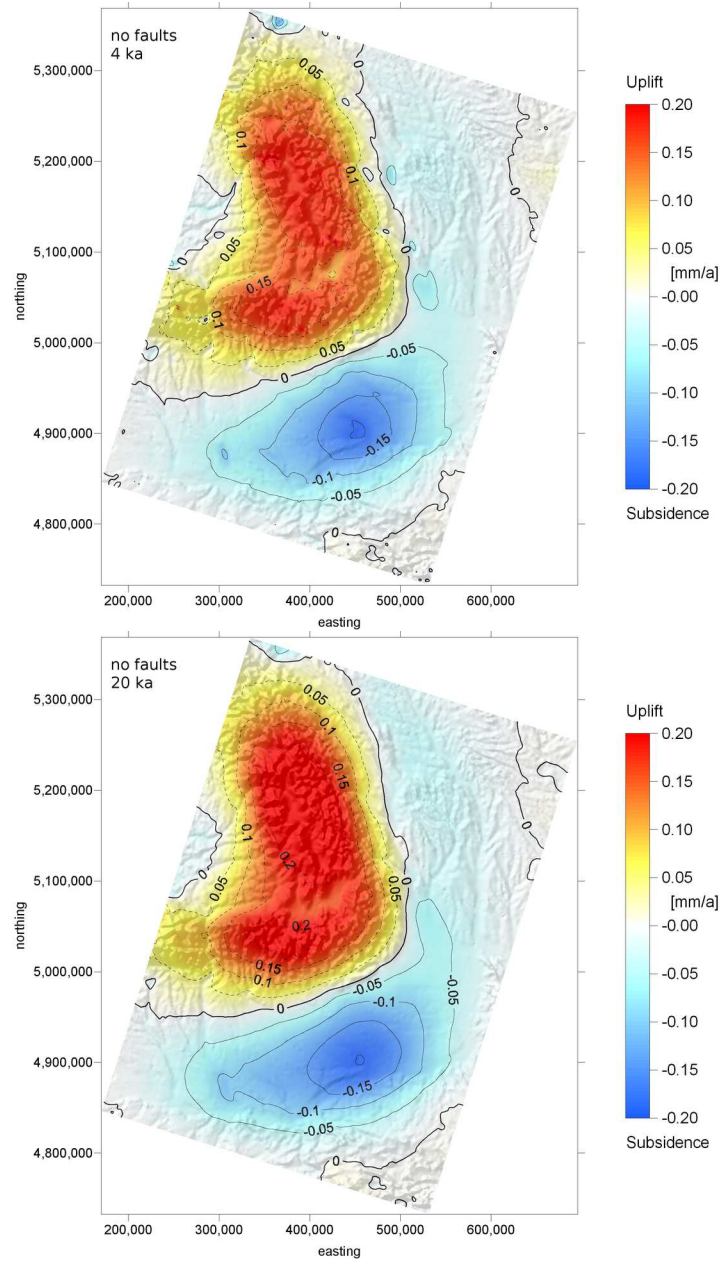


Figure 5.11 – Maps showing crustal uplift and subsidence rates color coded. **(top)** 4 ka model run without faults. **(bottom)** 20 ka model run without faults. Maximum subsidence rates in the foreland are slightly decreased compared to the above 4 ka model run, whereas maximum uplift rates within the Carpathians are slightly increased.

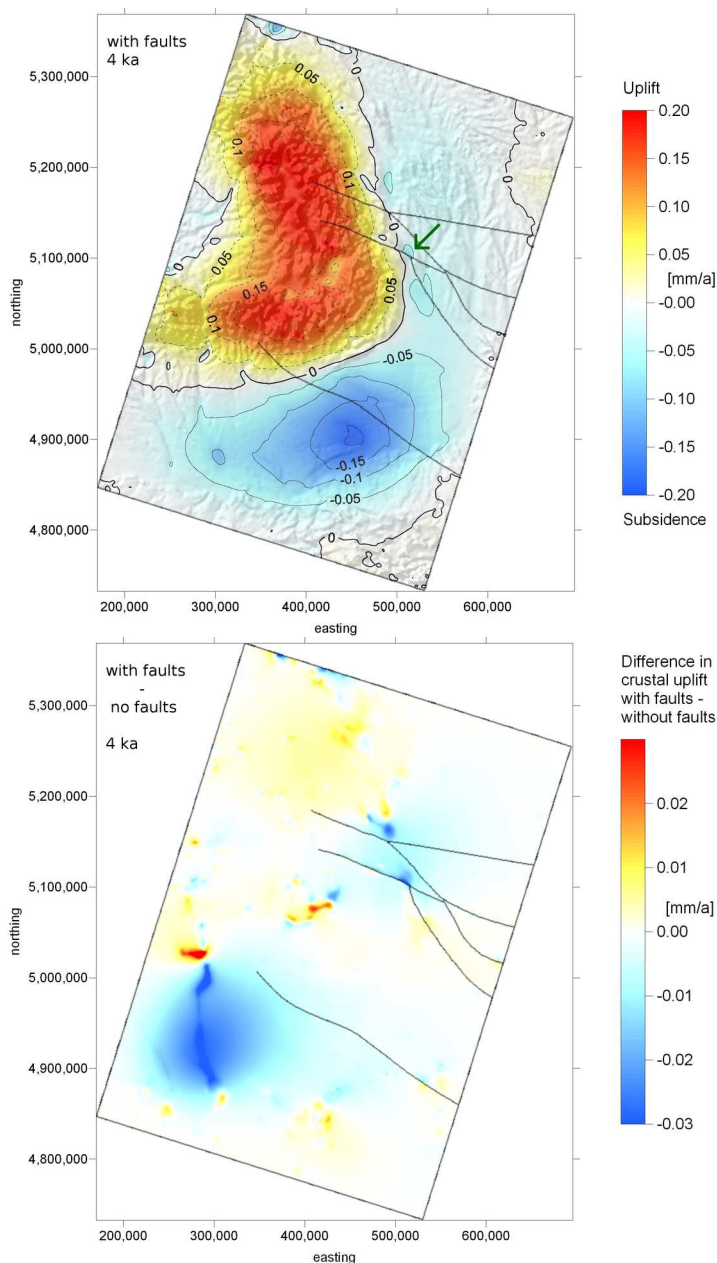


Figure 5.12 – (top) Map showing crustal uplift and subsidence rates for the 4 ka model run with active faults. The pattern does not vary significantly between the runs with and without faults, except of small changes (see arrow). (bottom) Map showing the difference between the 4 ka model runs with and without faults, $(\dot{u}_{ro})_{faults} - (\dot{u}_{ro})_{nofaults}$. Note the changes in color scale. Also note the significant differences at the river Olt, though all faults are far away. The increased subsidence rates along the river Olt result from the increased surface uplift/sedimentation rates there when faults are active, cf. arrow in figure 5.10.

5.4 Discussion

The simulation of the feedback between tectonic and surface processes for the SE Carpathian region has resulted in significant vertical crustal displacement rates that are generated only by fluvial mass redistribution. Both crustal uplift rates in the Carpathian mountains and subsidence rates in the foreland to the S of the SE Carpathians are up to 0.2 mm/a.

The subsurface model has been simulated by purely elastic material behavior. Viscous behavior of the subsurface has not been considered in this model, because it is assumed that it has no significant effect on the vertical crustal uplift rates generated by the continuous processes of erosion and sedimentation here. For the motivation of this assumption, note that viscous processes generally have the effect of damping subsurface movements, and compare the situation in Scandinavia after the last ice age: After the (on geological time scales) abrupt deglaciation, viscous processes prevented an instantaneous upward rebound of the crust. But the maximum observed uplift rates in Scandinavia are still in the order of 1 cm/a, i.e. around $(10 \dots 100) \times$ greater than the maximum crustal uplift rates resulting from the SE Carpathians model. As the mass redistribution rates by fluvial erosion and sedimentation are orders of magnitude less than those by deglaciation after the last ice age in Scandinavia, viscous processes would not significantly slow down vertical crustal displacement rates generated by fluvial surface processes, and so viscous effects can be neglected.

Uplift/subsidence patterns and uplift/subsidence rates are very similar for the model runs with and without faults. Thus the influence of tectonic faults can be neglected for the SE Carpathians as far as vertical displacement rates are concerned. This can be explained by the fact that major faults in this region are perpendicular to the mountain range. In regions where major faults are parallel to the mountains they may influence the uplift and subsidence pattern much more, because then rock material is redistributed by sediment transport from one side of the fault to the other. The faults would then probably support the natural pattern of uplift in the mountains and subsidence in the foreland. Another factor that significantly influences fault slip induced by surface mass redistribution is the dip of the fault. In the SE Carpathian region, all faults dip nearly vertically. Numerical studies have revealed that slip on faults with a dip of around 60° react much more sensitively to erosion and sedimentation processes than faults with a steeper dip [Maniatis et al., Subm.]. Thus, in regions with inclined-dipping faults, these faults can more significantly affect uplift/subsidence rates than in the SE Carpathians.

Considering the model results for *surface* displacement rates, in large parts of the SE Carpathian foreland the surface topography does not change signifi-

cantly. Here most rivers seem to have found a state of equilibrium with erosion and deposition, according to the concept of graded streams [Mackin, 1948]. This does not apply to the Focsani Basin area, where high sedimentation rates of more than 2 mm/a occur in the model, which is in agreement with geological observations that give characteristic sedimentation rates of (1...2) mm/a for the Focsani depression [Demetrescu et al., 2005].

As well, the result that the Carpathian arc is uplifted and that the foreland, in particular the Focsani Basin adjacent to the Carpathian bend zone, is subsiding is in agreement with geological studies [Bertotti et al., 2003; Matenco et al., 2003; Tarapoanca et al., 2003; and references therein]. According to these studies, also the Brasov Basin directly to the W of the Carpathian bend zone, surrounded by the S and the E Carpathians, is an area of subsidence. The numerical model does not show subsidence in the Brasov Basin, which indicates that subsidence in this area is not generated by fluvial mass redistribution.

Uplift rates determined by fluvial terrace analyses for the SE Carpathian region are around 0.5 mm/a, cf. section 5.1.3. Actually, river incision rates have been calculated from the fluvial terrace analyses, which have then been taken as crustal uplift rates by the authors [Gwendolyn Peters, personal communication, and Necea et al., 2005]. However, the calculation of these river incision rates is not only based on data from regions at the S or E margin of the SE Carpathians where uplift is obtained by the model, but it is also based on data from areas within the foreland where the model shows subsidence. Due to this inconsistency, and due to the fact that also for river segments crossing the Focsani Basin incision rates are taken as (positive) uplift rates, it is questionable whether it is appropriate to generally take incision rates equal to uplift rates in this region. Anyway, the vertical crustal displacement rates resulting from the numerical model, which are up to 0.2 mm/a, reach the same order of magnitude as the river incision rates.

In figure 5.13 (top), a continuous map of the vertical GPS signal is shown, based on the observations of the field campaign measurements at around 50 GPS stations introduced in section 5.1.3. For the continuous map, the station data is interpolated using a multilevel B-spline approximation by Nuckelt [2007]. In figure 5.13 (bottom), the vertical component of the GPS signal is corrected by the results from the numerical model. The resulting map is considered to reveal the part of the present-day uplift and subsidence rates that cannot be explained by fluvial mass redistribution.

Vertical crustal displacement rates resulting from the simulation of fluvial mass redistribution are about one order of magnitude smaller than the vertical displacement rates from the GPS campaign measurements. In the following this discrepancy will be discussed.

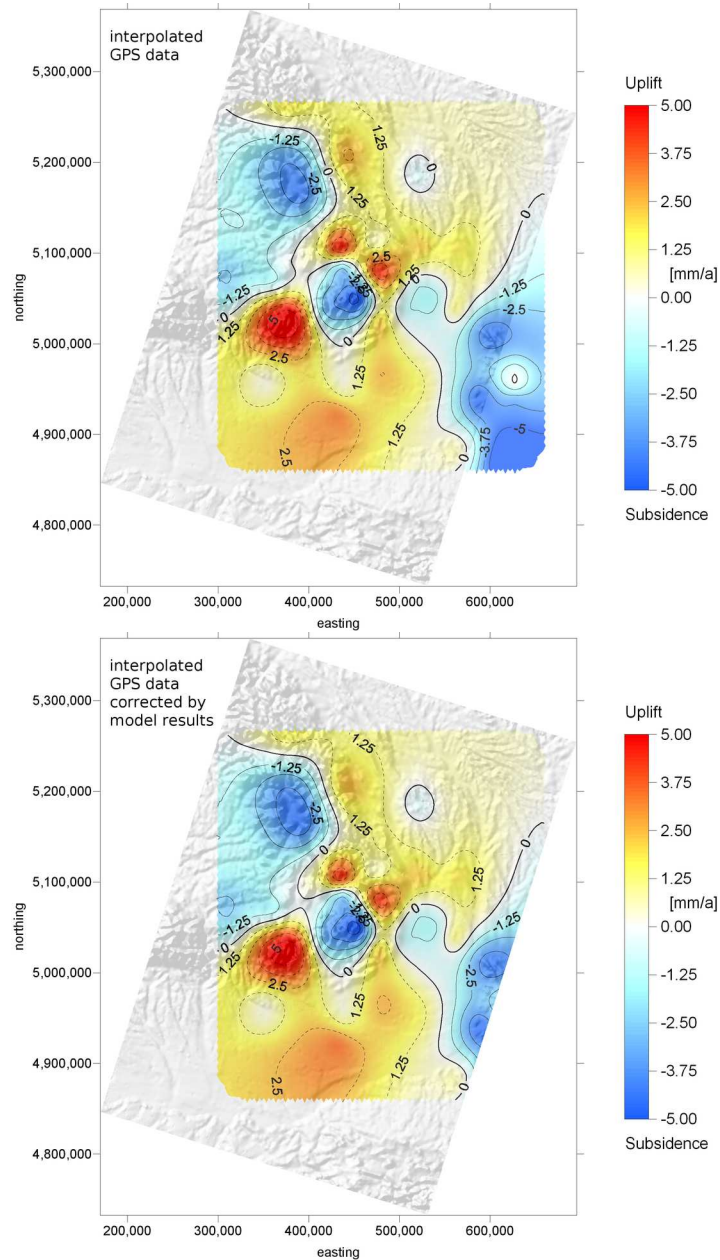


Figure 5.13 – (top) Map showing the vertical GPS signal, interpolated from the GPS data shown in figure 5.4 using multilevel B-spline approximation by Nuckelt [2007]. (bottom) Interpolated vertical GPS signal as shown above, corrected by the crustal uplift and subsidence rates resulting from the numerical model. (The rates from the 20 ka model run without faults are subtracted from the GPS rates.) Because the vertical GPS signals are around one order of magnitude greater than the numerical results, the correction does not lead to significant changes in the vertical displacement pattern.

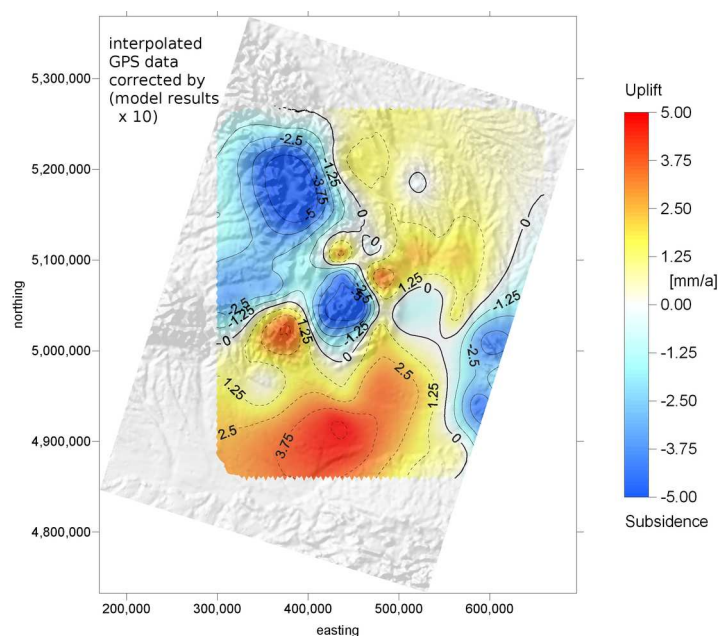


Figure 5.14 – Interpolated vertical GPS signal corrected by $10\times$ the crustal uplift and subsidence rates resulting from the numerical model. (The rates from the 20 ka model run without faults are multiplied by 10 and are then subtracted from the GPS rates.) The high uplift rates from the GPS observations within the S and the E Carpathians can be compensated to a large extent by the correction. In contrast, the high subsidence rates in the Brasov and the Transsylvanian Basin and the high uplift rates in the foreland to the S of the Carpathian bend zone are even increased by the correction.

First, the hypothesis must be discussed whether the maximum erosion rate of 1 mm/a for the Carpathian mountains that is taken to adjust the parameters for the surface processes computation is too low. The taken erosion rate is an average over some million years and may not represent the present-day erosion rate appropriately. This hypothesis of an underestimated erosion rate is supported by the drastic increase in river incision rates of around one order of magnitude at around 10 ka before present. Under the assumption that precipitation rates in the region have drastically increased during the last 10 ka, the numerical input parameters chosen for the surface processes computation would be far too low. Figure 5.14 shows the vertical GPS signal, but this time corrected by 10× the vertical displacement rates resulting from the numerical model. This corresponds to a factor of 10 for the precipitation rates used in the numerical model. Now the high uplift rates from the GPS observations within the S and the E Carpathians can be compensated to a large extent by the correction. But the high subsidence rates in the Brasov and the Transsylvanian Basin and the high uplift rates in the foreland to the S of the Carpathian bend zone are even increased by the correction. Anyway, a factor of 10 between the vertical displacement rates resulting from the numerical model and the GPS observations can hardly be explained by an increase in precipitation during the last 10 ka, because a drastic increase in rainfall of a factor 10 over such a short period of time is not realistic. So this hypothesis can be neglected.

Under the assumption that the GPS observations reliably represent the real vertical displacement rates in the SE Carpathian region, these high vertical displacement rates must have a tectonic origin. Small-scale tectonic processes must be active that can explain the high-amplitude short-range variations in vertical displacement rates across the Carpathian bend zone. Some neighboring GPS stations that are less than 20 km away from each other show differences in vertical displacement rates of more than 5 mm/a, cf. figure 5.4. However, such large variations over short distances would require active tectonic faults to compensate this large displacement rates. Obviously, if these faults existed they could be observed, as vertical slip on the faults would be in the order of 100 m during only 20 ka. But because such faults that are significantly active in the vertical direction are not observed in the SE Carpathian region, it is probable that the results from the GPS measurements overestimate the real vertical displacement rates there.

As stated above, the GPS data for the SE Carpathian region is derived from field campaign measurements. It is questionable whether GPS field campaigns that take place each few years and last only few days give reliable results. The International GNSS Service (IGS, formerly the International GPS Service)⁸ recommends that in order to derive vertical displacement rates from GPS it is

⁸<http://igsb.jpl.nasa.gov/>

necessary to measure continuously, i.e. using permanent GPS stations, during a period of at least 2 years [see the IGS Site Guidelines⁹, and Drewes et al., 2002].

This explains the very high standard deviations for the vertical rates measured by GPS, which are larger than the GPS results for several stations (figure 5.4). For some stations, even the sign of the vertical displacement rate from GPS is not safely determined. Figure 5.15 (top) shows the interpolated vertical rates from GPS subtracted by the standard deviations, i.e. the shown picture is a map of the smallest possible absolute uplift/subsidence rates from GPS that are within the standard deviation range. Note that vertical displacement rates of zero are within the error range of the GPS measurements for the largest part of the SE Carpathian area. Thus it is highly questionable whether the GPS results represent the real situation. This means that vertical displacement rates induced by fluvial mass redistribution are probably great enough to give significant contributions to the real vertical displacement rates occurring in the SE Carpathian region, see figure 5.15 (bottom).

⁹<http://igsb.jpl.nasa.gov/network/guidelines/guidelines.html>

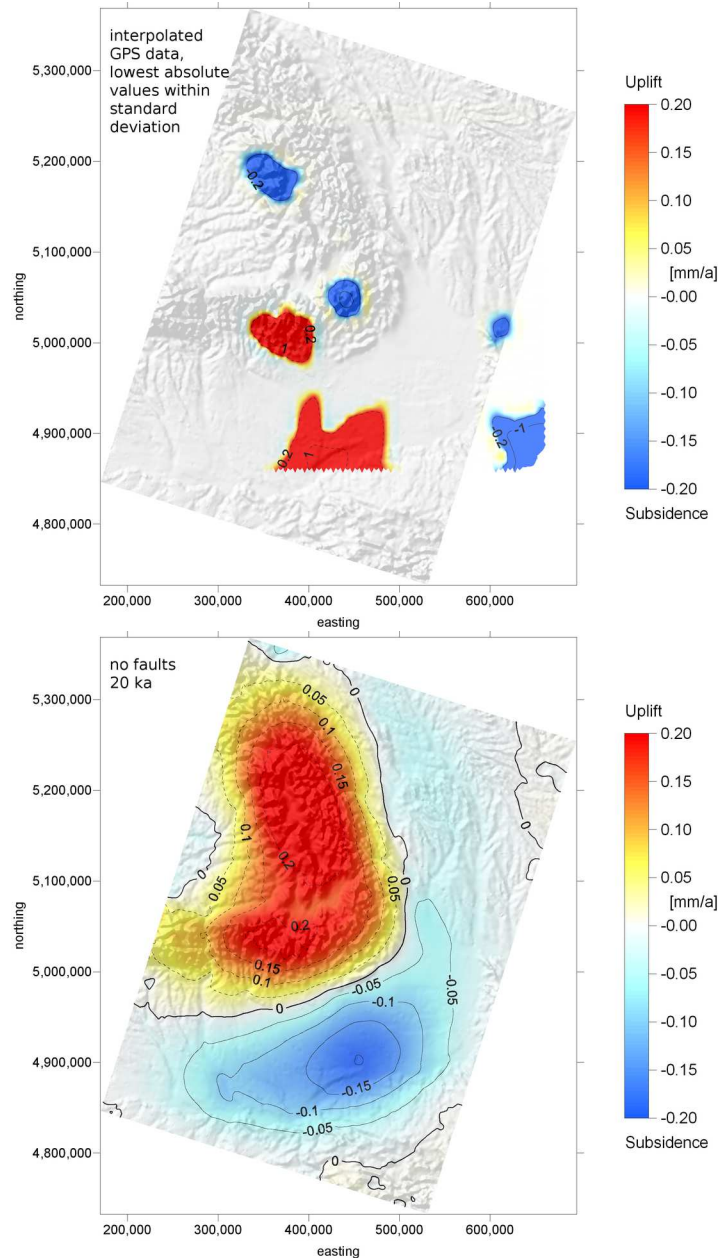


Figure 5.15 – (top) Map showing the vertical GPS signal like figure 5.13, but standard deviations of the GPS measurements are subtracted to give the smallest possible absolute uplift/subsidence rates that are within the standard deviation range. The very high standard deviations of the GPS data (figure 5.4) result in vertical displacement rates of around zero for the largest part of the GPS observation region. (bottom) Under the assumption that the vertical displacement rates from GPS campaign measurements in this region are highly defective, crustal uplift and subsidence rates resulting from the numerical model may give a significant contribution to vertical displacement rates in this region. Same picture as figure 5.11 (bottom).

5.5 Conclusions for slab attachment or detachment

The high sedimentation rates within the Focsani depression that have been found by geological observations are also found by the numerical simulation of fluvial surface processes. This high rate of sedimentation occurs for a large area of approximately $30 \times 50 \text{ km}^2$ within the Focsani Basin, cf. figure 5.9. The large amount of sediment material that is deposited here during a short period of time results in a crustal subsidence of the Focsani Basin, cf. figure 5.11.

This means that the subsidence of the Focsani Basin is not a clear evidence that the lithospheric slab below the basin is still attached to the crust, as proposed by some authors [Bertotti et al., 2003; Matenco et al., 2007]. As well, the tectonic response to mass redistribution due to erosion and sedimentation is able to explain the subsidence found in the Focsani Basin. This would agree with the hypothesis proposed by many authors that the slab has already detached and is now decoupled from the crust [Hauser et al., 2007; Heidbach et al., 2007b; Müller et al., Subm.]. In this case, no stress would be transferred from the slab into the crust or vice versa.

Chapter 6

Conclusions of the thesis

In the framework of this thesis, a new numerical modeling tool has been developed that enables the analysis of the impact of the interaction between tectonic and surface processes on vertical crustal displacement rates. It combines surface processes modeling including fluvial erosion and sedimentation with geomechanical Finite Element modeling of the subsurface. In contrast to previously existing software, the new tool allows for the simulation of heterogeneous subsurface structures including tectonic faults. With this numerical approach, the three questions raised in the objectives of this thesis have been answered:

1. *On which time scales does the feedback between tectonic and surface processes significantly contribute to observed erosion/sedimentation rates and vertical displacement rates?*

For the numerical simulation of the interaction between tectonic and surface processes the synchronization time between the surface processes computation and the geomechanical simulation of the subsurface is a very important numerical parameter. For synchronization times of more than a few ka – the exact value depends on the specific model situation – the mean erosion rates resulting from the simulation show numerical artefacts due to the inadequate coupling of tectonic and surface processes. For time spans that are shorter than a few ka, erosion/sedimentation rates are not significantly affected by the tectonic response that this erosion itself induces. On time scales of more than a few ka, the feedback process must be considered as it affects both erosion/sedimentation rates and thus also vertical displacement rates significantly. (Chapter 3)

2. *To what extent can fluvial erosion and sedimentation contribute to vertical crustal displacement rates?*

For a simple linear elastic model of the lithosphere with a small flexural rigidity, fluvial mass redistribution at the surface has been simulated with realistically high precipitation rates. The results of the model show that maximum vertical crustal displacement rates induced by fluvial erosion and sedimentation are in the order of few mm/a for extreme scenarios. (Chapter 4)

3. *To what extent can fluvial mass redistribution explain vertical crustal displacement rates in the region around the south-eastern Carpathians, both in terms of absolute rates and in terms of spatial distribution of uplift and subsidence?*

According to the results from a numerical model of the SE Carpathians, simulating fluvial erosion and sedimentation on top of the present-day topography, the tectonic response to fluvial mass redistribution is able to explain vertical crustal displacement rates of up to 0.2 mm/a. These absolute values are found both for uplift and for subsidence rates, and their order of magnitude is in agreement with geomorphological observations for river incision rates averaged over the last 100 ka. According to the numerical simulation, the complete Carpathian mountain range is continuously uplifted, whereas large parts of the foreland are subsiding. In particular, the observed ongoing subsidence of the Focsani Basin can be explained by the high sedimentation rates found there. This gives an alternative explanation for the Focsani subsidence in contrast to the hypothesis that the lithospheric slab below the Vrancea area is still attached to the crust. (Chapter 5)

Outlook The newly developed numerical tool to simulate the feedback between tectonic and surface processes is already used by other working groups. First results from advanced studies using the new software show that surface mass redistribution is able to significantly increase fault slip rates on normal faults in extensional regimes [Maniatis et al., Subm.]. The new approach has the potential to quantify the important contribution of surface processes to vertical crustal displacement rates, which are observed with continuously growing resolution and precision by constantly improved remote sensing techniques like global navigation satellite systems and InSAR.

Acknowledgments

Diese Arbeit wurde im Rahmen des Sonderforschungsbereichs 461 der Deutschen Forschungsgemeinschaft (DFG) mit Unterstützung des Landes Baden-Württemberg und der Universität Karlsruhe (TH) erstellt.

Some figures have been created using the software GMT (the Generic Mapping Tools) by P. Wessel and W. H. F. Smith [Wessel and Smith, 1991].

Ich möchte Prof. Dr. Friedemann Wenzel für die Übernahme des Referats meiner Dissertation und die hilfreichen guten Ideen zur Verbesserung meiner Arbeit danken. Meinem Korreferenten Prof. Dr. Karl Fuchs danke ich herzlich für die konstruktive Kritik und die erhellenden Diskussionen.

Besonderer Dank gilt Oliver Heidbach für die hervorragende Betreuung meiner Dissertation und die große Unterstützung.

Der ganzen Arbeitsgruppe “Tectonic Stress Group” gebührt großer Dank für die alltägliche Unterstützung meiner Arbeit, die hilfreichen Diskussionen und das ausgezeichnete Arbeitsklima. Besonders danke ich den Mitgliedern des SFB-Teilprojekts A6 für all das an mich weitergegebene Wissen und all die nützlichen Tipps und Hilfestellungen, namentlich Thies Buchmann, Jose Dirkwager, Oliver Heidbach, Paola Ledermann, Birgit Müller, Gwendolyn Peters und Blanka Sperner. Dafür danke ich auch meinen Kollegen Johannes Altmann, Tobias Hergert, Alik Ismael-Zadeh und John Reinecker, und ebenso Andreas Barth als meinem wunderbaren Bürokollegen.

In particular I would like to thank Jean Braun for kindly providing us with the CASCADE code.

Danken möchte ich auch meinen Bochumer Kollegen Andrea Hampel und Georgios Maniatis für die freundliche und konstruktive Zusammenarbeit.

Den Kollegen Andreas Knöpfler, André Nuckelt und Günter Schmitt vom Geodätischen Institut danke ich für die Bereitstellung der GPS-Daten und nützliche Tipps.

Danke auch an Michael Heintz für die großartige Hilfe und Unterstützung.

Ganz besonders danke ich schließlich Maïke, meiner Familie und meinen Freunden, die mich nach Möglichkeit unterstützten und die letzten Jahre immer hinter mir standen.

References

- ABAQUS, Inc. (2004). *ABAQUSTM Version 6.5 Documentation*.
- Ahnert, F. (1970). Functional relationships between denudation, relief, and uplift in large mid-latitude drainage basins. *American Journal of Science*, 268(3):243–263.
- Allen, P. A. (1997). *Earth surface processes*. Blackwell Science Ltd, Oxford.
- Avouac, J. P. and Burov, E. B. (1996). Erosion as a driving mechanism of intracontinental mountain growth. *Journal of Geophysical Research – Solid Earth*, 101(B8):17747–17769.
- Basile, C. and Allemand, P. (2002). Erosion and flexural uplift along transform faults. *Geophysical Journal International*, 151(2):646–653.
- Batt, G. E. and Braun, J. (1997). On the thermomechanical evolution of compressional orogens. *Geophysical Journal International*, 128(2):364–382.
- Beaumont, C., Fullsack, P., and Hamilton, J. (1992). Erosional control of active compressional orogens. In McClay, K. R., editor, *Thrust tectonics*, pages 1–18. Chapman & Hall, London.
- Berckhemer, H. (1997). *Grundlagen der Geophysik*. Wissenschaftliche Buchgesellschaft, Darmstadt, 2., durchgesehene und korrigierte auflage edition.
- Bertotti, G., Matenco, L., and Cloetingh, S. (2003). Vertical movements in and around the south-east Carpathian foredeep: lithospheric memory and stress field control. *Terra Nova*, 15(5):299–305.
- Bishop, P. (2007). Long-term landscape evolution: linking tectonics and surface processes. *Earth Surface Processes and Landforms*, 32(3):329–365.
- Bodine, J. H. and Watts, A. B. (1979). Lithospheric flexure seaward of the Bonin and Mariana trenches. *Earth and Planetary Science Letters*, 43(1):132–148.

- Braun, J. (2006). Recent advances and current problems in modelling surface processes and their interaction with crustal deformation. *Geological Society, London, Special Publications*, 253(1):307–325.
- Braun, J. and Sambridge, M. (1997). Modelling landscape evolution on geological time scales: a new method based on irregular spatial discretization. *Basin Research*, 9(1):27–52.
- Bronstein, I. N., Semendjajew, K. A., Musiol, G., and Mühlig, H. (1999). *Taschenbuch der Mathematik*. Verlag Harri Deutsch, Frankfurt am Main, Thun, 4., überarbeitete und erweiterte Auflage der Neubearbeitung edition.
- Buchmann, T. J. and Connolly, P. T. (2007). Contemporary kinematics of the Upper Rhine Graben: a 3D finite element approach. *Global and Planetary Change*, 58:287–309.
- Burbank, D. W. (1992). Causes of recent Himalayan uplift deduced from deposited patterns in the Ganges basin. *Nature*, 357(6380):680–683.
- Burbank, D. W. and Anderson, R. S. (2001). *Tectonic geomorphology*. Blackwell Science Ltd, Oxford.
- Burbank, D. W. and Pinter, N. (1999). Landscape evolution: the interactions of tectonics and surface processes. *Basin Research*, 11(1):1–6.
- Burgmann, R., Hilley, G., Ferretti, A., and Novali, F. (2006). Resolving vertical tectonics in the San Francisco Bay Area from permanent scatterer InSAR and GPS analysis. *Geology*, 34(3):221–224.
- Burov, E. and Toussaint, G. (2007). Surface processes and tectonics: forcing of continental subduction and deep processes. *Global and Planetary Change*, 58:141–164.
- Champagnac, J. D., Molnar, P., Anderson, R. S., Sue, C., and Delacou, B. (2007). Quaternary erosion-induced isostatic rebound in the western Alps. *Geology*, 35(3):195–198.
- Cloetingh, S., Horváth, F., Dinu, C., Stephenson, R. A., Bertotti, G., Bada, G., Matenco, L., Garcia-Castellanos, D., and The TECTOP Working Group (2003). Probing tectonic topography in the aftermath of continental convergence in central Europe. *Eos*, 84:89–96.
- Cloetingh, S., Ziegler, P. A., Beekman, F., Andriessen, P. A. M., Matenco, L., Bada, G., Garcia-Castellanos, D., Hardebol, N., Dezes, P., and Sokoutis, D. (2005). Lithospheric memory, state of stress and rheology: neotectonic controls on Europe’s intraplate continental topography. *Quaternary Science Reviews*, 24(3-4):241–304.

- Cloetingh, S. A. P. L., Burov, E., Matenco, L., Toussaint, G., Bertotti, G., Andriessen, P. A. M., Wortel, M. J. R., and Spakman, W. (2004). Thermo-mechanical controls on the mode of continental collision in the SE Carpathians (Romania). *Earth and Planetary Science Letters*, 218(1-2):57–76.
- Cloetingh, S. A. P. L., Ziegler, P. A., Bogaard, P. J. F., Andriessen, P. A. M., Artemieva, I. M., Bada, G., Balen, R. T., Beekman, F., Ben-Avraham, Z., Brun, J. P., Bunge, H. P., Burov, E. B., Carbonell, R., Facenna, C., Friedrich, A., Gallart, J., Green, A. G., Heidbach, O., Jones, A. G., Matenco, L., Mosar, J., Oncken, O., Pascal, C., Peters, G., Sliapura, S., Soesoo, A., Spakman, W., Stephenson, R. A., Thybo, H., Torsvik, T., de Vicente, G., Wenzel, F., and Wortel, M. J. R. (2007). TOPO-EUROPE: the geoscience of coupled deep Earth-surface processes. *Global and Planetary Change*, 58(1-4):1–118.
- Codilean, A. T., Bishop, P., and Hoey, T. B. (2006). Surface process models and the links between tectonics and topography. *Progress In Physical Geography*, 30(3):307–333.
- Coulthard, T. J. (2001). Landscape evolution models: a software review. *Hydrological Processes*, 15(1):165–173.
- Coward, M. P., Dietrich, D., and Park, R. G., editors (1989). *Alpine tectonics*, volume 45 of *Special Publications*. Geological Society, London.
- Csontos, L. (1995). Tertiary tectonic evolution of the Intra-Carpathian area: a review. *Acta Vulcanologica*, 7(2):1–13.
- Davis, R. O. and Selvadurai, A. P. S. (1996). *Elasticity and geomechanics*. Cambridge University Press, Cambridge, first published 1996 edition.
- Demetrescu, C., Wilhelm, H., Ene, M., Andreescu, M., Polonic, G., Baumann, C., Dobrica, V., and Serban, D. Z. (2005). On the geothermal regime of the foreland of the Eastern Carpathians bend. *Journal Of Geodynamics*, 39(1):29–59.
- DeMets, C., Gordon, R. G., Argus, D. F., and Stein, S. (1990). Current plate motions. *Geophysical Journal International*, 101(2):425–478.
- Drewes, H., Dodson, A. H., Fortes, L. P. S., Sanchez, L., and Sandoval, P., editors (2002). *Vertical reference systems*, volume 124 of *International Association of Geodesy Symposia*. Springer.
- Dyksterhuis, S., Albert, R. A., and Müller, R. D. (2005). Finite-element modelling of contemporary and palaeo-intraplate stress using ABAQUS™. *Computers & Geosciences*, 31(3):297–307.

- Ehlers, T. A. and Farley, K. A. (2003). Apatite (U-Th)/He thermochronometry: methods and applications to problems in tectonic and surface processes. *Earth and Planetary Science Letters*, 206(1-2):1–14.
- Ehlotzky, F. (2007). *Angewandte Mathematik für Physiker*. Springer.
- Ellis, S., Beavan, J., Eberhart-Phillips, D., and Stockhert, B. (2006). Simplified models of the Alpine fault seismic cycle: stress transfer in the mid-crust. *Geophysical Journal International*, 166(1):386–402.
- England, P. and Molnar, P. (1990). Surface uplift, uplift of rocks, and exhumation of rocks. *Geology*, 18(12):1173–1177.
- Fischer, K. D. (2001). *Dreidimensionale Modellierung der synorogenen Entwicklung des Variszischen Vorlandbeckens mit der Methode der Finiten-Elemente*. PhD thesis, Universität Jena, Institut für Geowissenschaften.
- Fischer, K. D. (2006). The influence of different rheological parameters on the surface deformation and stress field of the Aegean-Anatolian region. *International Journal Of Earth Sciences*, 95(2):239–249.
- Fischer, K. D., Jahr, T., and Jentzsch, G. (2004). Evolution of the Variscan foreland-basin: modelling the interactions between tectonics and surface processes. *Physics and Chemistry of the Earth*, 29(10):665–671.
- Friedrich, A. M., Wernicke, B. P., Niemi, N. A., Bennett, R. A., and Davis, J. L. (2003). Comparison of geodetic and geologic data from the Wasatch region, Utah, and implications for the spectral character of Earth deformation at periods of 10 to 10 million years. *Journal of Geophysical Research – Solid Earth*, 108(B4):2199.
- Fuchs, K., Bonjer, K. P., Bock, G., Cornea, I., Radu, C., Enescu, D., Jianu, D., Nourescu, A., Merkler, G., Moldoveanu, T., and Tudorache, G. (1979). Romanian earthquake of march 4, 1977; II. aftershocks and migration of seismic activity. *Tectonophysics*, 53(3-4):225–247.
- Fullsack, P. (1995). An arbitrary Lagrangian-Eulerian formulation for creeping flows and its application in tectonic models. *Geophysical Journal International*, 120(1):1–23.
- Gallagher, K., Brown, R., and Johnson, C. (1998). Fission track analysis and its applications to geological problems. *Annual Review Of Earth And Planetary Sciences*, 26:519–572.
- Garcia-Castellanos, D. (2002). Interplay between lithospheric flexure and river transport in foreland basins. *Basin Research*, 14(2):89–104.

- Garcia-Castellanos, D., Fernàndez, M., and Torne, M. (1997). Numerical modeling of foreland basin formation: a program relating thrusting, flexure, sediment geometry and lithosphere rheology. *Computers & Geosciences*, 23(9):993–1003.
- Garcia-Castellanos, D., Fernandez, M., and Torne, M. (2002). Modeling the evolution of the Guadalquivir foreland basin (southern Spain). *Tectonics*, 21(3):1018.
- Garcia-Castellanos, D., Verges, J., Gaspar-Escribano, J., and Cloetingh, S. (2003). Interplay between tectonics, climate, and fluvial transport during the Cenozoic evolution of the Ebro Basin (NE Iberia). *Journal of Geophysical Research – Solid Earth*, 108(B7):2347.
- Gilchrist, A. R. and Summerfield, M. A. (1990). Differential denudation and flexural isostasy in formation of rifted-margin upwarps. *Nature*, 346(6286):739–742.
- Girbacea, R. and Frisch, W. (1998). Slab in the wrong place: lower lithospheric mantle delamination in the last stage of the Eastern Carpathian subduction retreat. *Geology*, 26(7):611–614.
- Girbacea, R. and Frisch, W. (1999). Slab in the wrong place: lower lithospheric mantle delamination in the last stage of the Eastern Carpathian subduction retreat: reply. *Geology*, 27(7):666–666.
- Girbacea, R., Frisch, W., and Linzer, H. G. (1998). Post-orogenic uplift-induced extension: a kinematic model for the Pliocene to recent tectonic evolution of the Eastern Carpathians (Romania). *Geologica Carpathica*, 49(5):315–327.
- Gradstein, F. M., Ogg, J. G., Smith, A. G., Bleeker, W., and Lourens, L. J. (2004). A new Geologic Time Scale, with special reference to Precambrian and Neogene. *Episodes*, 27(2):83–100.
- Gvirtzman, Z. (2002). Partial detachment of a lithospheric root under the southeast Carpathians: toward a better definition of the detachment concept. *Geology*, 30(1):51–54.
- Haas, R., Gueguen, E., Scherneck, H. G., Nothnagel, A., and Campbell, J. (2000). Crustal motion results derived from observations in the European geodetic VLBI network. *Earth Planets And Space*, 52(10):759–764.
- Hampel, A. and Hetzel, R. (2006). Response of normal faults to glacial-interglacial fluctuations of ice and water masses on Earth’s surface. *Journal of Geophysical Research – Solid Earth*, 111(B6).

- Hauser, F., Raileanu, V., Fielitz, W., Dinu, C., Landes, M., Bala, A., and Prodehl, C. (2007). Seismic crustal structure between the Transylvanian Basin and the Black Sea, Romania. *Tectonophysics*, 430(1-4):1–25.
- Heidbach, O. and Drewes, H. (2003). 3-D finite element model of major tectonic processes in the Eastern Mediterranean. In Nieuwland, D., editor, *New insights in structural interpretation and modelling*, volume 212 of *Special Publications*, pages 259–272. Geological Society, London.
- Heidbach, O., Ledermann, P., Kurfeß, D., Peters, G., Buchmann, T., Mantenco, L., Negut, M., Sperner, B., Müller, B., Nuckelt, A., and Schmitt, G. (2007a). Attached or not attached: slab dynamics beneath Vrancea, Romania. In *International symposium on strong Vrancea earthquakes and risk mitigation, Oct. 4–6, 2007, Bucharest, Romania*.
- Heidbach, O., Müller, B., Peters, G., Kurfeß, D., Buchmann, T., and Ledermann, P. (2008). *Abschlussbericht Sonderforschungsbereich 461 – Starkbeben: Von geowissenschaftlichen Grundlagen zu Ingenieurmaßnahmen*, chapter Project A6 – Contemporary tectonic stress field and geodynamics, pages 57–87. Universitätsverlag Karlsruhe, Karlsruhe.
- Heidbach, O., Reinecker, J., Tingay, M., Müller, B., Sperner, B., Fuchs, K., and Wenzel, F. (2007b). Plate boundary forces are not enough: second- and third-order stress patterns highlighted in the World Stress Map database. *Tectonics*, 26(6).
- Hergert, T. and Heidbach, O. (2006). New insights into the mechanism of postseismic stress relaxation exemplified by the 23 June 2001 M_w=8.4 earthquake in southern Peru. *Geophysical Research Letters*, 33(2).
- Hetzl, R. and Hampel, A. (2005). Slip rate variations on normal faults during glacial-interglacial changes in surface loads. *Nature*, 435(7038):81–84.
- Horvath, F. (1993). Towards a mechanical model for the formation of the Pannonian Basin. *Tectonophysics*, 226(1-4):333–357.
- Houseman, G. A. and Gemmer, L. (2007). Intra-orogenic extension driven by gravitational instability: Carpathian-Pannonian orogeny. *Geology*, 35(12):1135–1138.
- Huhmann, M., Kremenetski, K. V., Hiller, A., and Bruckner, H. (2004). Late Quaternary landscape evolution of the upper Dnister valley, western Ukraine. *Palaeogeography Palaeoclimatology Palaeoecology*, 209(1-4):51–71.

- Johansson, J. M., Davis, J. L., Scherneck, H. G., Milne, G. A., Vermeer, M., Mitrovica, J. X., Bennett, R. A., Jonsson, B., Elgered, G., Elosegui, P., Koivula, H., Poutanen, M., Ronnang, B. O., and Shapiro, I. I. (2002). Continuous GPS measurements of postglacial adjustment in Fennoscandia – 1. geodetic results. *Journal of Geophysical Research – Solid Earth*, 107(B8):2157.
- Kalicki, T. and Sanko, A. F. (1998). Palaeohydrological changes in the Upper Dneper Valley, Belarus, during the last 20,000 years. In Benito, G. and et al., editors, *Palaeohydrology and environmental change*, pages 125–135. Wiley, Chichester, England.
- Kaniuth, K. and Vetter, S. (2005). Vertical velocities of European coastal sites derived from continuous GPS observations. *GPS Solutions*, 9(1):32–40.
- Kertz, W. (1969). *Einführung in die Geophysik I*, volume 275 of *BI Hochschultaschenbücher*. Bibliographisches Institut AG, Mannheim.
- Kooi, H. and Beaumont, C. (1994). Escarpment evolution on high-elevation rifted margins: insights derived from a surface processes model that combines diffusion, advection, and reaction. *Journal of Geophysical Research – Solid Earth*, 99(B6):12191–12209.
- Kooi, H. and Beaumont, C. (1996). Large-scale geomorphology: classical concepts reconciled and integrated with contemporary ideas via a surface processes model. *Journal of Geophysical Research – Solid Earth*, 101(B2):3361–3386.
- Koons, P. O. (1995). Modeling the topographic evolution of collisional belts. *Annual Review Of Earth And Planetary Sciences*, 23:375–408.
- Koons, P. O., Norris, R. J., Craw, D., and Cooper, A. F. (2003). Influence of exhumation on the structural evolution of transpressional plate boundaries: an example from the Southern Alps, New Zealand. *Geology*, 31(1):3–6.
- Kuo, C. Y., Shum, C. K., Braun, A., and Mitrovica, J. X. (2004). Vertical crustal motion determined by satellite altimetry and tide gauge data in Fennoscandia. *Geophysical Research Letters*, 31(1):L01608.
- Kurfeß, D. and Heidbach, O. (In Press). CASQUS: a new simulation tool for coupled 3D Finite Element modeling of tectonic and surface processes based on ABAQUSTM and CASCADE. *Computers & Geosciences*.
- Linzer, H. G. (1996). Kinematics of retreating subduction along the Carpathian arc, Romania. *Geology*, 24(2):167–170.

- Lister, G., Kennet, B., Richards, S., and Forster, M. (2008). Boudinage of a stretching slablet implicated in earthquakes beneath the hindu kush. *Nature Geoscience*, 1:196–201.
- Mackin, J. H. (1948). Concept of the graded river. *Geological Society of America Bulletin*, 59(5):463–511.
- Major, C. O., Goldstein, S. L., Ryan, W. B. F., Lericolais, G., Piotrowski, A. M., and Hajdas, I. (2006). The co-evolution of Black Sea level and composition through the last deglaciation and its paleoclimatic significance. *Quaternary Science Reviews*, 25(17-18):2031–2047.
- Maniatis, G., Kurfeß, D., Hampel, A., and Heidbach, O. (Subm.). Slip acceleration on normal faults due to erosion and sedimentation – results from a new three-dimensional numerical model coupling tectonics and landscape evolution. *Submitted to Earth and Planetary Science Letters*.
- Martin, M., Ritter, J. R. R., and the CALIXTO working group (2005). High-resolution teleseismic body-wave tomography beneath SE Romania – I. implications for three-dimensional versus one-dimensional crustal correction strategies with a new crustal velocity model. *Geophysical Journal International*, 162(2):448–460.
- Martin, M., Wenzel, F., and the CALIXTO working group (2006). High-resolution teleseismic body wave tomography beneath SE-Romania – II. imaging of a slab detachment scenario. *Geophysical Journal International*, 164(3):579–595.
- Masek, J. G., Isacks, B. L., Gubbels, T. L., and Fielding, E. J. (1994). Erosion and tectonics at the margins of continental plateaus. *Journal of Geophysical Research – Solid Earth*, 99(B7):13941–13956.
- Masterlark, T. (2007). Modeling earthquakes with realistic simulation software - FEA tools help researchers achieve more accurate earthquake predictions. *R&D Magazine*, 49(6):20–21.
- Matenco, L., Bertotti, G., Cloetingh, S., and Dinu, C. (2003). Subsidence analysis and tectonic evolution of the external Carpathian-Moesian Platform region during Neogene times. *Sedimentary Geology*, 156(1-4):71–94.
- Matenco, L., Bertotti, G., Leever, K., Cloetingh, S., Schmid, S. M., Tarapanca, M., and Dinu, C. (2007). Large-scale deformation in a locked collisional boundary: interplay between subsidence and uplift, intraplate stress, and inherited lithospheric structure in the late stage of the SE Carpathians evolution. *Tectonics*, 26(4).

- Molnar, P. (2001). Climate change, flooding in arid environments, and erosion rates. *Geology*, 29(12):1071–1074.
- Molnar, P. (2003). Geomorphology - nature, nurture and landscape. *Nature*, 426(6967):612–614.
- Molnar, P. and England, P. (1990). Late Cenozoic uplift of mountain ranges and global climate change: chicken or egg? *Nature*, 346(6279):29–34.
- Morra, G. and Regenauer-Lieb, K. (2006). A coupled solid-fluid method for modelling subduction. *Philosophical Magazine*, 86(21-22):3307–3323.
- Müller, B., Heidbach, O., Negut, M., Sperner, B., and Buchmann, T. (Subm.). Attached or not attached – evidence from crustal stress observations for a weak coupling of the Vrancea slab in Romania. *Submitted to Tectonophysics*.
- Necea, D., Fielitz, W., and Matenco, L. (2005). Late Pliocene-Quaternary tectonics in the frontal part of the SE Carpathians: insights from tectonic geomorphology. *Tectonophysics*, 410(1-4):137–156.
- New, M., Lister, D., Hulme, M., and Makin, I. (2002). A high-resolution data set of surface climate over global land areas. *Climate Research*, 21(1):1–25.
- Nuckelt, A. (2007). *Dreidimensionale Plattenkinematik: Strainanalyse auf B-Spline-Approximationsflächen am Beispiel der Vrancea-Zone / Rumänien*. Dissertation, Geodätisches Institut, Universität Karlsruhe (TH).
- Nuckelt, A., Nutto, M., Schmitt, G., van der Hoeven, A. G. A., Marcu, C., and Mocanu, V. (2005). Status report of the CRC 461 subproject “three dimensional plate kinematics in Romania”. In *EGU General Assembly 2005*, volume 7 of *Geophysical Research Abstract*. European Geosciences Union.
- Oncescu, M. C. and Bonjer, K. P. (1997). A note on the depth recurrence and strain release of large Vrancea earthquakes. *Tectonophysics*, 272(2-4):291–302.
- Oncescu, M. C., Marza, V. I., Rizescu, M., and Popa, M. (1999). The Romanian Earthquake Catalogue between 984–1997. In Wenzel, F., Lungu, D., and Novak, O., editors, *Vrancea earthquakes: tectonics, hazard and risk mitigation*, pages 43–47. Kluwer Academic Publishers, Dordrecht, Netherlands.

- Panaiotu, C. E., Vasiliev, I., Panaiotu, C. G., Krijgsman, W., and Langereis, C. G. (2007). Provenance analysis as a key to orogenic exhumation: a case study from the East Carpathians (Romania). *Terra Nova*, 19(2):120–126.
- Persson, K. S., Garcia-Castellanos, D., and Sokoutis, D. (2004). River transport effects on compressional belts: first results from an integrated analogue-numerical model. *Journal of Geophysical Research – Solid Earth*, 109(B1):B01409.
- Pinet, P. and Souriau, M. (1988). Continental erosion and large-scale relief. *Tectonics*, 7(3):563–582.
- Press, F. and Siever, R. (2001). *Understanding Earth*. W. H. Freeman and Company, New York.
- Pysklywec, R. N. (2006). Surface erosion control on the evolution of the deep lithosphere. *Geology*, 34(4):225–228.
- Radulian, M., Mandrescu, N., Panza, G. F., Popescu, E., and Utale, A. (2000). Characterization of seismogenic zones of Romania. *Pure And Applied Geophysics*, 157(1-2):57–77.
- Ranalli, G. (1987). *Rheology of the Earth*. Allen & Unwin Inc., Winchester.
- Robl, J., Stuwe, K., and Hergarten, S. (2008). Channel profiles around Himalayan river anticlines: constraints on their formation from digital elevation model analysis. *Tectonics*, 27(3):TC3010.
- Sanders, C. A. E., Andriessen, P. A. M., and Cloetingh, S. A. P. L. (1999). Life cycle of the East Carpathian orogen: erosion history of a doubly vergent critical wedge assessed by fission track thermochronology. *Journal of Geophysical Research – Solid Earth*, 104(B12):29095–29112.
- Schmitt, G., Nuckelt, A., Knöpfler, A., and Marcu, C. (2007). Three dimensional plate kinematics in Romania. In *International symposium on strong Vrancea earthquakes and risk mitigation, Oct. 4–6, 2007, Bucharest, Romania*.
- Schotman, H., Wu, P., and Vermeersen, L. (In Press). Regional perturbations in a global background model of glacial isostasy. *Physics of the Earth and Planetary Interiors*, Corrected Proof.
- Simpson, G. (2004). A dynamic model to investigate coupling between erosion, deposition, and three-dimensional (thin-plate) deformation. *Journal of Geophysical Research – Earth Surface*, 109(F2):F02006.

- Simpson, G. and Schlunegger, F. (2003). Topographic evolution and morphology of surfaces evolving in response to coupled fluvial and hillslope sediment transport. *Journal of Geophysical Research – Solid Earth*, 108(B6):2300.
- Snyder, N. P., Whipple, K. X., Tucker, G. E., and Merritts, D. J. (2000). Landscape response to tectonic forcing: digital elevation model analysis of stream profiles in the Mendocino triple junction region, northern California. *Geological Society Of America Bulletin*, 112(8):1250–1263.
- Sperner, B., Ioane, D., and Lillie, R. J. (2004). Slab behaviour and its surface expression: new insights from gravity modelling in the SE-Carpathians. *Tectonophysics*, 382(1-2):51–84.
- Sperner, B., Lorenz, F., Bonjer, K., Hettel, S., Müller, B., and Wenzel, F. (2001). Slab break-off – abrupt cut or gradual detachment? New insights from the Vrancea Region (SE Carpathians, Romania). *Terra Nova*, 13(3):172–179.
- Sperner, B., Ratschbacher, L., Zweigel, P., Moser, F., Hettel, S., Gîrbacea, R., and Wenzel, F. (1999). Lateral extrusion, slab-breakoff and subduction retreat: the Oligocene-Recent collision-subduction transition in the Alps and Carpathians. In Mann, P., Grindlay, N., and Dolan, J., editors, *Penrose Conference: Subduction to strike-slip transitions on plate boundaries (available on-line at <http://www.uncwil.edu/people/grindlayn/penrose.html>)*, Puerto Plata, Dominican Republic, pages 103–104.
- Sperner, B. and the CRC 461 team (2005). Monitoring of slab detachment in the Carpathians. In Wenzel, F., editor, *Perspectives in Modern Seismology*, volume 105 of *Lecture Notes in Earth Sciences*, pages 187–202. Springer, Berlin.
- Steffen, H., Kaufmann, G., and Wu, P. (2006). Three-dimensional finite-element modeling of the glacial isostatic adjustment in Fennoscandia. *Earth and Planetary Science Letters*, 250(1-2):358–375.
- Stüwe, K. (2000). *Geodynamik der Lithosphäre*. Springer-Verlag, Berlin.
- Tarapoanca, M., Bertotti, G., Matenco, L., Dinu, C., and Cloetingh, S. A. P. L. (2003). Architecture of the Focsani Depression: a 13 km deep basin in the Carpathians bend zone (Romania). *Tectonics*, 22(6):1074.
- Toussaint, G., Burov, E., and Avouac, J. P. (2004). Tectonic evolution of a continental collision zone: a thermomechanical numerical model. *Tectonics*, 23(6):TC6003.

- Tucker, G. E. and Slingerland, R. L. (1994). Erosional dynamics, flexural isostasy, and long-lived escarpments – a numerical modeling study. *Journal of Geophysical Research – Solid Earth*, 99(B6):12229–12243.
- Turcotte, D. L. and Schubert, G. (2002). *Geodynamics*. Cambridge University Press, second edition.
- van der Beek, P. and Braun, J. (1998). Numerical modelling of landscape evolution on geological time-scales: a parameter analysis and comparison with the south-eastern highlands of Australia. *Basin Research*, 10(1):49–68.
- van der Hoeven, A. G. A., Mocanu, V., Spakman, W., Nutto, M., Nuckelt, A., Matenco, L., Munteanu, L., Marcu, C., and Ambrosius, B. A. C. (2005). Observation of present-day tectonic motions in the Southeastern Carpathians: results of the ISES/CRC-461 GPS measurements. *Earth and Planetary Science Letters*, 239(3-4):177–184.
- Watts, A. B. (2001). *Isostasy and flexure of the lithosphere*. Cambridge University Press, Cambridge, United Kingdom.
- Wenzel, F., Lorenz, F., Sperner, B., and Oncescu, M. C. (1999). Seismotectonics of the Romanian Vrancea area. In Wenzel, F., Lungu, D., and Novak, O., editors, *Vrancea earthquakes: tectonics, hazard and risk mitigation*, pages 15–26. Kluwer Academic Publishers, Dordrecht, Netherlands.
- Wenzel, F., Sperner, B., Lorenz, F., and Mocanu, V. (2002). Geodynamics, tomographic images and seismicity of the Vrancea region (SE-Carpathians, Romania). In Cloetingh, S. A. P. L., Horváth, F., Bada, G., and Lankreijer, A. C., editors, *Neotectonics and surface processes: the Pannonian Basin and Alpine/Carpathian System*, volume 3 of *Stephan Mueller Special Publication Series*, pages 95–104. European Geosciences Union.
- Wessel, P. and Smith, W. H. F. (1991). Free software helps map and display data. *EOS*, 72:441.
- Wessel, P. and Smith, W. H. F. (1996). A global, self-consistent, hierarchical, high-resolution shoreline database. *Journal of Geophysical Research – Solid Earth*, 101(B4):8741–8743.
- Westerhaus, M., Altmann, J., and Heidbach, O. (2008). Using topographic signatures to classify internally and externally driven tilt anomalies at Merapi Volcano, Java, Indonesia. *Geophysical Research Letters*, 35(5):L05310.
- Willett, S. D. (1999). Orogeny and orography: the effects of erosion on the structure of mountain belts. *Journal of Geophysical Research – Solid Earth*, 104(B12):28957–28981.

- Willgoose, G., Bras, R. L., and Rodriguez-Iturbe, I. (1991a). A coupled channel network growth and hillslope evolution model, 1. theory. *Water Resources Research*, 27(7):1671–1684.
- Willgoose, G., Bras, R. L., and Rodriguez-Iturbe, I. (1991b). Results from a new model of river basin evolution. *Earth Surface Processes and Landforms*, 16(3):237–254.
- Wortel, M. J. R. and Spakman, W. (2000). Subduction and slab detachment in the Mediterranean-Carpathian region. *Science*, 290(5498):1910–1917.
- Wu, P. (2004). Using commercial finite element packages for the study of earth deformations, sea levels and the state of stress. *Geophysical Journal International*, 158(2):401–408.
- Zarifi, Z. and Havskov, J. (2003). Characteristics of dense nests of deep and intermediate-depth seismicity. *Advances In Geophysics*, 46:237–278.
- Zienkiewicz, O. C. (1977). *The finite element method*. McGraw-Hill, London, 3., expanded and rev. edition.